Adsorption by Powders and Porous Solids

Principles, Methodology and Applications

Françoise Rouquerol, Jean Rouquerol and Kenneth Sing

Centre de Thermodynamique et de Microcalorimétrie du CNRS and Université de Provence, 26 rue du 141ème RIA 13003 Marseille France

ACADEMIC PRESS
San Diego London Boston
New York Sydney Tokyo Toronto

This book is printed on acid-free paper.

ISBN 0-12-598920-2

ACADEMIC PRESS
24–28 Oval Road, London NW1 7DX, UK
http://www.hbuk.co.uk/ap/

ACADEMIC PRESS
a division of Harcourt Brace & Company
525 B Street, Suite 1900, San Diego, CA 92101, USA
http://www.apnet.com

Library of Congress Catalogue Card Number: 98-86248
A catalogue record for this book is available from the British Library

Typeset by Mathematical Composition Setters Ltd, Salisbury, Wiltshir
Printed in Great Britain by MPG Books Ltd, Bodmin, Cornwall

99 00 01 02 03 04 MP 9 8 7 6 5 4 3 2 1

Contents

List of Main Symbols

As far as possible, the notation used here follows the recommendations of the International Union of Pure and Applied Chemistry.

a	specific surface area
A	surface area
	A(ext) or a(ext) external surface area
b	Langmuir adsorption coefficient
$b(B)$	molality of a solute B
B_m	second virial (molar) coefficient
c	concentration
C	BET constant
d	molecular diameter or particle diameter
E	energy
	E_0 adsorption molar energy at infinitely low coverage
	E_1 adsorption molar energy for the first layer
	E^l liquefaction energy
F	Helmoltz energy defined as $U - TS$
G	Gibbs energy defined as $H - TS$
H	enthalpy defined as $U + pV$
H	distance between the nuclei in the parallel walls of a pore
i	intercept
k_H	Henry's law constant
K	equilibrium constant
K	Kelvin, SI unit
L	Avogadro constant
m	mass
M	molar mass
n	amount of substance
$\boldsymbol{n}$	specific surface excess amount
	n^σ surface excess amount (in the Gibbs representation)
	n^a adsorbed amount (in the layer representation)
	$\boldsymbol{n}_m$ monolayer capacity
	$\boldsymbol{n}_{(sat)}$ Specific surface excess amount corresponding to the saturation of pores
	n_p pore capacity

N number of elementary entities
p pressure
p° standard pressure (usually the saturation pressure)
Q heat
r pore radius
R gas constant
s slope
S entropy
t thickness of multimolecular layer
T thermodynamic temperature
U internal energy

U^σ surface excess (internal) energy

$u^\sigma = \dfrac{U^\sigma}{n^\sigma}$ molar surface excess (internal) energy

$\dot{u}^\sigma = \left(\dfrac{\partial U^\sigma}{\partial n^\sigma}\right)_{T,A.}$ differential surface excess (internal) energy

V volume

$v^\sigma(\mathrm{STP}) = \dfrac{V^\sigma(\mathrm{STP})}{m^s}$ specific gas volume (STP) corresponding to the specific surface excess amount n^σ.

w effective pore width
W work
x mole fraction
y mole fraction
z distance from surface

α polarizability
ε pairwise interaction energy
γ surface tension
Γ surface excess concentration defined as n^σ/A
θ surface coverage, defined as the ratio of two surface excess amounts, one of which is used as a reference
θ Celsius temperature
μ chemical potential
Π spreading pressure
ρ mass density
σ molecular cross sectional area
φ potential energy
ϕ heat flow

CHAPTER 1

Introduction

1.1. Importance of Adsorption

Adsorption occurs whenever a solid surface is exposed to a gas or liquid: it is defined as the enrichment of material or increase in the density of the fluid in the vicinity of an interface. Under certain conditions, there is an appreciable enhancement in the concentration of a particular component and the overall effect is then dependent on the extent of the interfacial area. For this reason, all industrial adsorbents have large specific surface areas (generally well in excess of $100\,m^2\,g^{-1}$) and are therefore highly porous or composed of very fine particles.

Adsorption is of great technological importance. Thus, some adsorbents are used on a large scale as desiccants, catalysts or catalyst supports; others are used for the separation of gases, the purification of liquids, pollution control or for respiratory protection. In addition, adsorption phenomena play a vital role in many solid state reactions and biological mechanisms.

Another reason for the widespread use of adsorption techniques is the importance now attached to the characterization of the surface properties and texture of fine powders such as pigments, fillers and cements. Similarly, adsorption measurements are undertaken in many academic and industrial laboratories on porous materials

appreciate the role of the solid surface. He proposed a general mathematical relation for the isotherm, which we now refer to as the Freundlich adsorption equation.

In 1909 McBain reported that the uptake of hydrogen by carbon appeared to occur in two stages: a rapid process of adsorption appeared to be followed by a slow process of absorption into the interior of the solid. McBain coined the term *sorption* to cover both phenomena. In recent years it has been found convenient to use 'sorption' when it is not possible to make a clear distinction between the stages of uptake, and also to use it to denote the penetration of molecules into very narrow pores (Barrer, 1978).

During the early years of the twentieth century, various quantitative investigations of gas adsorption were undertaken. The most important advances in the theoretical interpretation of gas adsorption data were made by Zsigmondy, Polanyi and Langmuir: their ideas set the scene for much of the research undertaken over the past 80 years.

In 1911 Zsigmondy pointed out that the condensation of a vapour can occur in very narrow pores at pressures well below the normal vapour pressure of the bulk liquid. This explanation was given for the large uptake of water vapour by silica gel and was based on an extension of a concept originally put forward by Thomson (Lord Kelvin) in 1871. It is now generally accepted that *capillary condensation* does play an important role in the physisorption by porous solids, but that the original theory of Zsigmondy cannot be applied to pores of molecular dimensions.

The theory proposed by Polanyi in 1914 was developed from an older idea of long-range attractive forces emanating from the solid surface. The adsorbed layer was pictured as a thick compressed film of decreasing density with increase in distance from the surface. The original 'potential theory' did not give an equation for the adsorption isotherm, but instead provided a means of establishing a 'characteristic curve' – relating adsorption potential to amount adsorbed – for a given system. In spite of its initial appeal, it soon became apparent that the principles underlying the potential theory were not consistent with the emerging treatment of intermolecular forces. However, more recently the concept of a characteristic curve has been modified and adopted by Dubinin and his co-workers in their theory of micropore filling.

The year 1916 brought a radical change in the approach to surface science. In that year the first of Langmuir's monumental papers appeared (1916, 1917, 1918). Lord Rayleigh's earlier conclusion that certain films of polar oils on water were one molecule thick had not received the attention it deserved and Langmuir's great contribution was to bring together all the available evidence to support the unifying concept of the monomolecular layer (the *monolayer*). He proposed that adsorption on both liquid and solid surfaces normally involved the formation of a monomolecular layer. In retrospect it is not surprising that the advent of the Langmuir theory produced a renaissance in surface science.

Langmuir's work on gas adsorption and insoluble monolayers prepared the way for more progress to be made in the interpretation of adsorption from solution data. In the light of the Langmuir theory, it seemed logical to suppose that the plateau of a solute isotherm represented monolayer completion and that the monolayer capacity could be derived by application of the Langmuir equation.

Another important stage in the history of gas adsorption was the work of Brunauer and Emmett, which preceded the publication of the Brunauer–Emmett–Teller (BET) theory in 1938. In 1934 Emmett and Brunauer made their first attempt to use low-temperature adsorption of nitrogen to determine the surface area of an iron synthetic ammonia catalyst. They noted that the adsorption isotherms of a number of gases, measured at temperatures at, or near, their respective boiling points, were all S-shaped with certain distinctive features. Others, including Langmuir, had recognized that this type of adsorption was not always restricted to monolayer coverage and an empirical approach was adopted by Emmett and Brunauer (1937) to ascertain the stage at which the multilayer adsorption began. They eventually decided that completion of the monolayer was characterized by the beginning of the middle nearly linear section of the adsorption isotherm (designated Point B – see Figure 1.7). The surface area was then evaluated from the amount adsorbed at Point B by making the further assumption that the completed monolayer was in a close-packed state. In 1938 the publication of the BET theory appeared to provide a sound basis for the identification of Point B as the stage of monolayer completion and the onset of multilayer adsorption.

It would be difficult to overestimate the historical importance of the BET theory since for over 50 years it has attracted an enormous amount of attention (Davis, 1991). Indeed, the BET method is now accepted as a standard procedure for the determination of the surface area of a wide range of fine powders and porous materials. On the other hand, it is generally recognized that the theory is based on an oversimplified model of multilayer adsorption and that the reliability of the BET method is questionable unless certain conditions are fulfilled.

There was a growing awareness in the early 1930s that a distinction could be made between physical adsorption (i.e. *physisorption*) in which the van der Waals interactions are involved and chemical adsorption (i.e. *chemisorption*) in which the adsorbed molecules are attached by chemical bonding. Taylor (1932) introduced the concept of 'activated adsorption' which, by analogy with the familiar idea of an energy of activation in chemical kinetics, attempted to explain the marked increase in rate of adsorption with rise in temperature in terms of surface bond formation. The activated adsorption theory aroused a good deal of early criticism and with the subsequent improvement of high vacuum techniques it was established that chemisorption of certain gases can take place very rapidly on clean metal surfaces. However, there are other chemisorption systems which do appear to exhibit some features of activated adsorption.

In his 1916 paper, Langmuir had stated that with highly porous adsorbents such as charcoal 'it is impossible to know definitely the area on which the adsorption takes place' and that 'there are some spaces in which a molecule would be closely surrounded by carbon atoms on nearly all sides'. He concluded that equations derived for plane surfaces were not applicable to adsorption by charcoal. Unfortunately, these observations have been overlooked by many investigators, who have applied the simple Langmuir monolayer equation to adsorption data obtained with zeolites and activated carbons.

The significance of Langmuir's comments was appreciated, however, by Dubinin

often difficult. Although many isotherms have a similar shape to the classical Langmuir isotherm, they rarely obey the Langmuir equation over an appreciable range of concentration. It is evident that consideration must be given to the competition between solute and solvent, the solvation of solute and, in many cases, lack of thermodynamic equilibration.

1.3. General Definitions and Terminology

Some of the principal terms and properties associated with adsorption, powders and porous solids are defined in Tables 1.1, 1.2 and 1.3. These definitions are consistent with those proposed by the International Union of Pure and Applied Chemistry (IUPAC) (see Sing *et al.* 1985; Haber, 1991; Rouquerol *et al.*, 1994) and by the British Standards Institution (1958, 1992) and other official organizations (see Robens and Krebs, 1991).

As noted earlier, the term *adsorption* is universally understood to mean the enrichment of one or more of the components in the region between between two bulk phases (i.e. the interfacial layer). In the present context, one of these phases is necessarily a solid and the other a fluid (i.e. gas or liquid). With certain systems (e.g. some metals exposed to hydrogen, oxygen or water), the adsorption process is accompanied by *absorption*, i.e. the penetration of the fluid into the solid phase. As already indicated, one may then use the term *sorption* (and the related terms *sorbent, sorptive* and *sorbate*). This is the convention that we shall adopt in the present book. The term sorption is used by some authors to denote the uptake of gas or liquid by a molecular sieve, but we do not favour this practice.

The terms *adsorption* and *desorption* are often used to indicate the direction from which the equilibrium states have been approached. *Adsorption hysteresis* arises when the amount adsorbed is not brought to the same level by the adsorption and desorption approach to a given 'equilibrium' pressure or bulk concentration. The relation, at constant temperature, between the amount adsorbed and the equilibrium pressure, or concentration, is known as the *adsorption isotherm.*

A powder is easily recognized as a mass of small dry particles, but the precise definition is inevitably somewhat arbitrary. The term *fine powder* is also used in an

Table 1.1. Definitions: adsorption

Term	Definition
Adsorption	Enrichment of one or more components in an interfacial layer
Adsorbate	Substance in the adsorbed state
Adsorptive[a]	Adsorbable substance in the fluid phase
Adsorbent	Solid material on which adsorption occurs
Chemisorption	Adsorption involving chemical bonding
Physisorption	Adsorption without chemical bonding
Monolayer capacity	*either* Chemisorbed amount required to occupy all surface sites *or* Physisorbed amount required to cover surface
Surface coverage	Ratio of amount of adsorbed substance to monolayer capacity

[a] Translated into French as 'adsorbable'.

Table 1.2. Definitions powders

Term	Definition
Powder	Dry material composed of discrete particles with maximum dimension less than about 1 mm
Fine powder	Powder with particle size below about 1 μm
Aggregate	Loose, unconsolidated assemblage of particles
Agglomerate	Rigid, consolidated assemblage or particles
Compact	Agglomerate formed by compression of powder
Acicular	Needle-shaped
Surface area	Extent of available surface as determined by a given method under stated conditions
Specific surface area	Surface area of unit mass of powder, as determined under stated conditions
External surface	Area of external surface of particles, as taking account of roughness (i e all cavities which are wider than they are deep), but not porosity
Roughness factor	Ratio of external surface area to area of smoothed envelope around particles
Divided solid	Solid made up of more or less independent particles which may be in the form of a powder, aggregate or agglomerate

imprecise manner, but it seems reasonable to apply it to a material consisting of particles less than about 1 μm (i.e. particles of colloidal dimensions). The unit mass of a fine powder contains a large number of small particles and hence exhibits an appreciable surface area. For example, in the simplest case of an assemblage of spherical particles, all with the same diameter, d, the specific surface area, a, is given by the relation

$$a = 6/\rho\, d \tag{1.1}$$

where ρ is the particle absolute density. Thus, a powder composed of smooth spherical particles of $d = 1$ μm and $\rho = 3\ \mathrm{g\ cm^{-3}}$ would have a specific surface of $2\ \mathrm{m^2\ g^{-1}}$. The same calculation would apply to cubic particles, but in this case d would equal the edge length of the cube. In fact, an area of about $2\ \mathrm{m^2 g^{-1}}$ turns out to be of the same order of magnitude as the lower limit amenable to investigation by the techniques most often used in routine adsorption measurements.

It is evident that it is more difficult to define particle size if the particle shape is not spherical or cubic. With some other simple geometric forms, a single linear dimension, d_x, may be used to calculate the surface area. In particular, when the particle aspect ratio is sufficiently large, d_x is taken as the *minimum* dimension. Thus, if the particles are thin or long (i.e. plates or rods), it is the thickness which mainly determines the magnitude of the specific surface area (Gregg and Sing, 1982).

Perfect spheres are rare, but spheroidal particles are present in some powders produced at high temperature (e.g. pyrogenic silicas) or by the sol-gel process. The term *sphericity* is useful for some purposes. Sphericity has been defined in various ways, the simplest definition being the ratio of the surface area of a sphere of the same volume as a given particle to the actual surface area of that particle (Allen, 1990).

The individual particles (primary particles) in a fine powder are usually clustered together in the form of *aggregates* or *agglomerates*. Loosely bonded aggregates are unconsolidated and non-rigid, but they may be converted into more rigid,

Table 1.3. Definitions: porous solids

Term	Definition
Porous solid	Solid with cavities or channels which are deeper than they are wide
Open pore	Cavity or channel with access to the surface
Interconnected pore	Pore which communicates with other pores
Blind pore[a] (Dead-end pore)	Pore with a single connection to the surface
Closed pore	Cavity not connected to the surface
Void	Space between particles
Micropore	Pore of internal width less than 2 nm
Mesopore	Pore of internal width between 2 and 50 nm
Macropore	Pore of internal width greater than 50 nm
Pore size	Pore width (diameter of cylindrical pore or distance between opposite walls of slit)
Pore volume	Volume of pores determined by stated method
Porosity	Ratio of total pore volume to apparent volume of particle or powder
Total porosity	Ratio of volume of voids and pores (open and closed) to volume occupied by solid
Open porosity	Ratio of volume of voids and open pores to volume occupied by solid
Surface area	Extent of total surface area as determined by given method under stated conditions
External surface area	Area of surface outside pores
Internal surface area	Area of pore walls
True density	Density of solid, excluding pores and voids
Apparent density	Density of material including closed and inaccessible pores, as determined by stated method

[a] In the sense of the French word '*borgne*'.

consolidated agglomerates as a result of sintering or ageing. The breakdown, or partial breakdown, of the consolidated material can be achieved by grinding. The process of agglomeration involves the bridging or cementation of particles and should not be confused with *Ostwald ripening*, which involves the growth of larger particles at the expense of smaller ones. It is evident that an agglomerate may be regarded as a 'secondary' particle, which always contains within it some internal surface. In many cases the *internal surface area* is much larger than the *external surface area* and the agglomerate then possesses a well-defined pore structure.

The classification of pores according to size has been under discussion for many years, but in the past the terms *micropore* and *macropore* have been applied in different ways by physical chemists and some other scientists. In an attempt to clarify this situation, the limits of size of the different categories of pores included in Table 1.3 have been proposed by the International Union of Pure and Applied Chemistry (Everett, 1972; Sing *et al.*, 1985). As indicated, the *pore size* is generally specified as the *pore width*, i.e. the available distance between the two opposite walls. Obviously, pore size has a precise meaning when the geometrical shape is well defined. Nevertheless, for most purposes the limiting size is that of the smallest dimension and this is generally taken to represent the effective pore size. Micropores and mesopores are especially important in the context of adsorption.

The hypothetical types of pores shown in Figure 1.1 relate to the definitions in

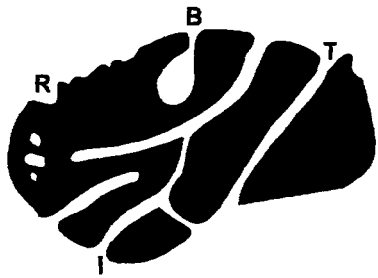

Figure 1.1. Cross-section of a hypothetical porous grain showing various types of pores: closed (C), blind (B), through (T), interconnected (I), together with some roughness (R) (Rouquerol, 1990).

Table 1.3. In addition to *closed pores* and *open pores*, we may distinguish between *blind pores* (or dead-end pores) and *interconnected pores*. Pores which are open at both sides of a membrane or porous plug are termed *through pores*.

Porosity is usually defined as the ratio of the volume of pores and voids to the volume occupied by the solid. However, it should be kept in mind that the recorded value of porosity is not always a simple characteristic property of the material, since it is likely to depend also on the methods used to assess both the pore volume and the volume of the solid. The pore volume is usually regarded as the volume of open pores, but it may include the volume of closed pores. Moreover, the recorded value may depend on the nature of the probe molecule or the experimental conditions.

It is not always easy to distinguish between roughness and porosity or between pores and voids. In principle, a convenient and simple convention is to refer to a solid as porous only if the surface irregularities are deeper than they are wide. Furthermore, the area of a rough surface is regarded as an external surface area, whereas the area of the pore walls is the internal surface area. We prefer to regard the porosity as an intrinsic property of the material and to designate void as the space between particles, which is dependent on the conditions of packing (and the particle coordination number).

It is evident that the description of many real porous materials is complicated by a wide distribution of pore size and shape and the complexity of the pore network. To facilitate the application of certain theoretical principles the shape is often assumed to be cylindrical, but this is rarely an accurate portrayal of the real system. With some materials, it is more realistic to picture the pores as slits or interstices between spheroidal particles. Computer simulation and the application of percolation theory have made it possible to study the effects of *connectivity* and *tortuosity*.

Pore structures can be created in a number of different ways. *Intracrystalline* pores are an inherent part of certain crystalline structures, e.g. of zeolites and certain clays. These pores are generally of molecular dimensions and are arranged as highly regular networks. A second type of porous material is composed of an assemblage of small particles (as mentioned earlier). The pore structure of the consolidated system (e.g. a xerogel) is mainly dependent on the size and packing density of the primary particles: the process is therefore *constitutive*. A third route is *subtractive* since inherent parts of the original structure are removed to create the pores, e.g. the thermal

barriers between adsorption sites are small enough to be overcome easily at the operational temperature: the adsorbed molecules therefore retain two translational degrees of freedom and can be regarded as *mobile*. On the other hand, if the energy barriers are much larger than kT, the adsorbed molecules are said to be *localized* since they spend most of their time on particular surface sites.

In the hypothetical case of a perfectly homogeneous surface, there is no variation of $\phi_i(z)$ in the xy plane – see Figure 1.4a. It is more realistic to picture a uniform surface, which gives rise to energy wells of the same depth. Now, the potential energy profiles corresponding to mobile and localized adsorption are shown respectively in Figures 1.4b and 1.4c. In the former case, there is a random distribution of

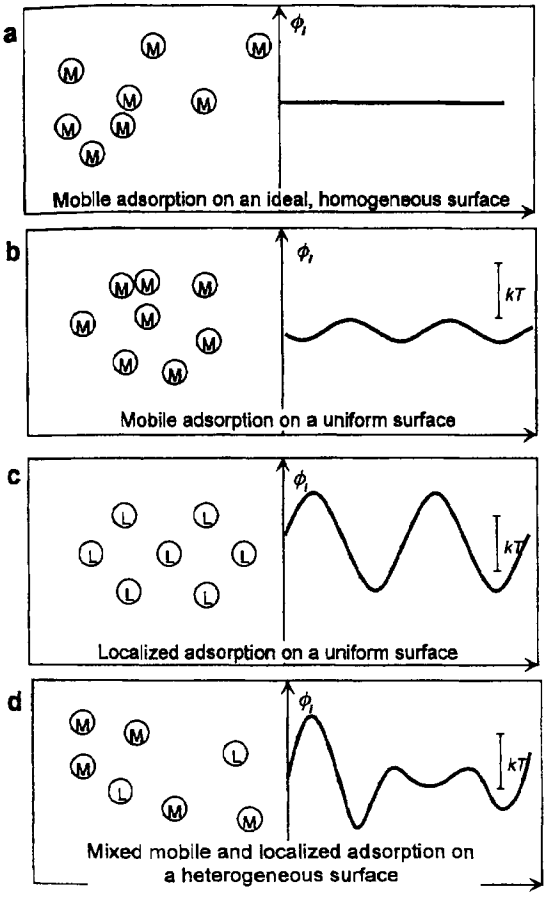

Figure 1.4. Distribution of adsorbed molecules on hypothetical surfaces (left) and corresponding variations of potential energy (right). M, mobile; L, localized. Adsorbate–adsorbate interactions are not taken into account.

adsorbed molecules across the surface; whereas in the latter case, the location of the adsorbed molecules is governed by the surface structure of the adsorbent.

Localization does not prevent the adsorbed molecules from 'hopping' from one site to another (unlike the situation in immobile chemisorption), but it is not compatible with the state of a close-packed completed monolayer.

1.7. Energetics of Physisorption

Provided that the experimental measurements are made under carefully controlled conditions and that the adsorption systems are well characterized, energy of adsorption data can provide valuable information concerning the mechanisms of physisorption.

When a polar molecule is adsorbed on an ionic or polar surface various types of specific interactions may contribute to the *adsorption energy*. A useful general expression for the adsorption energy, E_0, at very low surface coverage was first proposed by Barrer (1966) in the form of the sum

$$E_0 = E_D + E_R + E_P + E_{F\mu} + E_{FQ} \tag{1.6}$$

in which E_D and E_R represent the non-specific dispersion and repulsion contributions and the terms E_P, $E_{F\mu}$ and E_{FQ} represent, respectively, the three types of specific contributions: the polarization, field-dipole and field gradient-quadrupole energies.

For convenience, we may write Equation (1.6) in the form

$$E_0 = E_{ns} + E_{sp}$$

with E_{ns} now in place of $(E_D + E_R)$ representing the *non-specific* contributions and E_{sp} representing the various *specific* contributions.

If we wish to study the adsorbent–adsorbate interactions we must undertake adsorption calorimetry or analysis of the isotherm data at very low surface coverage. It is only under these conditions that we can eliminate, or at least minimize, the adsorbate–adsorbate interactions. At higher coverage, an additional (self-potential) term, E_{aa}, must be added to E_0 to allow for the latter interactions.

It is evident that the adsorption energy is controlled by the nature of the adsorption *system* (i.e. by both adsorbent and adsorptive). There are a few adsorbents which give rise to essentially non-specific interactions with a wide range of different adsorptives. The most important non-porous adsorbent of this type is graphitized carbon black, which in its most uniform state has a surface structure composed almost entirely of the graphitic basal planes. When a polar molecule is adsorbed on this surface, E_{ns} is much larger than E_{sp}, which is unlikely to contribute more than 10% to the total interaction energy. In the case of graphite, the E_{sp} contribution is largely due to the polarization component arising from the interaction between a polar adsorptive molecule and the induced dipoles in the graphite lattice.

It follows from Equations (1.2) and (1.5) that the magnitude of E_{ns} is dependent on the polarizabilities of the adsorptive and the adsorbent and the density of the principal force centres in the outer part of the adsorbent (i.e. in the surface layer). It is only

Table 1.4. Enthalpies in kJ mol^{-1} of adsorption at low coverage for *n*-hexane and benzene on graphitized carbon, silica (hydroxylated, dehydroxylated and modified), and barium sulfate

Adsorbent	n-Hexane	Benzene	Reference
Graphitized carbon black	42	42	Avgul and Kiselev (1965)
Hydroxylated silica	46	55	Kiselev (1965)
Dehydroxylated silica	48	38	Kiselev (1965)
Trimethylsilylated silica	29	34	Kiselev (1967)
Barium sulfate	47	70	Belyakova *et al.* (1970)

has resulted in a much greater effect. In this case the weakening of the adsorbent–adsorbate interactions is mainly due to the fact that the surface modification has resulted in a reduction in the density of the force centres.

The polarizabilities of benzene and hexane are very similar, but because of its electronic structure benzene exhibits significant specificity in its interaction with ionic or polar surfaces (e.g. hydroxylated silica and barium sulphate). Considerable attention has been given to the specificity associated with hydroxylated silica, but some specific adsorbent–adsorbate interactions are enhanced to an even greater extent by the exposure at the surface of ionic sites. This is illustrated by the benzene data on $BaSO_4$ in Table 1.4 and the nitrogen data on rutile in Table 1.5.

One might expect argon and nitrogen to be similar in their physisorption behaviour since their physical properties are not very different (e.g. molecular sizes, boiling points and polarizabilities). However, the energy data in Table 1.5 show that this is true only if the nitrogen interaction is non-specific (e.g. on graphitized carbon). The field gradient-quadrupole term in Equation (1.6) makes an important contribution when nitrogen

Table 1.5. Differential enthalpies of adsorption, $|\Delta_{ads}h|$ (kJ mol^{-1}), of argon and nitrogen at 'zero' and half coverage

Adsorbent	Argon		Nitrogen		Reference
	$\theta \to 0$	$\theta = 0.5$	$\theta \to 0$	$\theta = 0.5$	
Graphitized carbon	10	12	10	11	Grillet *et al.* (1979)
Hydroxylated silica (mesoporous)	15	9	> 20	12	Rouquerol *et al.* (1979)
Dehydroxylated silica (mesoporous)	15	9	17	11	
Zinc oxide (450 °C)[a]	12	11	21	20	Grillet *et al.* (1989)
Rutile (150 °C)	13	9	> 20	10	Furlong *et al.* (1980)
(400 °C)	15	11	30	13	
Molecular sieve carbon	20	15[b]	22	17[b]	Atkinson *et al.* (1987)
Microporous carbon	21	15[b]	25	15[b]	Rouquerol *et al.* (1989)
Silicalite I	14	14[b]	15	14[b]	Llewellyn *et al.* (1993a, b)
H-ZSM5 (Si/Al = 16)	14	14[b]	18	15[b]	
$AlPO_4$-5	11	14[b]	13	14[b]	Grillet *et al.* (1993)
Sepiolite	14	15	17	15	Grillet *et al.* (1988)
Attapulgite (130 °C)	15	13	18	17	Cases *et al.* (1991)

[a] Outgassing temperature.
[b] θ = fraction of pore filling.

decay, rather than the inverse 12th power in Equation (1.4). For this reason, low-coverage isotherm and adsorption energy data are used to refine the evaluation of the adsorbent–adsorbate interaction energy Another source of uncertainty is the magnitude of three-body effects, e.g. involving two adsorbate molecules and a substrate atom, which with some systems are likely to be significant even at very low coverage (Nicholson, 1996).

1.9.2. Molecular simulation

The two simulation methods in general use for solving the statistical mechanical equations are Monte Carlo (MC) and molecular dynamics (MD). The two techniques have several common features, but each has certain advantages and limitations.

Monte Carlo (MC) simulation

In this method a random number generator is used to move and rotate molecules in a random fashion. If the system is held under specified conditions of temperature, volume and number of molecules, the probability of a particular arrangement of molecules is proportional to $\exp(-U/kT)$, where U is the total intermolecular energy of the assembly of molecules and k is the Boltzmann constant. Thus, within the MC scheme the movement of individual molecules is accepted or rejected in accordance with a probability determined by the Boltzmann distribution law. After the generation of a long sequence of moves, the results are averaged to give the equilibrium properties of the model system.

An advantage of MC simulation is that it is not difficult to program. Also, the thermodynamic, canonical, variables may be readily changed. For gas adsorption studies it is generally more useful to specify μ, V, T (the grand canonical variables of chemical potential, volume and temperature) rather than N, V, T (the number of molecules, volume and temperature), so that μ is an independent variable. For this reason grand canonical Monte Carlo (GCMC) molecular simulation has been favoured by most investigators.

Molecular dynamics (MD)

By the application of Newton's equations of motion, the trajectories and velocities of the molecular motion can be obtained. Averaging over time then gives the properties of the system. Since it is possible to simulate a few nanoseconds of real time, transport properties can be evaluated as well as equilibrium states. MD is more difficult to program than MC, but the molecular motions are more realistic and therefore computer graphics can be used to give a more accurate impression of the actual movement of molecules moving through or into pores.

1.9.3. Density functional theory (DFT)

As a means of establishing the density profile, $\rho(r)$, two free energy functionals are introduced: $\Omega[\rho(r)]$ and $F[\rho(r)]$. Ω is a form of thermodynamic potential and is generally known as the grand potential, or grand free energy. In general, for a system

containing a mixture of components, which is characterized by the grand canonical variables T, V, μ_a, ..., μ_i, we may write

$$\Omega = F - \sum \mu_i N_i \tag{1.10}$$

where F is the Helmholtz free energy (see Chapter 2) and N_i is the number of molecules of component i. For a single-component fluid in the presence of a spatially varying external potential $V_{ext}(r)$, the grand potential functional can be expressed in the form

$$\Omega[\rho(r)] = F[\rho(r)] - \int dr\, \rho(r)[\mu - V_{ext}(r)], \tag{1.11}$$

where ρ is the local fluid density at position r and the integration is performed over the pore volume.

The Helmholtz energy F represents the intrinsic free energy in the absence of any external field, whereas Ω is dependent on all the interactions within the pore together with a surface contribution. When Ω is allowed to vary in response to a change in $\rho(r)$, its overall minimum corresponds to the equilibrium density profile of the system. The equilibrium density profile is therefore determined by minimizing the grand potential functional with respect to $\rho(r)$. Since $\rho(r)$ is the local density, the amount adsorbed (usually expressed as the surface excess number of molecules adsorbed) must be obtained by integration over the internal volume of the pore. By repeating this procedure for different values of μ (and hence values of $p/p°$) it is possible to construct the adsorption isotherm.

The value of DFT is evidently dependent on the accessibility and accuracy of the grand potential functional, Ω $[\rho(r)]$. The usual practice is to treat the molecules as hard spheres and divide the fluid–fluid potential into attractive and repulsive parts. A mean field approximation is used to simplify the former by the elimination of correlation effects. The hard sphere term is further divided into an ideal gas component and an excess component (Lastoskie *et al.*, 1993). The ideal component is considered to be exactly local, since this part of the Helmholtz free energy per molecule depends only on the density at a particular value of r.

The evaluation of the excess free energy is a more difficult problem. This is because in the inhomogeneous fluid the energy distribution is non-local, that is it depends on the correlations within the overall density profile. Various attempts have been made to overcome this difficulty by the introduction of weighting or smoothing functions (Gubbins, 1997). This approach has led to the development of the non-local density functional theory (NLDFT), which *inter alia* has been used for the derivation of the pore size distribution from adsorption isotherm data (see Chapter 7). The use of DFT and MC simulation for the study of micropore filling is also under active investigation (see Chapter 8).

With a number of fairly simple systems, excellent agreement has been obtained between the corresponding DFT-predicted and MC-generated isotherms, 2-D phase transitions and adsorption energies. These are encouraging results, but it must be kept in mind that the computational procedures are not entirely independent. As we have seen, they are dependent on the same model parameters of adsorbent structure and potential functions. At present, there are only a few porous adsorbents which have the

Grillet Y, Llewellyn P L, Tosi Pellenq N and Rouquerol J (1993) In *Proc Fourth International Conference on Fundamentals of Adsorption* (M Suzuki, ed), Kodansha, Tokyo, p 235
Gubbins K E (1997) In *Physical Adsorption Experiment Theory and Applications* (J Fraissard and W C Connor, eds) Kluwer Dordrecht, p 65
Gurvich L G (1915) *J Russ Phys Chim*, **47**, 805
Haber J (1991) *Pure Appl Chem*, **63**, 1227
Kiselev A V (1965) *Disc Faraday Soc*, **40**, 205
Kiselev A V (1967) *Adv Chromatogr*, **4**, 113
Langmuir I (1916) *J Am Chem Soc*, **38**, 2221
Langmuir I (1917) *J Am Chem Soc*, **39**, 1848
Langmuir I (1918) *J Am Chem Soc*, **40**, 1361
Lastoskie C, Gubbins K E and Quirke N (1993) *J Phys Chem*, **97**, 4786
Lennard Jones J E (1932) *Trans Faraday Soc* **28**, 333
Llewellyn P L, Coulomb J P, Grillet Y, Patarin J, Lauter H Reichert H and Rouquerol J (1993a) *Langmuir*, **9**, 1846
Llewellyn P L, Coulomb J P, Grillet Y, Patarin J André G and Rouquerol J (1993b) *Langmuir* **9**, 1852
London F (1930) *Z Phys*, **63** 245
Mandelbrot B B (1975) *Les Objets Fractals Forme, Hasard et Dimension*, Flammarion, Paris
McBain J W (1909) *Phil Mag*, **18**, 916
Nicholson D (1996) *J Chem Soc, Faraday Trans* **92**, 1
Nicholson D and Pellinq R J M (1998) In *Advances in Colloid and Interface Science*, vols 76 and 77 (A V Neimark, ed), Elsevier, Amsterdam, pp 76–77
Overbeek J Th G (1970) In *Surface Area Determination* (D H Everett and R H Ottewill, eds), Butterworths, London, p 3
Polanyi M (1914) *Verb Deutsch Phys* Ges, **16**, 1012
Pouillet M C S (1822) *Ann Chim Phys*, **20**, 141
Ravikovitch P, Haller G and Neimark A V (1998) In *Advances in Colloid and Interface Science*, vols 76 and 77 (A V Neimark, ed) Elsevier, Amsterdam, p 203
Ricca, F, Pisani, C and Garrone, E (1971) In *Adsorption–Desorption Phenomena*, Academic Press, London, p 111
Rideal E K (1932) In *The Adsorption of Gases by Solids*, Disc Faraday Society, London, p 139
Robens E (1994) In *Characterization of Porous Solids III* (J Rouquerol, F Rodriguez-Reinoso, K S W Sing and K K Unger, eds), Elsevier, Amsterdam, p 109
Robens E and Krebs K F (1991) In *Characterization of Porous Solids II* (F Rodriguez-Reinoso, J Rouquerol, K S W Sing and K K Unger eds), Elsevier, Amsterdam, p 133
Rouquerol J (1990) *Impact of Science on Society*, UNESCO, Paris, vol 157, p 5
Rouquerol J, Rouquerol F, Pérès C, Grillet Y and Boudellal M (1979) In *Characterization of Porous Solids* (S J Gregg, K S W Sing and H F Stoeckli, eds) Society of Chemical Industry, London, p 107
Rouquerol J, Rouquerol F and Grillet Y (1989) *Pure Appl Chem*, **61**, 1933
Rouquerol J, Avnir D, Fairbridge C W, Everett D H, Haynes J H, Pernicone N, Ramsay J D F, Sing K S W and Unger K K (1994) *Pure Appl Chem*, **66**, 1739
Sing K S W, Everett D H, Haul R A W, Moscou L, Pierotti R A, Rouquerol J and Siemieniewska T (1985) *Pure Appl Chem*, **57**, 603
Steele W A (1996) *Langmuir*, **12**, 145
Steele W A (1974) *The Interaction of Gases with Solid Surfaces*, Pergamon, Oxford
Steele W A and Bojan M J (1989) *Pure Appl Chem*, **61**, 1927
Steele W A and Bojan M J (1997) In *Characterization of Porous Solids IV* (B McEnaney, T J Mays, J Rouquerol, F Rodriguez-Reinoso, K S W Sing and K K Unger, eds), Royal Society of Chemistry, London, p 49
Steele W A and Bojan, M J (1998) In *Advances in Colloid and Interface Science*, vols 76 and 77 (A V, Neimark, ed) Elsevier, Amsterdam, p 153
Taylor H S (1932) In *The Adsorption of Gases by Solids*, Disc Faraday Society, London, p 131
Thomson W T (Lord Kelvin) (1871) *Phil Mag*, **42** (4), 448
Zsigmondy A (1911) *Z Anorg Chem*, **71**, 356

surface; at distance $z = t$, this concentration reaches the constant value of the gas phase c^g. This form of hypothetical variation of local concentration is shown schematically in Figure 2.1a, where we also identify three zones (I, II and III).

We shall assume that there is no penetration of gas into the solid (i.e. no *absorption*) so that zone I is occupied solely by the adsorbent and therefore $c^s = 0$. In zone III, the adsorbable gas is at sufficient distance from the solid surface to have a uniform concentration, c^g, and here $z > t$. In this region the concentration is dependent only on the equilibrium pressure and temperature. In Figure 2.1a, zone II is the 'adsorbed layer', which is an intermediate region confined within the limits $z = 0$ and $z = t$. Here, the local concentration, c, is higher than the concentration of the gas in zone III and is dependent on z.

It follows from this simple picture that the volume, V^a, of the adsorbed layer can be expressed as the product of the interfacial area, A, and the thickness, t. Thus

$$V^a = At \tag{2.1}$$

We may define the amount adsorbed, n^a, of the substance in the adsorbed layer as

$$n^a = \int_0^{V^a} c \, dV$$

$$= A \int_0^t c \, dz \tag{2.2}$$

In Figure 2.1a, n^a is equivalent to the hatched area (d + e).

The total amount, n, of the adsorbable substance in the whole system can be divided into two parts, the amount adsorbed and the amount remaining in the gas phase:

$$n = A \int_0^t c \, dz + c^g V^g$$

where the volume occupied by the gas at the concentration c^g is V^g, therefore:

$$n^a = n - c^g V^g \tag{2.3}$$

It is evident that the exact evaluation of n^a requires a knowledge of either the exact value of V^g or of the variation of the local concentration, c, with respect to z. In practice, it is not easy to attain either of these requirements.

To overcome this problem, Gibbs (1877) proposed an alternative approach. This makes use of the concept of 'surface excess' to quantify the amount adsorbed. Comparison is made with a reference system, which is divided into two zones (A, of volume $V^{s,\circ}$ and B, of volume $V^{g,\circ}$) by an imaginary surface – the *Gibbs dividing surface* (or GDS) – which is placed parallel to the adsorbent surface. The reference system occupies the same volume V as the real system, so that:

$$V = V^{s,\circ} + V^{g,\circ} = V^s + V^a + V^g \tag{2.4}$$

In the reference system the concentration of the gaseous adsorptive remains constant

in the volume $V^{g,\circ}$, i.e. up to the GDS. This is shown in pictorial form in Figure 2.1b. In this model, the *surface excess amount*, n^σ, represented by hatched area d, is defined as the difference between the total amount, n, of the adsorptive (hatched and crossed areas) and the amount which would be present in the volume $V^{g,\circ}$ of the reference system if the final equilibrium concentration c^g were constant up to the GDS (crossed area e + f). Thus:

$$n^\sigma = n - c^g V^{g,\circ}$$

It is convenient (although, in principle, not compulsory), for the sake of the physical interpretation of the data, to locate the GDS exactly on the surface which is accessible to the adsorptive used, so that $V^{g,\circ} = V^a + V^g$. This is what was actually done in Figure 2.1b. The experimental determination of $V^{g,\circ}$ in order to meet the above requirement is examined in Section 3.4.1.

Under these conditions:

$$n^\sigma = n - c^g V^g - c^g V^a \tag{2.5}$$

Combining with Equation (2.3), one gets:

$$n^a = n^\sigma + c^g V^a \tag{2.6}$$

In Figure 2.1b, the surface excess amount n^σ is represented by hatched area d; whereas the amount adsorbed n^a, which also includes term $c^g V^a$, is represented in Figure 2.1a by area (d + e).

Generally, the experimental conditions are such that the final concentration c^g of the gas is small and the volume V^a of the adsorbed layer is negligible in comparison with the gas volume V^g. Under these conditions

$$n^a \approx n^\sigma \tag{2.7}$$

However, at high temperature or pressure it may become necessary to make some allowance for the difference between these two quantities.

The amounts n^a and n^σ are extensive quantities, which depend on the extent of the interface. The related 'surface excess concentration', Γ, is an intensive quantity, which is defined as

$$\Gamma = n^\sigma / A \tag{2.8}$$

where the surface area, A, is associated with the mass m^s of the adsorbent. The specific surface area is therefore:

$$a = A/m^s \tag{2.9}$$

What is usually measured and recorded is the specific surface excess amount n^σ/m^s, where

$$n^\sigma/m^s = \Gamma a$$

As we have seen already, n^σ/m^s is dependent on the equilibrium pressure, p, and the adsorbent temperature, T. The usual practice is to maintain constant temperature

The *differential standard entropy of adsorption*, $\Delta_{ads}\dot{s}^{\circ}_{T,\Gamma}$, is:

$$\Delta_{ads}\dot{s}^{\circ}_{T,\Gamma} = \dot{s}^{\sigma}_{T,\Gamma} - s^{g,\circ}_{T} \tag{2.55}$$

The differential entropy of adsorption can be readily calculated from the differential enthalpy of adsorption since from Equations (2.46), (2.51) and (2.54) we obtain:

$$\Delta_{ads}\dot{s}_{T,\Gamma} = \frac{\Delta_{ads}\dot{h}_{T,\Gamma}}{T} \tag{2.56}$$

It is important not to confuse the differential (or isosteric) enthalpy of adsorption with the *transformed differential enthalpy of adsorption* $\Delta_{ads}\hat{h}_{T,\Gamma}$, which is derived from Equation (2.45):

$$\Delta_{ads}\hat{h}_{T,\Gamma} = \dot{u}^{\sigma}_{T,\Gamma} + A\left(\frac{\partial \Pi}{\partial n^{\sigma}}\right)_{T,A} - u^{g} - RT \tag{2.57}$$

so that:

$$\Delta_{ads}\hat{h}_{T,\Gamma} = \Delta_{ads}\dot{h}_{T,\Gamma} + A\left(\frac{\partial \Pi}{\partial n^{\sigma}}\right)_{T,A} \tag{2.58}$$

2.5.2. Definitions of the integral molar quantities of adsorption

The difference between a molar surface excess thermodynamic quantity $x^{\sigma}_{T,\Gamma}$ and the corresponding molar quantity $x^{g}_{T,p}$ for the gaseous adsorptive at the same equilibrium T and p is usually called the *integral molar quantity of adsorption*, and is denoted $\Delta_{ads}x_{T,\Gamma}$:

$$\Delta_{ads}x_{T,\Gamma} = x^{\sigma}_{T,\Gamma} - x^{g}_{T,p}$$

We can thus define the *integral molar energy of adsorption*:

$$\Delta_{ads}u_{T,\Gamma} = u^{\sigma}_{T,\Gamma} - u^{g}_{T} \tag{2.59}$$

and the *integral molar entropy of adsorption*:

$$\Delta_{ads}s_{T,\Gamma} = s^{\sigma}_{T,\Gamma} - s^{g}_{T,p} \tag{2.60}$$

We may derive the relation between these integral molar quantities of adsorption from Equations (2.20) using the expression of surface excess chemical potential μ^{σ} given by Equation (2.41) and assuming the gas to be ideal:

$$u^{\sigma}_{T,\Gamma} + \frac{\Pi}{\Gamma} - Ts^{\sigma}_{T,\Gamma} = u^{g}_{T} + RT - Ts^{g}_{T,p} \tag{2.61}$$

Then, from Equation (2.40), the *transformed integral molar enthalpy of adsorption* is obtained:

$$\Delta_{ads}\hat{h}_{T,\Gamma} = u^{\sigma}_{T,\Gamma} + \frac{\Pi}{\Gamma} - u^{g}_{T} - RT \tag{2.62}$$

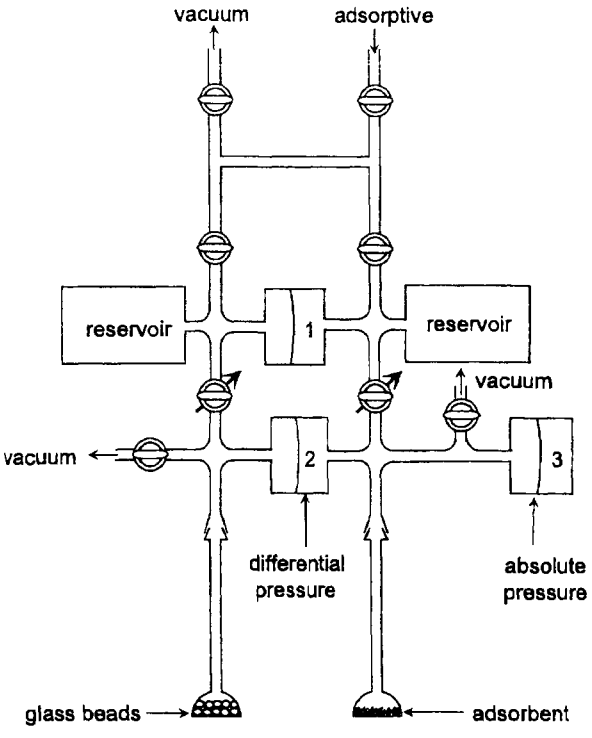

Figure 3.6. Differential gas adsorption manometry with double reservoir and triple pressure mea
ment (after Camp and Stanley, 1991).

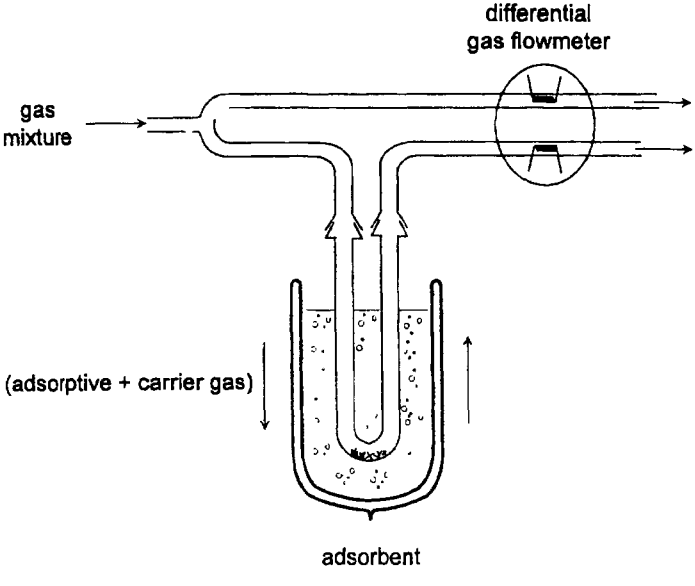

Figure 3.7. Differential flow technique for gas adsorption (after Nelsen and Eggertsen, 1958).

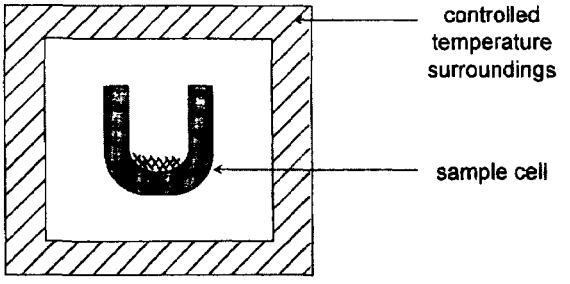

Figure 3.13. Schematic representation of a calorimeter.

- *Diathermal-compensation calorimeters*: here again, sample temperature follows surroundings temperature (usually constant in adsorption experiments), but now by means of a power compensation within the sample cell (i.e. Joule or Peltier effect). This reduces the response time.
- *Isoperibol calorimeters*: no special connection between sample temperature and surroundings temperature and, generally, the latter is kept constant. This is the conventional 'temperature rise', 'Thomsen', or 'Berthelot' calorimeter. The word 'isoperibol' was coined by Kubachewski and Hultgren (1962), from the Greek, to mean 'with isothermal surroundings'.

Adiabatic adsorption calorimetry

Here, the heat evolved on adsorption increases the temperature of the sample and its container (usually a copper cylinder). The heat is prevented from flowing to the peripheral shield (the 'surroundings') by an appropriate control of the shield temperature. Thus, the shield is usually maintained at the same temperature as the sample container by the use of a differential thermocouple and a heat coil – as indicated in Figure 3.14. The temperature rise is measured by means of a resistance thermometer attached to the sample container.

Adiabatic calorimetry is particularly useful for the study of closed adsorption systems at low temperatures (where radiation losses are small) and for temperature scanning experiments. It is the preferred type of measurement for the determination of the heat capacity of adsorption systems, especially in the temperature range 4–300 K (Morrison *et al.*, 1952; Dash, 1975). The temperature scan is obtained by means of the Joule effect applied to the sample container: the sample heating coil shown in Figure 3.14 is used for this purpose.

In some respects, adiabatic calorimetry provides information which is complementary to that provided by heat-flow calorimetry. The latter allows a study to be made of the full composition range at constant temperature, whereas the adiabatic calorimetry study is carried out over the prescribed range of temperature with a constant amount of adsorptive in the adsorption cell (of course, this does not mean that a constant amount is adsorbed). Adiabatic calorimetry allows direct measurements of the heat capacities of adsorbed films, although they are difficult to make accurately

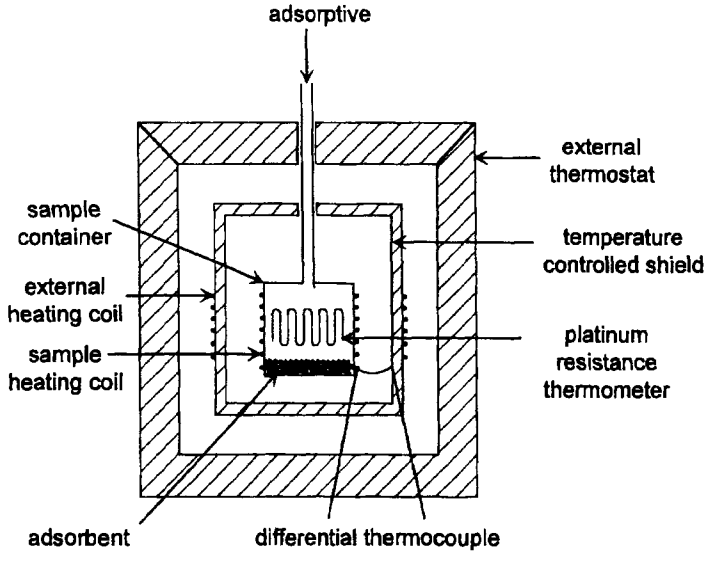

Figure 3.14. Gas adsorption cell (or sample container) in an adiabatic calorimeter.

because the mass of the film is usually a small fraction of the total mass of the calorimetric cell and sample. Fortunately, phase changes of the adsorbed film give rise to large changes in heat capacity which are easily detected by adiabatic calorimetry: this technique can be used in the same way as thermal analysis (for 3-D systems) to determine phase diagrams of 2-D systems (Morrison, 1987). Because of the desorption that takes place on heating it is necessary to allow for the enthalpy of desorption (e.g. by application of the isosteric method).

Diathermal-conduction adsorption calorimetry

This is now the most useful category for adsorption studies, especially for isothermal measurements. There are two main types.

Phase-change adsorption calorimetry. This was the earliest type of diathermal-conduction calorimetry and was originally developed in the form of 'ice calorimetry' by Lavoisier and Laplace (1783), who weighed the liquid water, and by Bunsen (1870), who measured the change of volume. Dewar (1904) devised an elegant adsorption calorimeter at liquid air temperature: the heat was evaluated from the volume of air vaporized. Of course, the temperature of the calorimeter is imposed by the temperature of the phase change. Because these calorimeters lack adaptability and cannot be readily automated, they are mainly of historical interest.

Heat-flow adsorption microcalorimetry. The most important type of isothermal calorimeter in current use is that based on the principle of the heat flowmeter, which was first applied by Tian (1923) and improved by Calvet (Calvet and Prat, 1958,

taken into account:

- The adsorptive must be carefully brought to the temperature of the microcalorimeter before entering the adsorption bulb.
- It must also be introduced very slowly, so that the heat effect corresponding to the gas compression in the calorimeter may be calculated accurately, as explained by Rouquerol and Everett (Rouquerol *et al.*, 1980). This also helps to meet the previous requirement of efficient adsorptive pre-cooling or pre-heating.
- The outgassing must be carried out carefully, bearing in mind that the adsorption bulbs used in a microcalorimeter usually have much longer necks than standard adsorption bulbs. Also, this arrangement may drastically change the actual residual pressure in the immediate vicinity of the sample during outgassing.

Diathermal-compensation adsorption calorimetry

At a time when the means for recording and integrating the signal from a heat flowmeter were of limited accuracy, Tian (1923) proposed a way of compensating the major part of the heat liberation by a steady Peltier or Joule effect taking place just against the sample. This idea was refined and adapted to adsorption experiments by Kiselev and his co-workers (Dzhigit *et al.*, 1962). By means of a continuous Joule effect in the vicinity of the adsorbent, they maintained a constant temperature difference ΔT through the heat flowmeter. As soon as adsorption produced an evolution of heat, the Joule effect was interrupted discontinuously, just enough to keep ΔT unchanged. The heat evolved on adsorption was simply derived from the sum of all non-heating periods. This approach was no longer used when the quality of the recordings allowed an accurate integration. Nevertheless, it would be worthwhile updating it (with proportional, integral and differential – PID – control and with integration of the variable Joule power) with the objective of speeding up the experiments, since this *in situ* power compensation shortens the time needed to reach the desired thermal equilibrium. The same can be done using a Peltier effect (keeping $\Delta T = 0$).

Isoperibol adsorption calorimetry

The first experiments of gas adsorption calorimetry by Favre (1854) were made with an isoperibol calorimeter. More recently, refinements were introduced by Beebe and his co-workers (1936) and by Kington and Smith (1964). Because of the uncontrolled difference between the temperature of the sample and that of the surroundings, Newton's law of cooling must be applied to correct the observed temperature rise of the sample. In consequence, any slow release of heat (over more than, say, 30 minutes), which would produce a large uncertainty in the corrective term, cannot be registered. For this reason, isoperibol calorimetry cannot be used to follow slow adsorption equilibria. However, its main drawback is that the experiment is never isothermal: during each adsorption step, a temperature rise of a few kelvins is common. The corresponding desorption (or lack of adsorption) must then be taken into account and, after each step, the sample must be 'thermally earthed' so as to start each step at the same temperature. In view of these drawbacks,

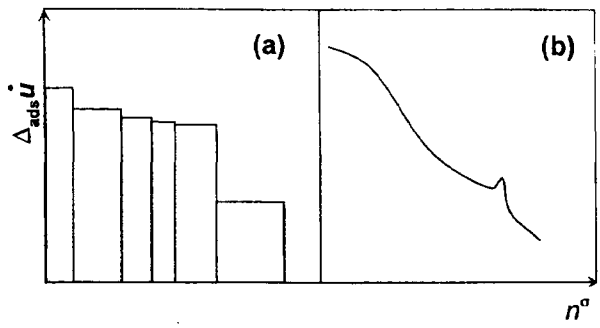

Figure 3.16. Pseudo-differential (left) and differential (right) energies of adsorption, as obtained with a discontinuous or continuous procedure, respectively.

involves the use of the following equation:

$$\Delta_{ads}\dot{h} = \frac{1}{f^\sigma}\left(\phi + V_C \frac{dp}{dt}\right) \tag{3.2}$$

The 'rate of adsorption' f^σ is determined with the help of Equation (2.80) from the experimental rate of introduction, f, of the adsorptive, the dead volumes V_C and V_E and their temperatures T_C and T_E, and the slope dp/dt. The only extra information needed is a continuous recording of the heat-flow ϕ from the beginning to the end of the experiment. To obtain these data, a convenient procedure is described in the following steps.

Steps 1–5 as for the discontinuous experiment. Dead space volume determination (Step 4) also possible by the discontinuous sonic nozzle procedure (Section 3.3.2).

6. Adsorbent bulb and calibrated volumes evacuated. Adsorbent bulb isolated.
7. Gas flow rate calibrated (cf. Step 3 of continuous sonic nozzle procedure).
8. Calibrated volume evacuated, while adsorptive still introduced at constant rate.
9. Evacuation valve closed (starting time of experiment).
10. Adsorption bulb opened and heat-flow $\phi = (dQ/dt)_T$ and quasi-equilibrium pressure p recorded.
11. Adsorbent bulb evacuated when final pressure reached.

The results can be presented in the form of a continuous curve of differential enthalpies of adsorption $\Delta_{ads}\dot{h}$ versus n^σ, as shown in Figure 3.16b, with a resolution which is much higher than that obtained by the discontinuous procedure (Figure 3.16a). If the adsorption calorimeter cannot be easily connected to a well-calibrated and well-temperature-controlled adsorption sonic nozzle set-up, or when the adsorption isotherm is difficult to determine (e.g. if very small amounts are adsorbed), there remains the possibility of determining, separately, the adsorption isotherm by any of the discontinuous or continuous procedures described in Sections 3.3.1 or 3.3.2. A simple procedure can be applied which does not require the gas flow rate calibration:

bulb when immersed in liquid nitrogen during Step 2 (with reproducible but unknown temperature gradients). V_{up} does not depend on the presence or absence of the sample. From V_f and V_{up} we therefore obtain the modified V_{lo}, which takes account of the presence of the adsorbent. Since V_{up} remains constant, only Step 3 is required for a new sample.

The gas to be used in the dead space determination must be carefully selected. In the procedure described, Step 1 can be carried out with any permanent gas (e.g. helium or nitrogen), whereas for Step 2 it is advisable to use a gas with the same virial coefficient B_m as the adsorptive, since B_m and the subsequent correction can vary considerably from one gas to another (see Section 3.4.8). Since the measured value of V_a depends on the virial coefficient B_m of the gas used, the simplest procedure is to use the adsorptive itself. Step 3 is also preferably carried out with a gas whose accessibility to the sample is comparable to that of the adsorptive: here again the adsorptive itself, at a temperature at which it is known not to adsorb, is the best.

As can be seen, helium, in contrast to what was once assumed, is not necessarily the best gas to select for the determination of dead space. It is sometimes thought that helium allows dead space to be determined directly at 77 K in the presence of the sample, since it will not adsorb. However, since its virial coefficient is much smaller than that of most adsorptives (see Table 3.2), and because of the possibility of adsorption in micropores (see Chapter 9), its use cannot be recommended. This problem has been discussed recently by Neimark and Ravikovitch (1997).

The indirect route for determining the dead space volume makes use of an estimated volume of the adsorbent sample. This volume can be obtained in two ways:

(a) From the theoretical density. This leads to a dead space which, by definition, contains all pores of any size (including closed pores and also any micropores inaccessible to the adsorptive).
(b) From pycnometric measurements (in a liquid or in a gas) carried out separately. In this case the nature and temperature of the fluid must always be stated.

Both have the advantage of giving a sample volume (and therefore a location of the dividing surface) which is, by definition, perfectly reproducible from one adsorption bulb to another and from one laboratory to another. Even if not always realistic, it is a sound convention, if the aim is to obtain reproducible measurements and calculations and is consistent with the spirit of the Gibbs representation. It is, for these reasons, certainly well suited for the study of reference materials. Of course, this approach would replace Step 3 in the procedure described above, whereas Steps 1 and 2 would remain necessary.

In the case of differential or twin arrangements of adsorption manometry (cf. Figures 3.4–3.6), the dead volume determination is not required, but the volume equalization and the symmetry of the set-up are essential. The volume equalization is usually obtained with glass beads on the reference side and sometimes also with adjustable bellows or a piston. The check or adjustment is normally carried out at ambient temperature: the introduction of an identical amount of gas on both sides must result in a zero pressure difference between them.

described just above, but it may allow the balance to be used over a smaller range, where a higher sensitivity is available.

A pertinent question is: as the volume of the adsorbed phase increases, do we have to take into account the corresponding increase of buoyancy? (e.g. the buoyancy doubles after saturation of an adsorbent with 50% porosity). The answer is no, provided we want to assess the surface excess mass m^{σ}. As illustrated in Figure 3.22, because of the buoyancy effect, we do not measure the total mass of the adsorbed layer (shaded + hatched areas) but simply a surface excess mass (hatched area only). Thus, adsorption gravimetry and the Gibbs representation are highly compatible (Findenegg, 1997).

Finally, it may be worth considering the effect of buoyancy correction on the magnitude of the error in the determination of the BET(N_2) surface area. This is indicated in Figure 3.23 for surface areas ranging from 1 to 1000 $m^2\,g^{-1}$ and adsorbent densities in the range 1 to 8. The buoyancy is calculated by taking into account the density of nitrogen vapour at a temperature of 77 K and a pressure of 100 mbar, which is assumed enough to complete the monolayer. For a sample of 1 $m^2\,g^{-1}$, with a density of 2 (for instance, a finely ground quartz), the error amounts to 80%! At the other extreme, for a sample of 1000 $m^2\,g^{-1}$, with a density of 1.5 (for instance, an active carbon), the error will be as small as 0.1%.

3.4.5. Adsorption equilibrium

By convention, 'adsorption isotherms' are generally assumed to correspond to a thermodynamic equilibrium: if this is not true, use of the term 'adsorption isotherm' is questionable. The confirmation of adsorption equilibrium is therefore of crucial significance.

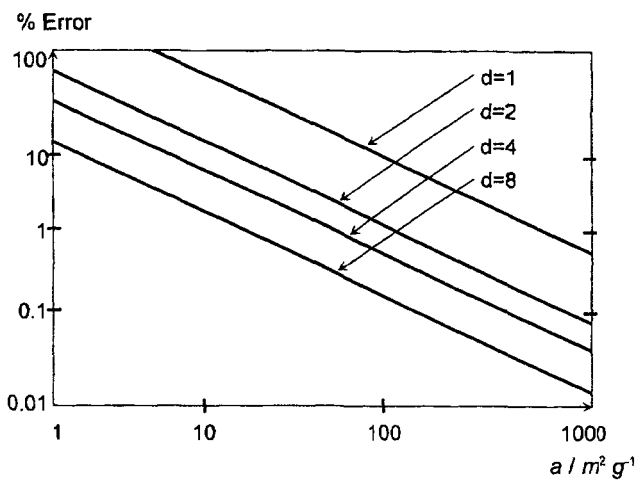

Figure 3.23. Gas adsorption gravimetry: percentage error in surface area as a result of neglecting totally the buoyancy effect on the adsorbent (assumptions: nitrogen BET, monolayer at 100 mbar, bulk density of adsorbent from 1 to 8).

Table 3.1. Thermal transpiration: coefficients of the Takaishi and Sensui equation, for various gases.

Gas	*A*	*B*	*C*	Temperature range (K)
Hydrogen	1.24	8.00	10.6	14–673
Neon	2.65	1.88	30.0	20.4–673
Argon	10.8	8.08	15.6	77–673
Krypton	14.5	15.0	13.7	77–673
Methane	14.5	15.0	13	473–673
Xenon	35	41.4	10	77–90
Helium	1.5	1.15	19	4.2–90
Nitrogen	12	10	14	77–195
Oxygen	8	17.5	–	90

3.4.8. Correction for non-ideality

At the temperatures normally used for physical adsorption, the correction for the non-ideality of real gases generally amounts to several percent. It can be reasonably taken into account by using the first two terms of the virial equation:

$$v^{\circ}_{\text{real}} = \frac{V}{n} = v^{\circ}_{\text{id}} + B_{\text{m}} \tag{3.7}$$

where v°_{real} and v°_{id} are the real and ideal molar volumes of the gas at a given temperature T and reference pressure (normally 1 bar), respectively, V is the total volume occupied by the given amount of gas, and B_{m} is the second molar virial coefficient, which is usually negative under the conditions of physisorption experiments. Its value for a large number of gases can be found in a critical compilation by Dymond and Smith (1969) and in the thermodynamic tables published by Marsh (1985).

To determine the real amount of gas present in a given volume V, at temperature T and pressure p, it is convenient to use the relation:

$$n = \frac{V}{T} \times \frac{273.15}{22711}\left(1 + \frac{\alpha p}{100}\right) \tag{3.8}$$

where V is expressed in cm^3 and p in bar and where $\alpha = -100B_{\text{m}}/v^{\circ}_{\text{id}} = -(10B_{\text{m}}/RT) \times p^{\circ}$.

Values of α for a number of gases and temperatures used in adsorption studies are given in Table 3.2. They were calculated with help of the data provided by Dymond and Smith (1969). A detailed study of the incidence of these corrections on the adsorption isotherms and the BET surface areas was made by Jelinek *et al.* (1990).

An elegant way to avoid this non-ideality correction, especially when operating at high pressures (up to 16.5 MPa), where it can become predominant, was proposed by Bose *et al.* (1987). In their method, for each equilibrium point the density of the adsorptive is determined experimentally from its dielectric constant, which is measured in a gas capacitance cell at the same temperature and pressure as the adsorption system studied. The rest of their adsorption procedure is comparable to the

Table 3.2. Correction for non-ideality for a few gases commonly used in adsorption experiments.

Gas	Formula	T (K)	α = % correction
Nitrogen	N_2	77.3	4.0
		90.0	3.1
Argon	Ar	77.3	4.8
		90.0	3.6
Oxygen	O_2	77.3	5.1
		90.0	3.8
Helium	He	77.3	0.2
Carbon monoxide	CO	77.3	1.3
Ammonia	NH_3	273.15	1.5
		298.15	1.2
Neopentane	$(CH_3)_4C$	273.15	4.4
		298.15	3.9
n-Butane	C_4H_{10}	273.15	4.1
		298.15	3.2

discontinuous manometric procedure (see Section 3.3.1), the dosing volume being made up of the gas capacitance cell at the temperature of the adsorbent.

3.4.9. Presentation and use of the experimental data

The raw experimental data (temperatures, pressures, flow-rates, equilibration times, sample treatment) should be stored, together with all calibration data of the set-up. It is highly desirable to plot the adsorption isotherm as soon as possible and preferably during the experiment itself.

The commercial software generally includes a smoothing procedure in the first processing stage of the experimental data. This certainly improves the appearance of the data and may be useful for routine measurements, but the smoothing tends to hide systematically small events (including small phase changes) which may be highly informative about the mechanism of adsorption. It is therefore preferable to store the data in their raw form, before any smoothing has been applied, so that the experimental results are available for subsequent analysis.

References

Ajot H., Joly J.F., Raatz F. and Russmann C. (1991) In: *Studies in Surface Science and Catalysis*, vol. 62, Elsevier, Amsterdam, p. 161.
Atkins J.H. (1964) *Anal. Chem.* **36**, 579.
Beebe R.A., Low G.W. and Goldwasser S. (1936) *J. Am. Chem. Soc.* **58**, 2196.
Bose T.K., Chahine R., Marchildon L. and St Arnaud J.M. (1988) *Rev. Sci. Instrum.* **58**(12), 2279.
Bunsen R.W. (1870) *Ann. Phys.* **141**, 1.
Calvet E. and Prat H. (1958) *Récents Progrès en Microcalorimétrie*, Dunod, Paris.
Calvet E. and Prat H. (1963) *Recent Progress in Microcalorimetry*, Pergamon Press, Oxford.
Camp R.W. and Stanley H.D. (1991) *American Laboratory* September, p. 34.
Dash J.G. (1975) *Films on Solid Surfaces*, Academic Press, New York.

Here the pre-exponential factor, K, is equal to the ratio of the adsorption and desorption coefficients, α/β. Alternatively, b may be regarded as a function of the enthalpy and entropy of adsorption (Everett, 1950; Barrer, 1978, p. 117).

In his early treatment, Langmuir assumed that the energy of adsorption for the first layer is generally considerably larger than for the second and higher layers, and therefore multilayer formation is possible only at much greater pressures than the pressure required for monolayer completion. Thus, the formation of second or higher layers would be indicated by the appearance of a discontinuous isotherm. In fact, this situation does arise in the case of a stepwise, Type VI, isotherm. However, the lateral adsorbate–adsorbate interactions, which are associated with all known stepwise isotherms, are not compatible with the Langmuir model.

It is evident that Equation (4.11) is of a very general mathematical form (i.e. a hyperbolic function). At low θ it reduces to Henry's law; at high surface coverage, a plateau is reached as $\theta \rightarrow 1$. Other equations of the same mathematical form as Equation (4.11) have been derived from a classical thermodynamic standpoint (Brunauer, 1945) and by application of the principles of statistical mechanics (Fowler, 1935).

Equation (4.11) is usually applied in the linear form

$$p/n = 1/n_m b + p/n_m \tag{4.13}$$

where n is the specific amount of gas adsorbed at the equilibrium pressure p and n_m is the monolayer capacity (as before, $\theta = n/n_m$).

Many systems give linear plots of p/n against p over a limited ranges of pressure, but such linearity does not by itself imply conformity with the Langmuir model. As already indicated, a second condition is that the energy of adsorption should be independent of surface coverage. Thirdly, the differential entropy of adsorption should vary in accordance with the ideal localized model (Everett, 1950). That no real system has been found to satisfy all these requirements is not surprising in view of the complexities noted here and in subsequent chapters.

Various attempts have been made to modify the Langmuir model. One of the best known is that of Fowler and Guggenheim (1939), which allowed for adsorbate–adsorbate interactions in a localized monolayer on a uniform surface. However, on an empirical basis the Fowler–Guggenheim equation turns out to be no more successful than the original Langmuir isotherm. The highly complex problem of localized adsorption on heterogeneous surfaces has been discussed by Rudzinski and Everett (1992).

4.2.4. The Brunauer–Emmett–Teller (BET) theory

By introducing a number of simplifying assumptions, Brunauer, Emmett and Teller (1938) were able to extend the Langmuir mechanism to multilayer adsorption and obtain an isotherm equation (the BET equation), which has Type II character. The original BET treatment involved an extension of the Langmuir kinetic theory of monomolecular adsorption to the formation of an infinite number of adsorbed layers.

According to the BET model, the adsorbed molecules in one layer can act as

changed and the point of inflection is lost. The BET equation then gives a Type III isotherm. In practice, the range of validity of Equation (4.32) is always confined to a limited part of the isotherm.

If the adsorption at saturation is restricted to a finite number of layers, N, the BET treatment leads to a modified equation which includes this additional parameter (cf. Chapter 6). Naturally, in the special case when $N = 1$, the extended BET equation corresponds to the Langmuir equation.

The BET model appears to be unrealistic in a number of respects. For example, in addition to the Langmuir concept of an ideal localized monolayer adsorption, it is assumed that all the adsorption sites for multilayer adsorption are energetically identical and that all layers after the first have liquid-like properties. It is now generally recognized that the significance of the parameter C is oversimplified and that Equation (4.33) cannot provide a reliable evaluation of E_1.

A recent molecular simulation study (Seri-Levy and Avnir, 1993) has also revealed the artificial nature of the BET model and has illustrated the effect of taking adsorbate–adsorbate interactions into account. Thus, the addition of lateral interactions appears to flatten the BET stacks into more realistically shaped islands.

In spite of the inadequacy of the underlying theory, the BET equation remains the most used of all adsorption isotherm equations. The reasons for this situation and the advantages and limitations of the BET method are discussed in Chapter 6.

4.2.5. Multilayer equations

An extension to the BET model was put forward by Brunauer, Deming, Deming and Teller (BDDT) in 1940. The BDDT equation contains four adjustable parameters and was designed to fit the isotherm Types I–V. From a theoretical standpoint, the BDDT treatment appears to offer very little more than the original BET theory and the cumbersome equation has very rarely been applied to experimental data.

Several other attempts have been made to modify the BET equation in order to improve the agreement with isotherm data in the multilayer region. Brunauer *et al.* (1969) pointed out that the BET assumption of an infinite number of molecular layers at saturation pressure is not always justified. By replacing p by kp, where k is an additional parameter with a value less than unity, they arrived at the following equation, which has the same form as that originally proposed by Anderson (1946):

$$\frac{kp}{n(p^\circ - kp)} = \frac{1}{n_m C} + \frac{(C-1)}{n_m C} \times \frac{kp}{p^\circ} \tag{4.34}$$

On an empirical basis, this Anderson–Brunauer equation can be applied to some isotherms (e.g. nitrogen and argon at 77 K on various non-porous oxides) over a much wider range of p/p° than the original BET equation.

When the adsorbate reaches a thickness of several molecular layers, the effects of surface heterogeneity are considerably reduced. If the temperature is not too low, some – but not all – multilayers appear to undergo a continuous increase in thickness as the pressure approaches saturation and bulk behaviour is gradually developed (Venables *et al.*, 1984). With such systems, it seems reasonable to assume that the

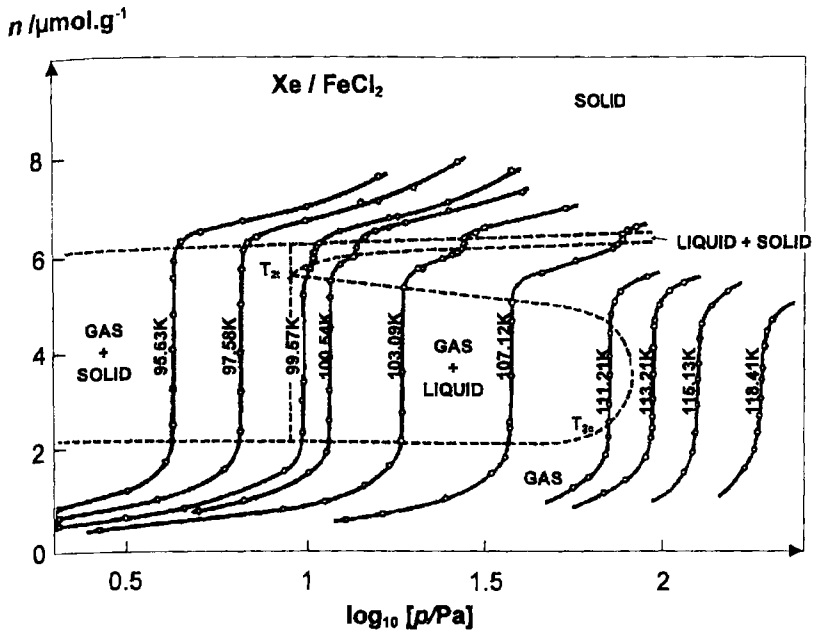

Figure 4.2. Adsorption isotherms of xenon on $FeCl_2$ (courtesy of Larher, 1992).

was displayed up to four molecular layers, as can be seen in Figure 4.1. Each vertical 'riser' (at constant p/p°) can be regarded as a phase transition between one adsorbed layer and the next higher layer.

In the sub-monolayer range, three distinctive regions were identified and attributed by Thomy and Duval to 2-D 'gas', 'liquid' and 'solid' phases. These measurements provided the first unambiguous evidence for the existence of sub-steps in the monolayer region of a stepwise, Type VI, isotherm.

To illustrate the interpretation of such sub-steps, the monolayer isotherms for the adsorption of Xe on $FeCl_2$ (Larher, 1992) are shown in Figure 4.2. At temperatures below 99.57 K, there is a single vertical step, which corresponds to the transformation of 2-D gas to the solid phase. Very little further compression of the monolayer is possible before its completion at Point B. A smaller sub-step becomes apparent at temperatures above 99.57 K. As a result of the careful studies of Thomy and Duval and Larher, the consensus interpretation is that this small sub-step represents a first-order transition between the 2-D liquid and solid phases. It is evident that, in the case of the $Xe/FeCl_2$ system, 99.57 K is the two-dimensional triple point.

Two-dimensional phase diagrams are often displayed in the form of ln [p] against $1/T$ (at a constant specific amount adsorbed), which provides a convenient way of indicating the conditions for the coexistence of two phases (see Figure 4.3). Indeed, the application of the Phase Rule indicates that when two adsorbed phases coexist in equilibrium, the system has one degree of freedom: therefore, at constant

Langmuir equation contains the two disposable constants, n_m and b, which cannot be evaluated by any independent method.

It is now generally accepted that there is no sound reason why isotherms on microporous solids should conform any more closely to the classical Langmuir mechanism than isotherms on non-porous or mesoporous adsorbents. Indeed, a considerable amount of the evidence now available gives strong support to the view that the limiting uptake is controlled rather by the accessible micropore volume than by the internal surface area (Gregg and Sing, 1982).

In the context of gas separation (see Yang, 1987) or for some other purposes, it may be expedient to apply an equation of the Langmuir form; but we consider it advisable to treat this as empirical relation. Thus, we may write

$$\frac{n}{n_L} = \frac{bp}{1+bp} \tag{4.38}$$

where the parameters n_L and b are to be regarded as empirical constants within stated ranges of p and T.

We have concluded that the limiting uptake at the plateau of a Type I isotherm is not directly related to the surface area. However, it is now appropriate to return briefly to the initial stage of physisorption by microporous solids and consider the question: does monolayer adsorption ever precede micropore filling ?

Some time ago Brunauer (1970) argued that monolayer adsorption of nitrogen and other small molecules does occur on the walls of micropores wider than about 0.7 nm. Although as we have seen, Brunauer's original theory is now questionable, some recent evidence does support his view that monolayer adsorption can take place on the walls of the wider micropores before secondary micropore filling occurs. These aspects are discussed in later chapters.

4.4.4. The Dubinin–Stoeckli theory

Dubinin was the pioneer of the concept of micropore filling. His approach was based on the early potential theory of Polanyi, in which the physisorption isotherm data were expressed in the form of a temperature-invariant 'characteristic curve'.

In 1947 Dubinin and Radushkevich put forward an equation for the characteristic curve in terms of the fractional filling, W/W_0, of the micropore volume, W_0. This relation is usually expressed in the form

$$W/W_0 = \exp\left[-(A/E)^2\right] \tag{4.39}$$

where A, the Polanyi 'adsorption potential', is an adsorption affinity,

$$A = -RT \ln (p/p^\circ) \tag{4.40}$$

and E is a characteristic energy for the given system.

The isotherm equation is obtained by combining Equations (4.39) and (4.40). With the introduction of a scaling factor, β, it becomes

$$W/W_0 = \exp\{-[RT \ln (p^\circ/p)]^2/(\beta E_0)^2\} \tag{4.41}$$

where E_0 is a 'characteristic energy'.

Equation (4.47) and obtain an isotherm equation in which the distribution function, f(B) was expressed in an analytical form (Huber *et al.*, 1978; Bansal *et al.*, 1988). In principle, f(B) provides an elegant basis for relating the micropore size distribution to the adsorption data. However, it must be kept in mind that the validity of the approach rests on the assumption that the DR equation is applicable to each pore group and that there are no other complicating factors such as differences in *surface* heterogeneity.

4.4.5. Empirical isotherm equations

Many different equations have been applied to physisorption isotherms on microporous adsorbents. The first and best known empirical equation was proposed by Freundlich (1926) in the form

$$n = kp^{1/m} \tag{4.49}$$

where k and m are constants ($m > 1$).

According to Equation (4.49), the plot of ln [n] against ln [p] should be linear. In general, activated carbons give isotherms which obey the Freundlich equation in the middle range of pressure (Brunauer, 1945), but the agreement is usually poor at high pressures and low temperatures. These limitations are partly due to the fact that the Freundlich isotherm does not give a limiting value of n as $p \rightarrow \infty$.

It is possible to achieve an improved fit at higher pressures by a combination of the Freundlich and Langmuir equations (Sips, 1948),

$$n/n_L = (kp)^{1/m}/[1 + (kp)^{1/m}] \tag{4.50}$$

where n_L is the limiting adsorption capacity. Equation (4.50) has been applied as a 'generalized Freundlich' isotherm to multisite occupancy by long-chain hydrocarbons (Rudzinski and Everett, 1992, p. 491). However, as in the case of the Freundlich isotherm itself, the Sips equation does not reduce to Henry's law as $p \rightarrow 0$.

Another empirical variant is Toth equation,

$$n/n_L = p/(b + p^m)^{1/m} \tag{4.51}$$

which also contains three adjustable parameters (n_L, b and m), but has the advantage that it appears to give the correct limits for both $p \rightarrow 0$ and $p \rightarrow \infty$. Thus, although it was originally proposed for monolayer adsorption (Toth, 1962), the Toth equation actually gives a more extensive range of fit when applied to Type I isotherms (Rudzinski and Everett, 1992).

In spite of the availability of modern computer-aided techniques for curve fitting, these and other relatively simple, empirical equations are still found to be useful for the analysis of chemical engineering data (e.g. in the context of pressure swing adsorption or other separation processes).

There is a growing interest in the presentation of physisorption isotherms in a generalized integral form. This approach was first applied to physisorption in the submonolayer region (Adamson *et al.*, 1961), but much of the current interest is centred on the analysis of micropore filling isotherms. An apparent advantage is that it provides a means of constructing a series of model isotherms by systematically

purpose, empirical methods of isotherm analysis are extremely useful. These procedures are introduced in Chapters 6, 7 and 8.

The pragmatic approach adopted in the following chapters involves the identification and characterization of the various mechanisms of adsorption and pore filling. By making use of standard data on well-defined adsorbents and proceeding step-by-step, we endeavour to extract the maximum amount of useful information without having to rely completely on any of the oversimplified models discussed in this chapter.

References

Adamson A.W., Ling I. and Datta S.K. (1961) *Adv. Chem. Series* **33**, 62.

Anderson R.B. (1946) *J. Am. Chem. Soc.* **68**, 686.

Avgul N.N. and Kiselev A.V. (1970) In: *Chemistry and Physics of Carbon*, vol. 6 (P.L. Walker, ed.), Marcel Dekker, New York, p.1

Avgul N.N., Bezus A.G., Dobrova E.S. and Kiselev A.V. (1973) *J. Colloid Interface. Sci.* **42**, 486.

Bansal R.C., Donnet J.B. and Stoeckli H.F. (1988) *Active Carbon*, Marcel Dekker, New York.

Barrer (1978) *Zeolites and Clay Minerals as Sorbents and Molecular Sieves*, Academic Press, London, p. 117.

Block J.H., Bradshaw A.M., Gravelle P.C., Haber J , Hansen R.S., Roberts M.W., Sheppard N. and Tamaru K. (1990) *Pure Appl. Chem.* **62**, 2297.

Bonnetain L., Duval X. and Letort M. (1952) *C.R. Acad. Sci. Fr.* **234**, 1363.

Broekhoff J.C.P. and van Dongen R.H. (1970) In: *Physical and Chemical Aspects of Adsorbents and Catalysts* (ed. B.G. Linsen), Academic Press; London, p. 63.

Brunauer S. (1945) *The Adsorption of Gases and Vapours*, Princeton University Press, Princeton.

Brunauer S. (1970) In: *Surface Area Determination* (D.H. Everett and R.H. Ottewill, eds.) Butterworths, London, p. 63.

Brunauer S., Emmett P.H. and Teller E. (1938) *J. Am. Chem. Soc.* **60**, 309.

Brunauer S., Deming L.S., Deming W.L. and Teller E. (1940) *J. Am. Chem. Soc.* **62**, 1723.

Brunauer S., Skalny J. and Bodor E.E. (1969) *J. Colloid Interface Sci.* **30**, 546.

Carrott P.J.M. and Sing K.S.W. (1989) *Pure Appl Chem.* **61**(11) 1835.

Carrott P.J.M., McLeod A.J. and Sing K.S.W. (1982) In: *Adsorption at the Gas–Solid and Liquid–Solid Interface* (J. Rouquerol and K.S.W. Sing, eds.) Amsterdam, p. 403.

Carrott P.J.M., Roberts R.A. and Sing K.S.W. (1987) *Carbon* **25**(6), 769.

Cole J.H., Everett D.H., Marshall C.T., Paniego A.R., Powl J.C. and Rodriguez-Reinoso F. (1974) *J. Chem. Soc., Faraday Trans. I* **70**, 2154.

Coulomb J.P., Sullivan T.J. and Vilches (1984) *Phys. Rev. B* **30**(8), 4753.

Dash J.G. (1975) *Films on Solid Surfaces*, Academic Press, New York.

de Boer J.H. (1968) *The Dynamical Character of Adsorption*, Oxford University Press, London, p. 179.

Dubinin M.M. (1966) In: *Chemistry and Physics of Carbon* (P.L. Walker, ed.), Marcel Dekker, New York, p. 51

Dubinin M.M (1975) In: *Progress in Surface and Membrane Science*, vol. 9 (D.A. Cadenhead ed.), Academic Press, New York, p. 1.

Dubinin M.M. and Astakhov V.A. (1970) *Adv. Chem. Series* **102**, 69.

Dubinin M.M. and Radushkevich L.V. (1947) *Proc. Acad. Sci.* USSR, **55**, 331.

Everett D.H. (1950) *Trans Faraday Soc.* **46**, 453, 942, 957.

Everett D.H. (1970) In: *Surface Area Determination* (D.H. Everett and R.H. Ottewill, eds.), Butterworth, London, p. 181.

Everett D.H. (1972) *Pure Appl. Chem.* **31**, 579.

Everett D.H. and Powl J.C. (1976) *J. Chem. Soc., Faraday Trans. I* **72**(3), 619.

Fowler R.H. (1935) *Proc. Cambridge Phil. Soc.* **31**, 260.

Fowler R H and Guggenheim E A (1939) *Statistical Thermodynamics* Cambridge University Press, London, p 429
Freundlich H (1926) *Colloid and Capillary Chemistry*, Methuen, London, p 120
Gregg S J (1961) *The Surface Chemistry of Solids*, Chapman & Hall, London
Gregg S J and Sing K S W (1982) *Adsorption, Surface Area and Porosity*, Academic Press, London
Halsey G D (1948) *J Chem Phys* **16**, 93
Hill T L (1946) *J Am Chem Soc* **68**, 535
Hill T L (1952) *Adv Catalysis* **4**, 211
Huber U, Stoeckli H F and Hourlet J P (1978) *J Colloid Interface Sci* **67**(2), 195
Jaroniec M, Kruk M and Choma J (1997) In *Characterization of Porous Solids IV* (B McEnaney, T J Mays, J Rouquerol, F Rodriguez-Reinoso, K S W Sing and K K Unger, eds) Royal Society of Chemistry, London, p 163
Lamb A B and Coolidge A S (1920) *J Am Chem Soc* **42**, 1146
Langmuir I (1916) *J Am Chem Soc* **38**, 2221
Langmuir I (1918) *J Am Chem Soc* **40**, 1361
Larher Y (1992) *Surface properties of layered structures* (G Benedek, ed), Kluwer Dordrecht, p 261
McEnaney B (1988) *Carbon* **26**, 267
Pierotti R A and Thomas H E (1971) In *Surface and Colloid Science* (E Matijevic, ed) Wiley-Interscience, New York, p 93
Price G L and Venables J A (1976) *Surface Sci* **59**(2), 509
Reichert H Muller U, Unger K K, Grillet Y, Rouquerol F, Rouquerol J and Coulomb J P (1991) In *Characterization of Porous Solids II* (F Rodriguez-Reinoso, J Rouquerol, K S W Sing and K K Unger, eds), Elsevier, Amsterdam, p 535
Ross S and Clark H (1954) *J Am Chem Soc* **76**, 4291
Ross S and Olivier J P (1964) *On physical adsorption*, Wiley-Interscience, New York
Rudzinski W and Everett D H (1992) *Adsorption of Gases on Heterogeneous Surfaces*, Academic Press, London
Ruthven D M (1984) *Principles of Adsorption and Adsorption Processes*, Wiley-Interscience, New York
Sahouli, B, Blacher, S and Brouers, F (1997) *Langmuir* **13**, 4391
Seri-Levy, A and Avnir, D (1993) *Langmuir* **9**, 2523
Sing K S W (1973) In *Colloid Science I*, The Chemical Society, London, p 30
Sing K S W (1979) In *Characterization of Porous Solids* (S J Gregg, K S W Sing and H F Stoeckli, eds), Society of Chemical Industry, London, p 98
Sing K S W, Everett D H, Haul R A W, Moscou L, Pierotti R A, Rouquerol J and Siemieniewska T. (1985) *Pure Appl Chem* **57**, 603
Sips R (1948) *J Chem Phys* **16**, 490
Steele W A (1974) *The Interaction of Gases with Solid Surfaces*, Pergamon, New York, p 131
Steele W A (1996) *Langmuir* **12**, 145
Stoeckli H F (1977), *J Colloid Interface Sci* **59**, 184
Stoeckli H.F (1993) *Adsorption Sci Tech* **10**, 3
Stoeckli H F, Hourlet J P, Perret A and Huber U (1979) In *Characterization of Porous Solids* (S J Gregg, K S W Sing and H F Stoeckli, eds), Society of Chemical Industry, London, p 31
Stoeckli, F, Hugi-Cleary, D and Centeno, T A (1998), *J Eur Ceramic Soc* in press
Suzanne J and Gay J M (1996) In *Handbook of Surface Science*, vol 1, Physical Structure (W N Unertl, vol ed, N V Richardson and S Holloway, series eds), North-Holland Elsevier, Amsterdam, p 503
Terlain A and Larher Y (1983) *Surface Sci* **125**, 304
Thomy A and Duval X (1970) *J Chim Phys Fr* **67**, 1101
Thomy A, Regnier J and Duval X (1972) In *Thermochimie* Colloques Internationaux du CNRS no 201, Editions du CNRS, Paris, p 511
Toth J (1962) *Acta Chim Acad Sci Hung* **35**, 416
Venables J A, Seguin J L, Suzanne I and Bienfait M (1984) *Surface Sci* **145**, 345
Yang R T (1987) *Gas Separation by Adsorption Processes* Butterworths, London
Young D M and Crowell A D (1962) *Physical Adsorption of Gases*, Butterworths London, p 124

5.1. Introduction

Adsorption at the liquid–solid interface is of great importance in industry and everyday life (e.g. in detergency, adhesion, lubrication, flotation of minerals, water treatment, oil recovery, and in pigment and particle technology). Adsorption from solution measurements have been used for many years for the determination of the surface area of certain industrial materials. Immersion microcalorimetry has also been applied for the characterization of such materials as clays and activated carbons. The application of the energetics of immersion is based on the observation by Pouillet in 1822 that the immersion of an insoluble solid in a liquid is a measurable exothermic phenomenon. To gain an understanding of liquid–solid adsorption phenomena, it is not enough to know the surface area and porosity of the adsorbent. In addition, it is necessary to know how the solid behaves in the liquid medium.

The comparison with adsorption at the gas–solid interface is further complicated by the fact that some adsorbents cannot be outgassed without an irreversible change in their texture. Also, changes in texture may occur when the adsorbent is immersed in a pure liquid or a solution. For these reasons, it is necessary to utilize special methods which provide direct information on the particular liquid–solid interactions.

In this chapter, our aim is to give an introductory account of the methodology and underlying thermodynamic principles of adsorption at the liquid–solid interface. We are mainly, but not exclusively, concerned with the characterization of the liquid–solid interface. In this context, there are two relevant topics:

(a) the energetics of immersion of solids in liquids;
(b) isothermal adsorption from solutions.

Many attempts have been made to employ immersion calorimetry and solution adsorption measurements for the determination of the surface area of porous and non-porous materials (see Gregg and Sing, 1967), but in our view insufficient attention has

at the solid–liquid film interface and

$$U^{\sigma}(\mathrm{LG}) = Au^{\mathrm{i}}(\mathrm{LG}) \tag{5.11}$$

at the liquid film–vapour interface.

The maximum energy of immersion, which we designate $\Delta_{\mathrm{imm}}U^{\circ}$, is liberated when the vacuum–solid interface is replaced by the liquid–solid interface. Thus, for the immersion of an outgassed adsorbent of surface area A, we obtain:

$$\Delta_{\mathrm{imm}}U^{\circ} = A[u^{\mathrm{i}}(\mathrm{SL}) - u^{\mathrm{i}}(\mathrm{S0})] \tag{5.12}$$

where $u^{\mathrm{i}}(\mathrm{SL})$ and $u^{\mathrm{i}}(\mathrm{S0})$ are the areal surface excess energies corresponding to $U^{\sigma}(\mathrm{SL})$ and $U^{\sigma}(\mathrm{S0})$ in Figure 5.1. (Note that since the process is exothermic, the $\Delta_{\mathrm{imm}}U$ values are all negative.)

When area A is already covered with a physisorbed layer at surface excess concentration Γ (i.e. n^{σ}/A), the energy of immersion becomes

$$\Delta_{\mathrm{imm}}U^{\Gamma} = \mathrm{A}[u^{\mathrm{i}}(\mathrm{SL}) - u^{\mathrm{i}}(\mathrm{SG})] \tag{5.13}$$

Finally, when the adsorbed layer is thick enough to behave as a liquid film, the energy of immersion, $\Delta_{\mathrm{imm}}U^{\mathrm{l}}$, which corresponds to the disappearance of the liquid–gas interface, is simply:

$$\Delta_{\mathrm{imm}}U^{\mathrm{l}} = -Au^{\mathrm{i}}(\mathrm{LG}) \tag{5.14}$$

The above equations are all based on the internal energy. Similar equations can be written with the enthalpy since the surface excess enthalpy and energy are identical in the Gibbs representation when $V^{\sigma} = 0$ (Harkins and Boyd, 1942). Therefore the various energies of immersion defined by Equations (5.6)–(5.8) are all virtually equal to the corresponding enthalpies of immersion, i.e. ($\Delta_{\mathrm{imm}}H^{\circ}$, $\Delta_{\mathrm{imm}}H^{\Gamma}$ and $\Delta_{\mathrm{imm}}H^{\mathrm{l}}$), thus:

$$\Delta_{\mathrm{imm}}H^{\circ} = \Delta_{\mathrm{imm}}U^{\circ} \tag{5.15}$$

The latter definition of the enthalpy of immersion is that given by Everett (1972, 1986).

Nevertheless, in this chapter we shall refer to the energy of immersion which is unambiguous and consistent with our thermodynamic treatment.

In fact, 'energy of immersion' was the term originally used by Harkins in his early papers (Harkins and Dahlstrom, 1930), before resorting to the usual laboratory term of 'heat of immersion'. Although the latter term is still used by a few authors, it is to be discouraged since 'heat' is not a precise term and is not directly related to any thermodynamic state of the system: as will be stressed in Section 5.2.2 describing experimental techniques, in practice, the microcalorimetric measurement of the heat exchanged is never equal to the required energy of immersion.

Relation between the energies of immersion and gas adsorption

The process of the immersion of a clean solid surface (which gives rise to $\Delta_{\mathrm{imm}}U^{\circ}$)

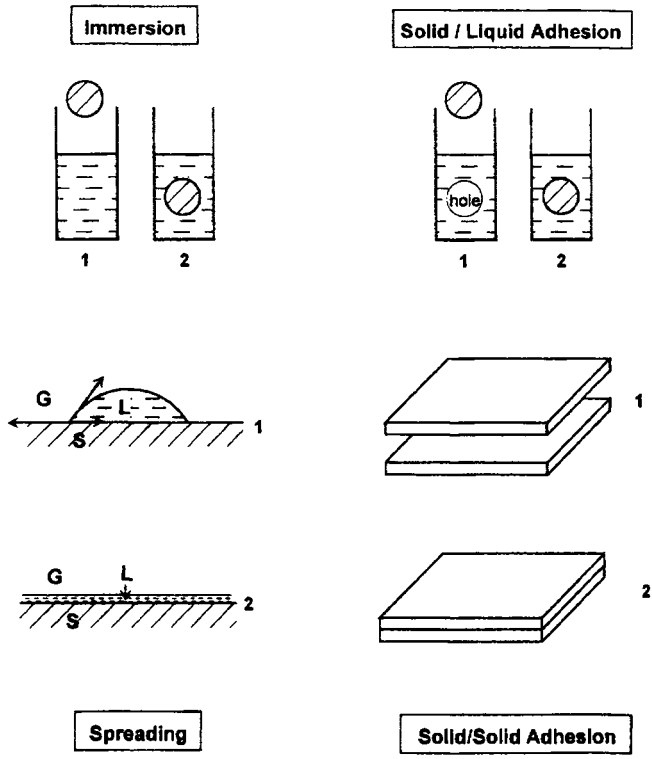

Figure 5.4. Interfaces lost or formed during immersional, adhesional and spreading wetting and during solid–solid adhesion.

At this stage, it may be noted (Jaycock and Parfitt, 1981) that the above types of wetting do not all have the same contact angle requirement ($\theta < 90°$) for spontaneous occurrence. Thus:

(a) adhesional wetting requires $\theta < 180°$, which is of course the most general case;
(b) immersional wetting requires $\theta < 90°$ (otherwise external work must be applied);
(c) spreading and condensational wetting require $\theta = 0$.

Wettability of a solid surface: definition and assessment

The concept of wettability of a solid by a liquid is directly related to the wetting processes. This concept is specially useful in the fields of detergency, lubrication or enhanced oil recovery. In the context of the oil industry, proposals were made by Briant and Cuiec (1972) for the experimental assessment of wettability, which was defined in terms of the thermodynamic affinity of a solid surface for a liquid.

According to this approach wettability is equated to the work exchanged by the immersion system with its surroundings when the process of immersional wetting of

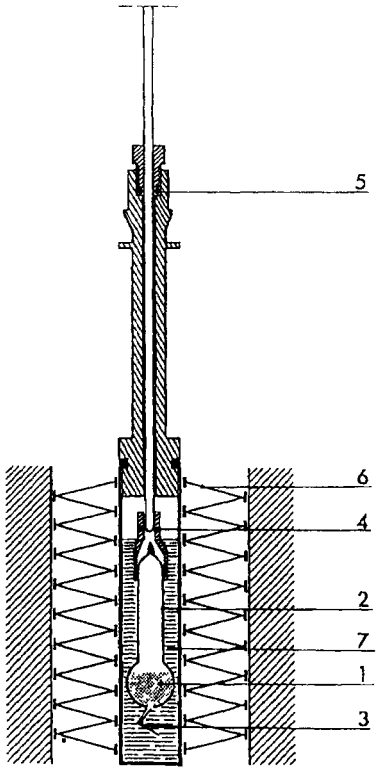

Figure 5.5. Set-up for immersion microcalorimetry (see text for details).

9. Allowance of time for temperature equilibration in the microcalorimeter may require 3 hours for high sensitivity).
10. Breaking of capillary tip by slowly and gently depressing glass rod microcalorimetric signal starts to respond.
11. Recording of microcalorimetric signal until it returns to baseline (this us requires *c.* 30 min).
12. Careful removal of sample bulb and broken tip from microcalorimetric cell
13. Determination of weight of sample bulb filled with immersion liquid (wiped outside), together with broken tip.
14. Determination of dead volume V of sample bulb from the information gain Steps 5 and 13, knowing mass and density of immersion liquid.
15. Determination of total experimental heat of immersion by integration o whole microcalorimetric signal (including the small endothermal peak d vaporization of the first droplet of immersion liquid into dead volume, before immersion proper (Partyka *et al.*, 1979).
16. Calculation of correction terms and, finally, of the energy of immersion.

5.3.1. Quantitative expression of the amounts adsorbed from a binary solution

Scope and limitations of the normal surface excess amounts

As for adsorption from the gas phase, one must be able to express unambiguously and quantitatively the observed adsorption phenomenon without reference to any prior knowledge concerning the structure of the adsorbed layer. For this reason, the concept of the Gibbs dividing surface (GDS) and the associated surface excess amounts are just as useful as for gas adsorption. Figure 5.10 represents the concentration of species 1 and 2 and also the total concentration c (expressed as the amount per unit volume of solution) as one moves away from the adsorbing surface. Figure 5.10a represents a hypothetical adsorption system where the molar volumes of species 1 and 2 are equal, so that any enrichment of the adsorption layer in component 2 (i.e. positive adsorption) is necessarily accompanied by an equal loss of component 1 (i.e. negative adsorption).

Figure 5.10b represents another adsorption system, in which the molar volumes of species 1 and 2 are different, so that adsorption also affects the total concentration c in the solution. Although these are representative of real systems, it must be stressed that in most cases these concentration profiles are unknown.

Finally, Figure 5.10c gives a Gibbs representation of the simple case where the GDS coincides with the real adsorbing surface. By convention, the concentrations in the solution are taken as constant up to the GDS. The hatched areas represent the amounts apparently lost (for component 2) or gained (for component 1) by the solution when the adsorption changes the concentrations from c_1° and c_2° to c_1 and c_2. These are the amounts counted as the 'surface excess amounts' on the GDS, one being positive (for component 2) and the other negative (for component 1). Now, one advantage of the GDS is that it can be located arbitrarily, allowing a change at will of the volume $V^{l,\sigma}$ of the liquid. Thus the calculation of the surface excess amount n_i^σ

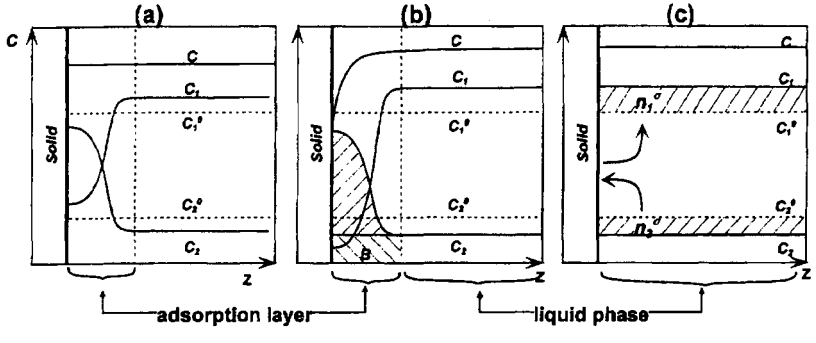

Figure 5.10. Concentrations in a liquid–solid adsorption system (competitive adsorption from binary mixture or solution).
(a) Real state after preferential adsorption of 2 (molecular volumes and cross-sectional areas of 1 and 2 supposed equal).
(b) Same as (a), but with different molecular volumes and/or cross-sectional areas for 1 and 2.
(c) Gibbs representation of system (b) for the case where GDS coincides with real adsorbing surface.

location of the GDS on the surface excess amounts of components 1 and 2. Here GDS 'L' provides the special condition for $n_1^\sigma = 0$.

Turning to Equation (5.55), we now require a GDS where n^σ (the whole surface excess amount $n_1^\sigma + n_2^\sigma$) equals zero. In Figure 5.12, this is the case for GDS 'D', where $n_2^\sigma = -n_1^\sigma$.

From Equation (5.55) we now obtain:

$$n_2^{\sigma(n)} = n_2^\sigma = -n_1^\sigma = -n_1^{\sigma(n)} \tag{5.59}$$

which shows that the reduced surface excess amounts of 1 and 2 are equal and opposite in sign. It turns out that this remains true whatever the position of the GDS. As underlined by Defay and Prigogine (1951, p. 26), this representation in terms of the reduced surface excess 'treats the components on an equal footing'. A practical consequence is that the same curve (either U or S as illustrated in Figure 5.13) provides the adsorption isotherm for both components. We also note that it is only when the partial molar volumes of 1 and 2, together with their molecular cross-sectional areas, are equal, that for $n_1^\sigma + n_2^\sigma = 0$ the GDS coincides with the real adsorbing surface.

By combining Equations (5.51), (5.54) and (5.55), we obtain the relationship between the relative and reduced surface excess quantities:

$$n_2^{\sigma(1)} = n_2^{\sigma(n)}/x_1^1 \tag{5.60}$$

and:

$$\Gamma_2^{(1)} = \Gamma_2^{(n)}/x_1^1 \tag{5.61}$$

and also:

$$m_2^{\sigma(1)} = m_2^{\sigma(m)}/w_1^1 \tag{5.62}$$

Adsorption isotherms expressed in reduced surface excess amounts

The reduced surface excess amounts, whose use is recommended by the IUPAC (Everett, 1986), offer much more than a form of precise mathematical accounting of the adsorption experiment: they also offer the most convenient way of reporting the experimental results. For decades this presentation was intuitively chosen as a way of plotting adsorption data, without any reference to the Gibbs formalism. The quantity plotted to represent adsorption of component 2 was often in the form of either $n^\circ \Delta x_2^1$, which is consistent with Equation (5.54), or $[m_2 - m^\circ w_2^1]$, which is consistent with Equation (5.57). The isotherm obtained is generally termed a 'composite isotherm' or an 'isotherm of apparent adsorption', or less often an 'isotherm of concentration change'. The term 'composite' refers to the fact that this single isotherm contains information about the adsorption of both components 1 and 2. This is shown in Figure 5.13, which gives the two most important shapes of reduced surface excess (or 'composite') isotherms (S-shape and inverted U-shape) for completely miscible liquids. Depending on the axis chosen, one obtains the isotherm for component 2. These shapes were the basis for a more detailed classification given by Schay and Nagy (1961).

When the adsorption is studied from *dilute solutions* (where by convention, we shall consider that component 1 is the solvent), the experimental isotherms are still plotted, strictly speaking, in terms of reduced surface excess. Nevertheless, since

5.3.3. Basic experimental methods for the study of adsorption from solution

We may divide the experimental techniques available for the study of adsorption from solution into three main categories: (a) for the determination of adsorption isotherms, (b) for the measurement of the energies involved, and (c) for the provision of extra information on the properties of the adsorbed layer.

Methods for determining the amounts adsorbed

A first distinction must be made between the methods which use one sample for each point on the adsorption isotherm (i.e. immersion methods) and those using a single sample through which the solution of increasing concentration is allowed to flow (i.e. flow-through methods). A critical outline of most of these methods is given by Everett (1986).

Immersion methods. These are the oldest and the easiest to apply with conventional bench-type equipment but may suffer, as we shall see, from a lack of accuracy or from a large sample consumption.

In the *standard immersion method*, the dry sample is immersed in the solution (see Figure 5.15a). In a slightly different version (Rouquerol and Partyka, 1981), the sample is initially covered with the pure solvent (protected from any contact with ambient atmosphere) before receiving an appropriate dose of mother solution (see Figure 5.15b).

Equilibration may take between 1 minute and more than a day, in a thermostatted bath with continuous and slow tumbling. The suspension, still kept at the controlled temperature, is allowed to settle, which may take one full day, or, more frequently, the suspension is centrifuged (taking care, in the case of polymers, not to produce a measurable concentration gradient) and the supernatant is then pipetted and analysed. The analysis may involve differential refractometry, UV or IR spectroscopy (the former mainly for aqueous solutions, the latter for organic solutions), organic carbon analysis, colorimetry (for dye adsorption) or surface tension measurements. As mentioned in Section 5.3.1, this method has the advantage that it directly gives the reduced surface excess amounts. Since one experiment only provides one point of the adsorption isotherm, it is usual to undertake a number of simultaneous measurements (each requiring a fresh sample) in order to cover the desired portion of the adsorption isotherm.

A possible way to increase the accuracy of this immersion approach is to use the *slurry method* and to analyse a weighed sample of the slurry in the bottom of the test-tube, instead of analysing the supernatant (Nunn *et al.*, 1981). One then simply makes use of Equation (5.49), the operational expression of the relative surface excess of the solute with respect to the solvent. Here n_1 and n_2 are the total amounts of solute and solvent in the sample of slurry (either adsorbed or in solution) and c_2^l and c_1^l their concentrations in the solution. If one uses a liquid–solid ratio large enough to avoid any measurable change in concentration on adsorption, then c_2^l and c_1^l are simply the concentrations in the starting solution. The measurement is accurate provided the quantitative analysis of the slurry, which involves measuring the total amounts of 2 and 1

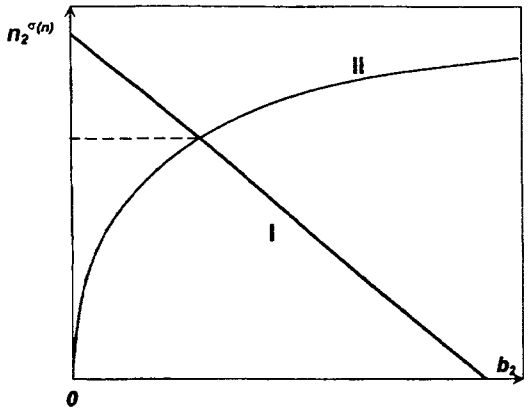

Figure 5.17. Graphical calculation of amount adsorbed in batch calorimetry experiment after introducing amount n_2 of solute (after Trompette, 1995). Curve II is the adsorption isotherm. For straight line I, see text. Crossing represents final adsorption equilibrium.

In Figure 5.17, for a given total amount of solute n_2 introduced into the microcalorimetric cell, the line I gives the dependence of the reduced surface excess amount $n_2^{\sigma(n)}$ on the equilibrium molality b_2. In order to plot line I we first consider the extreme case of $b_2 = 0$, that is all the solute is considered to be adsorbed so that

$$\frac{n_2^{\sigma(n)}}{m^s} = \frac{b_{2,0} \times \Delta m_i}{1000 + b_{2,0} M_2} \times \frac{1}{m^s} \tag{5.76}$$

where $b_{2,0}$ is the molality of the added solution, Δm_i is the mass of the first increment of solution, M_2 is the molar mass of the solute, and m^s is the mass of the adsorbent.

The other extreme of the line is determined by considering that $n_2^{\sigma(n)} = 0$, when all the solute is considered to remain in solution. Then:

$$b_2 = \frac{1000 b_{2,0} \Delta m_i}{(m_0 + \Delta m_i)\left[1000 + b_{2,0} M_2\right] - b_{2,0} m_0} \tag{5.77}$$

where m_0 is the initial mass of the pure solvent.

Curve II is simply the adsorption isotherm: the crossing provides the actual values of $n_2^{\sigma(n)}$ and b_2 after the introduction of Δm_i of solution. A blank experiment with the same set-up provides the curve of $\Delta_{mix} H$ versus b_2.

A batch microcalorimetric experiment, very similar to the one just described, is possible with a diathermal heat flowmeter type of microcalorimeter, which is less versatile than the Tian–Calvet microcalorimeter (especially in its temperature range and ultimate sensitivity), but of a simpler design. In the 'Montcal' microcalorimeter (Partyka *et al.*, 1989), the thermopile with up to 1000 thermocouples is replaced by a few thermistors.

Flow-through adsorption microcalorimetry. Flow-through adsorption microcalorimetry is not as versatile as the batch procedure. The grain size must be

such as

$$N_m = k\sigma^{-D_a/2} \tag{6.29}$$

where N_m is the number of molecules in the completed monolayer, σ is the adsorptive molecular area and D_a is now the fractal dimension of the accessible surface (Farin and Avnir, 1989).

The magnitude of D_a is determined *inter alia* by the degree of surface roughness or porosity. In principle, a lower limit of $D_a = 2$ is obtained with a perfectly smooth surface on the molecular scale. Most non-porous materials would be expected to exhibit some surface roughness. With such a material, a constant value of D_a between 2 and 3 implies that there is a degree of self-similarity: the shape of the surface irregularities thus remains invariant over a certain range of resolution. The physical structure of a fractal surface will therefore appear similar when viewed at different magnifications.

Fractal plots of log n_m versus log σ for two porous silicas are shown in Figure 6.3 (here, n_m is the BET monolayer capacity). Both plots are linear, giving $D_a = 2.98$ for the silica gel and $D_a = 2.09$ for the controlled pore glass. These values reflect the extremes of the fractal scale, the latter being close to the ideal value for a flat surface.

Some of the many values of D_a compiled by Farin and Avnir (1989) and Avnir *et al.*, (1992) are given in Table 6.2. Most values are within the theoretical fractal range, $D_a = 2$–3 and it is noteworthy that $D_a \approx 2$ for the graphitized carbon blacks and the pillared clays.

The values of D_a of (1.89 ± 0.09) and (1.94 ± 0.10) reported by Van Damme and Fripiat (1985) for pillared clays were derived from the multilayer capacities of nitrogen and various organic adsorptives. The fact that $D_a \approx 2$ appeared to confirm that the basal smectite surface was smooth and that the pillars were regularly distributed. It was argued by Van Damme and Fripiat that a random distribution of the pillars would necessarily lead to some localized molecular sieving and that this in turn would result in $D_a > 2$.

Various other aspects of fractal analysis have been discussed by Van Damme and Fripiat and their co-workers. For example, by extending the BET model to fractal surfaces, Fripiat *et al.* (1986) were able to show that the apparent fractal dimension is reduced by the progressive smoothing of a molecularly rough surface. Alternatively, the effect of a micropore filling contribution is to enhance the fractal dimension.

Other investigators, including Pfeifer and Obert (1989), Pfeifer *et al.* (1990), Krim and Panella (1991), Panella and Krim (1994) and Neimark and Unger (1993), have also studied multilayer adsorption on fractally rough surfaces. In particular, Pfeifer and his co-workers point out that the interpretation of a fractal dimension of a porous surface

Table 6.2. Values of accessible fractal dimension evaluated from adsorption data (taken from Farin and Avnir, 1989)

Adsorbent	Adsorptives	Fractal dimension, D_a
Graphitized carbon blacks	N_2 and alkanes	1.9–2.1
Activated carbons	N_2 and organic molecules	2.3–3.0
Pillared clays	N_2 and organic molecules	1.8–2.0
Silica gels	Alkanes	2.9–3.4
Other oxides	N_2 and alkanes	2.4–2.7

presents problems when it is associated with the BET theory. In contrast, an FHH-fractal treatment appears to be more promising, provided that wetting effects are taken into account. This was exactly the approach adopted by Krim and her co-workers.

In their work on carefully prepared homogeneous silver films, Krim and Panella (1991) and Panella and Krim (1994) applied the FHH equation in the form

$$\ln(p/p^\circ) = -\alpha/(kT\theta^n) \tag{6.30}$$

where the coefficient α is dependent on the nature of the adsorbent–adsorbate and adsorbate–adsorbate interactions and the corresponding fractal dimension is determined by the magnitude of the exponent n (de Gennes, 1985). Nitrogen and oxygen isotherms at 77.4 K gave linear FHH plots over a wide range of multilayer coverage. The values of n for nitrogen on smooth and rough silver substrates were 3.0 and 4.7, respectively, the former giving the expected fractal dimension, $D_a = 2$. However, the value $n \approx 3$ was also obtained for oxygen on the *rough* surface, which was attributed to surface tension effects (since the surface tension of liquid oxygen is much higher than that of liquid nitrogen).

Panella and Krim suggested that the high value $n = 4.7$ was more consistent with the properties of a self-affine surface rather than a self-similar one. Self-affine fractals are associated with asymmetric scaling, that is different scaling relations in different directions (Avnir, 1997).

The FHH-fractal approach was also adopted by Ehrburger-Dolle *et al.* (1994) as part of a systematic study of the properties of silica aerogels. The value $D_a = 2.1$ was evaluated from the linear FHH plot for nitrogen on Aerosil 200, whereas values of 2.64 and 2.95 were obtained from the nitrogen multilayer isotherms on various aerogels. The latter value, which is obviously close to 3, appeared to be consistent with

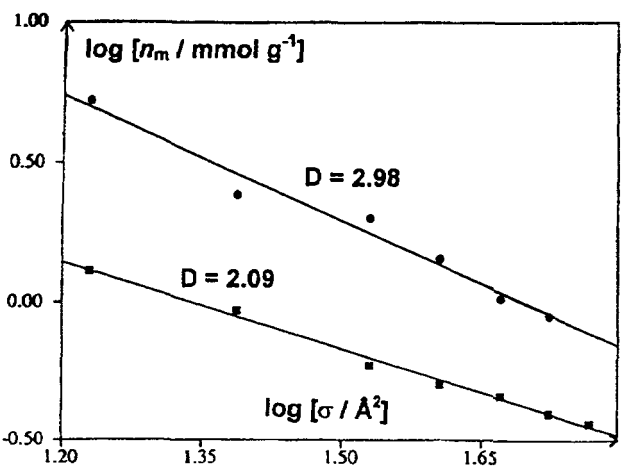

Figure 6.3. Fractal plots for the adsorption of organic vapours on the silica gel and a controlled porous glass (after Farin *et al.*, 1985 and Christensen and Topsoe, 1987): part of Fig. 1, Farin and Avnir, 1989.

contact of the particles. The initial interparticle condensation is reversible, but as the advancing menisci meet the narrow openings between the particles (i.e. the 'windows' or 'throats') are spontaneously filled. The third stage involves the filling of the larger voids (or cavities) within the packed particles.

The initial process of monolayer–multilayer adsorption on the available surface of the packed spherical particles is complicated by two opposing effects. First, there is always a significant reduction in adsorption due to the loss of surface area between adjacent particles (see Figure 7.2a). On the other hand, because of the close proximity of the two surfaces, the adsorption is enhanced in the inner part of the annular space (i.e. similar to small-scale micropore filling).

A saddle-shaped meniscus (or pendular ring) is developed in the first stage of condensation. Application of Equation (7.10) now requires the designation of two radii of curvature of opposite sign, one being concave and the other convex. The Kelvin equation therefore takes the form

$$\ln (p/p^\circ) = -\frac{\gamma v^l}{RT}\left[\frac{1}{r_1} - \frac{1}{r_2}\right] \tag{7.14}$$

where r_1 is the concave radius and r_2 is the convex radius, which is directly related to the particle radius. If we assume that the spherical particles all have the same radius, R, the radius of curvature r_2 as given by Wade (1964, 1965) is $\{[(R+t+r_1)^2 - R^2]^{1/2} - r_1 + R + t\}/2$.

The second and third stages of capillary condensation are evidently dependent on both the particle size and the degree of packing (i.e. the coordination number) of the spherical particles. The windows may be pictured as the space between three or four neighbouring particles as in Figure 7.2. If the particles are in a triangular array, the second stage of condensation is controlled by the radius of the inscribed circle. Although the amount taken up may be relatively small, this stage is important in relation to hysteresis (see Section 7.5).

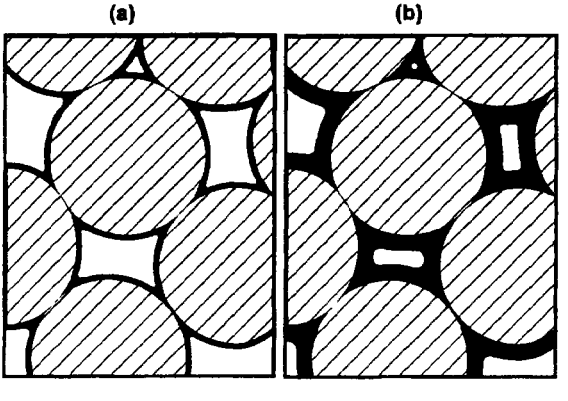

Figure 7.2. Sections of the pore space between solid spheres in irregular packing. First (a) and second (b) stage of condensation.

condensation occurs in an open-ended cylinder. Since a cylindrical meniscus is unstable, a spontaneous change leads to the development of an unduloid. In the next stage, the pore becomes blocked by the formation of a biconcave lens of liquid. The evaporation process proceeds in a thermodynamically reversible manner, however, and in accordance with the Kelvin equation, the relative pressure is now dependent on the radius of curvature of the hemispherical menisci. Thus, in the case of this simple system, it is the location of the desorption branch which should be used for the calculation of r_p.

A different approach was adopted by Saam and Cole (1975), who attempted to explain the hysteresis exhibited by a cylindrical pore in terms of the regimes of stability, metastability and instability of the multilayer film. The applicability of the Saam–Cole theory has been explored in some detail by Findenegg *et al.* (1994), Lewandowski *et al.* (1991) and Michalski *et al.* (1991).

According to the Saam–Cole theory, there are two opposing effects which govern the range of metastability of a multilayer film in a cylindrical mesopore. Thus, long-range adsorption forces help to stabilize the film, while capillary forces are responsible for the condensation of the liquid. At a critical film thickness, t_c, the curved film becomes unstable and condensation occurs. Evaporation of the liquid condensate requires a lower $p/p°$ and now the residual film thickness, is t_m. We may therefore regard the difference $(t_c - t_m)$ as the metastability thickness range of the multilayer film.

On the basis of the Saam–Cole–Findenegg approach, we are now able to revise the 'ideal isotherm' for capillary condensation. A more realistic isotherm for the physisorption of a vapour in an assemblage of uniform cylindrical mesopores is shown in Figure 7.5. Here, C represents the limit of metastability of the multilayer (of thickness t_c) and M the point at which the three phases (multilayer, condensate and gas) all coexist. Along MC the multilayer and gas are in metastable equilibrium.

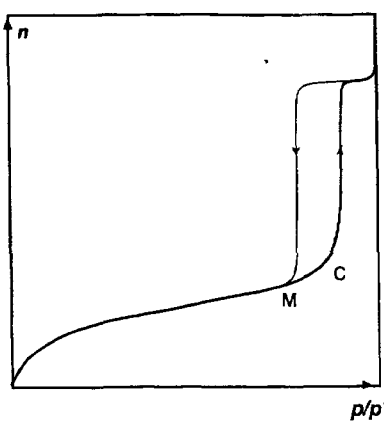

Figure 7.5. An adsorption–desorption isotherm for a mesoporous solid with cylindrical pores, all having the same radius.

(e) the adsorptive molecular size and shape;
(f) the operational temperature.

In addition, we should keep in mind that the micropore filling capacity is dependent on both the available pore volume and the packing of the adsorbed molecules.

In this chapter, we introduce the currently most popular adsorption methods used for micropore size analysis: our aim is to outline in general terms the relative merits and limitations of these procedures. Their application is discussed more fully in later chapters in relation to the characterization of particular adsorbents.

As we have already seen, an ideal Type I isotherm has a long, almost horizontal plateau, which extends up to $p/p^\circ \rightarrow 1$, as in Figure 8.1a. In this case, the micropore capacity, $n_p(\text{mic})$, is registered directly as the amount adsorbed at the plateau. Such well-defined Type I isotherms are given by large crystals of a molecular sieve zeolite.

Many porous adsorbents contain pores with a wide range of sizes which cross the micropore–mesopore boundary. Also, some microporous adsorbents are composed of very small agglomerated particles, which exhibit a significant external area. Such materials give composite isotherms with no distinctive plateau. The presence of mesopores can often be detected by the appearance of a hysteresis loop – as in Figure 8.1b.

A third possibility is a Type I isotherm with a short plateau, which terminates at $p/p^\circ < 1$. An upward deviation, as indicated in Figure 8.1c, occurs at high p/p° when the microporous adsorbent also contains some wide mesopores or narrow macropores. Since the wall area of such relatively wide pores is likely to be much smaller than the micropore area, the scale of multilayer development or mesopore filling may be quite small.

Many attempts have been made to obtain the micropore capacity by the analysis of composite isotherms. The calculation of the micropore volume, $v_p(\text{mic})$, from $n_p(\text{mic})$ is almost invariably based on the assumption that the adsorbate in the micropores has the same density as the adsorptive in the liquid state at the operational

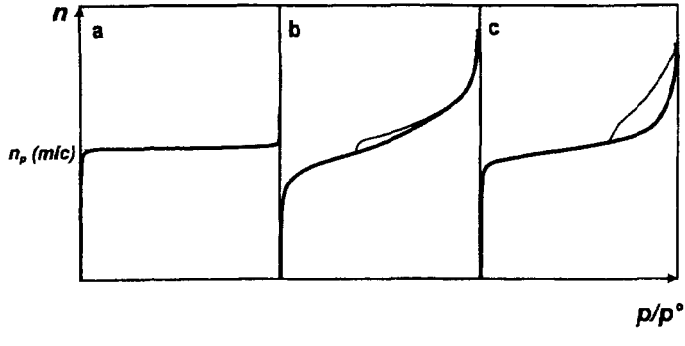

Figure 8.1. Nitrogen isotherms corresponding to adsorption: (a) in ultramicropores; (b) in wider micropores and on external surfaces; (c) in micropores and wide mesopores.

temperature. As we saw in Chapter 7, for the condensate in a mesoporous adsorbent this assumption (i.e. the Gurvich rule) appears to be justified. The situation is quite different, however, with a microporous material – particularly when the pore dimensions are in the ultramicropore range.

Studies of the packing of molecules in cylindrical and slit-shaped pores have revealed the importance of both the width and the shape of narrow pores (Carrott *et al.*, 1987; Balbuena and Gubbins, 1994). An indication of the effect of pore size on the packing density of spherical molecules is given in Figure 8.2. Here, the degree of packing in cylinders and slits is expressed as a percentage of the packing density in the corresponding close-packed state. Although this is an oversimplified picture since it does not allow for the adsorption forces, it does illustrate the difficulty of arriving at an unambiguous assessment of the accessible pore volume. Inspection of

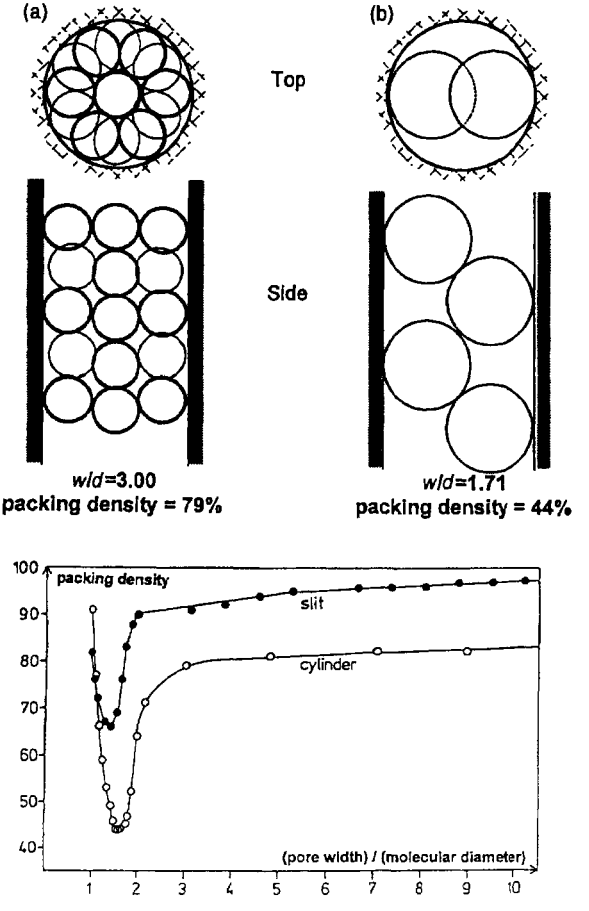

Figure 8.2. Packing of spherical molecules in narrow cylinders and slits.

Stoeckli H.F. (1977) *J. Colloid Interface Sci.* **59**, 184.
Stoeckli F. (1993) *Adsorption Sci. Tech.* **10**, 3.
Stoeckli H.F. and Ballerini L. (1991) *Fuel* **70**, 557.
Stoeckli H.F. and Huguenin D. (1992) *J. Chem. Soc., Faraday Trans.* **88**(5), 737.
Stoeckli H.F., Houriet J.Ph., Perret A. and Huber U. (1979) In: *Characterisation of Porous Solids* (S.J. Gregg, K.S.W. Sing and H.F. Stoeckli, eds) *Society of Chemical Industry*, London, p. 31.
Stoeckli H.F., Centeno T.A., Fuertes A.B. and Muniz J. (1996) *Carbon* **34**, 10.
Venero A. F. and Chiou J. N. (1988) *M.R.S. Symp. Proc.* **111**, 235.
Walton J.P.R.B. and Quirke N. (1989) *Mol. Simul.* **2**, 361.

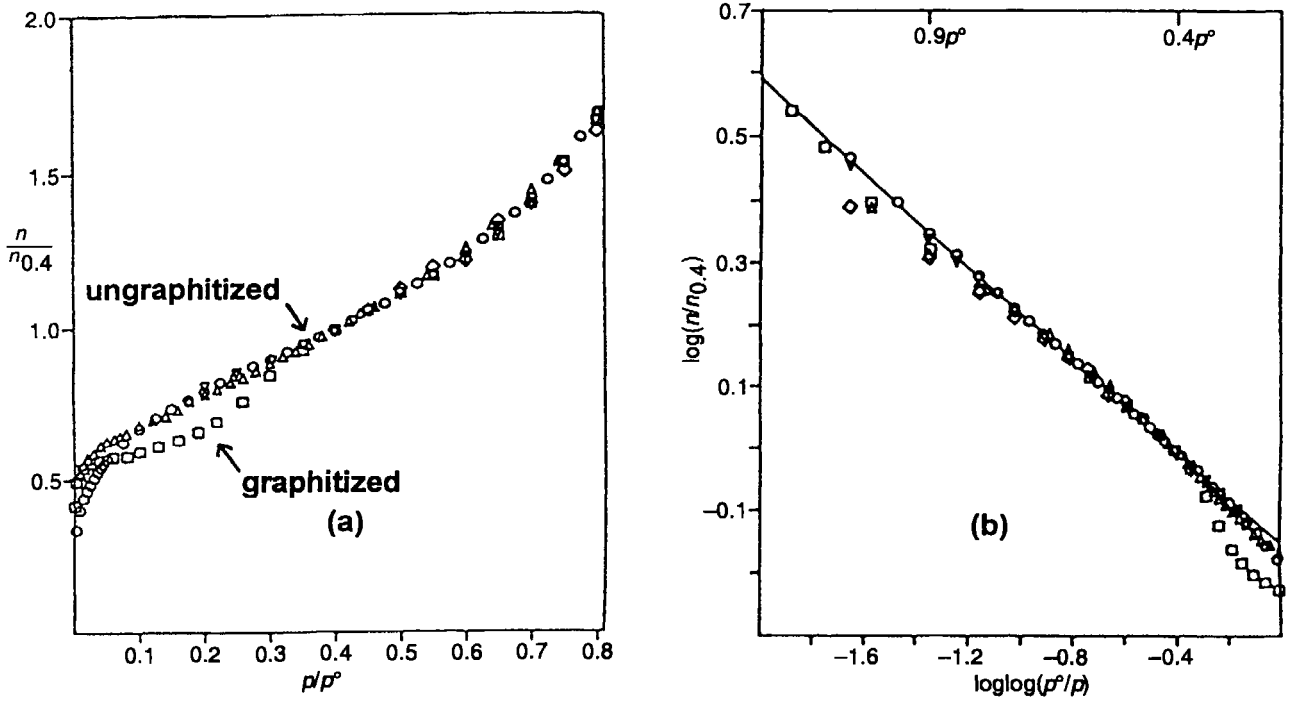

Figure 9.4. Standard nitrogen isotherms for carbons (a), and corresponding FHH plots (b) (circles, Carrott *et al.*, 1988a; diamonds, Voloshchuk *et al.*, 1988, squares, Isirikyan and Kiselev, 1961; triangles down, Pierce, 1968; triangles up, Rodriguez-Reinoso *et al.*, 1987). Reproduced from Carrott and Sing (1989).

could serve as standard for both graphitized and non-graphitized carbons. There are three main reasons why there are significant discrepancies between proposed standard data to be found in the literature. First, any significant differences in the graphitic surface structure will have some effect on the isotherm shape – especially at low surface coverage. Second, any interparticle capillary condensation will produce an upward deviation in the multilayer/capillary condensation region. Third, any microporosity will enhance the adsorption in the sub-monolayer region and will tend also to reduce the isotherm slope in the multilayer region.

As explained in Chapters 6 and 8, by applying the α_S-method we have a simple way of checking the validity of the BET area and detecting the presence of microporosity. Many carbon blacks have been found to be essentially non-microporous (Carrott *et al.*, 1987; Bradley *et al.*, 1995), in which case the corresponding values of BET area and α_S area are in good agreement. However, in a few cases the back-extrapolation of the α_S-plot has given a positive intercept on the adsorption axis which is an indication of some microporosity. The microporous nature of some carbon blacks has been confirmed in several recent investigations (Stoeckli *et al.*, 1994a; Kruk *et al.*, 1996). As one might expect, oxidation leads to a considerable increase in the level of the microporosity (Bradley *et al.*, 1995).

The strong energetic heterogeneity exhibited by Spheron 6 was first shown calorimetrically by Beebe and his co-workers (Beebe *et al.*, 1947; Kington *et al.*, 1950). This work also revealed that the surface of Graphon was much less heterogeneous than that of the original carbon black. The results of a more detailed investigation of the effect of thermal treatment of carbon black on the energetics of nitrogen adsorption (i.e. variation of $\Delta_{ads}h$ with coverage θ) are shown in Figure 9.5. Microcalorimetric measurements were undertaken on a sample of heat-treated Sterling FT-FF (i.e. a thermal black).

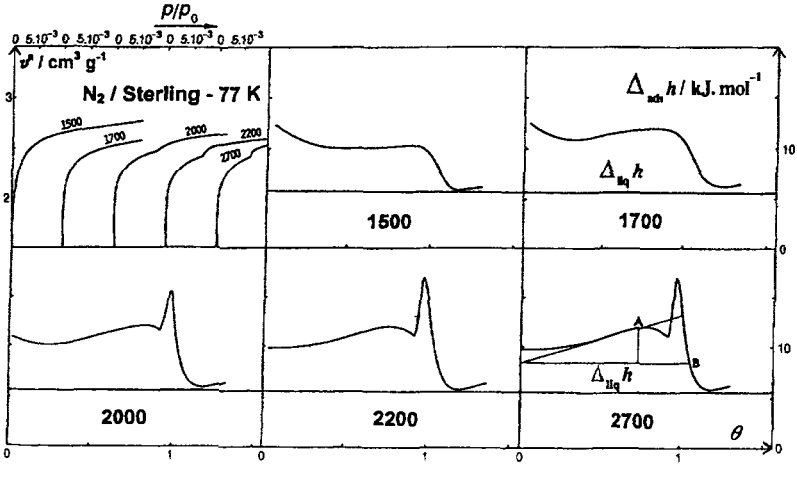

Figure 9.5. Differential enthalpies of N_2 adsorption at 77 K on heat-treated blacks (at temperatures from 1500 to 2700°C), as a function of coverage (Grillet *et al.*, 1979).

The energetic heterogeneity of the original ungraphitized surface was revealed by the careful adsorption calorimetric measurements undertaken by Beebe *et al.*, (1953). By comparing the changes in the differential energies of adsorption for argon on Spheron and Graphon, these investigators found that the initial steep decline in 'differential heat of adsorption' was largely removed as a result of graphitization. Instead, an increase in the differential energy was observed at a higher surface coverage: it is now generally agreed that this was due to the adsorbate–adsorbate interaction becoming apparent as the degree of energetic heterogeneity was reduced.

A systematic study of krypton adsorption on exfoliated graphite was subsequently undertaken by Thomy and co-workers (Thomy and Duval, 1969; Thomy *et al.*, 1972). Their stepwise isotherm, determined at 77.3 K, is shown in Figure 4.1. The layer-by-layer nature of the physisorption process is clearly evident – at least up to four molecular layers. This isotherm shape is remarkably similar to that of the krypton isotherm on graphitized carbon black reported by Amberg *et al.*, (1955).

The work of Thomy and co-workers (Thomy and Duval, 1969; Thomy *et al.*, 1972) provided the first well-documented evidence for the presence of a sub-step in the krypton isotherm. The effect of temperature on the shape and the location of the sub-step is shown in Figure 9.7. The fact that the riser of the sub-step remained vertical over the temperature range of 77.3–96.3 K served to confirm that the sub-step was

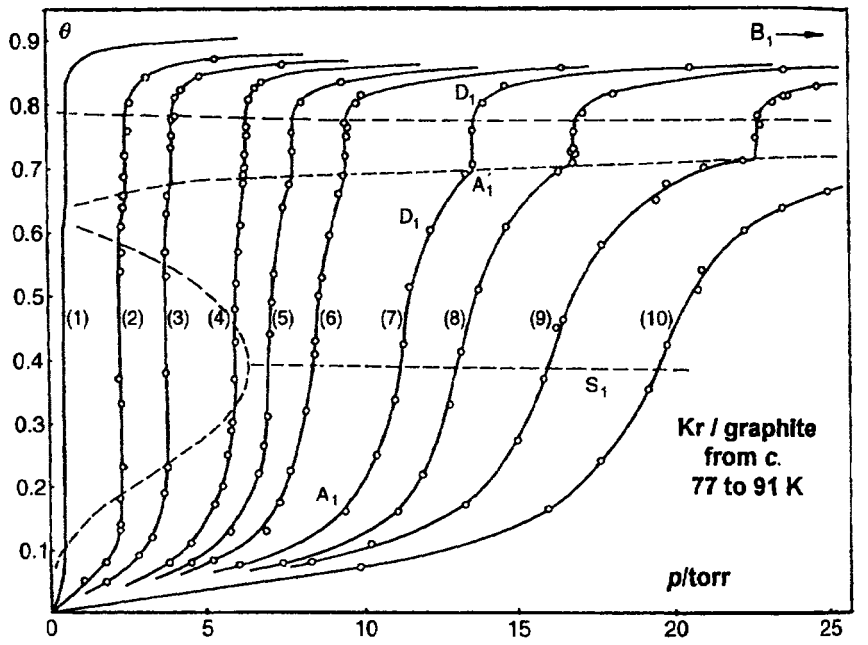

Figure 9.7. Adsorption isotherms of krypton on exfoliated graphite. Curves labelled from 1 to 10, obtained at 77.3, 82.4, 84.1, 85.7, 86.5, 87.1, 88.3, 89.0, 90.1 and 90.9 K, respectively (courtesy Thomy *et al.*, 1972).

micropores (i.e. the ultramicropores) occurs at very low $p/p°$, the change in amount adsorbed at $p/p° > 0.01$ is quite small (Atkinson *et al.*, 1987; Kenny *et al.*, 1993) and therefore it is not surprising to find that the DR plot is virtually linear over a fairly wide range of $p/p°$.

In some investigations (Fernandez-Colinas *et al.*, 1989a; Kakei *et al.*, 1991; Kenny *et al.*, 1993; Kaneko, 1996) it has been found that the shapes of high-resolution α_S-plots and DR plots provide strong evidence for a sequential filling of several groups of micropores. For example, the nitrogen isotherms in Figure 9.12a were determined on a series of activated pine wood charcoals (Fernandez-Colinas *et al.*, 1989a). The change in isotherm shape is the first indication that pore widening has occurred as a result of progressive activation in steam. The α_S-plots in Figure 9.12b confirm this interpretation and indicate that this was mainly due to the development of a supermicropore structure. It appears that the initial stage of primary micropore filling at very low $p/p°$ (i.e. $p/p° < 0.01$) was followed by the more gradual filling of supermicropores.

Surface coverage of the supermicropore walls is indicated by the appearance of a short linear section at $\alpha_S > 0.5$. Extrapolation of this section to $\alpha_S = 0$ provides an approximate evaluation of the *effective ultramicropore volume*, v_p(u, mic).

The second linear section extends over the multilayer range of each α_S-plot in Figure 9.12b. Backward extrapolation of this branch gives the total effective micropore volume, v_p(mic), from the intercept on the v^a axis. It follows that the effective supermicropore volume, v_p(sup, mic), can be regarded as the difference v_p(mic) – v_p(u, mic). It is of interest that after an initial small change in v_p(u, mic), this has remained constant during further activation while the magnitude of v_p(sup, mic) has increased steadily.

As discussed in Chapter 8, the pre-adsorption of *n*-nonane can be used as a means of blocking narrow micropore entrances (see Section 8.2.3). Thus, in the case of an ultramicroporous adsorbent such as Carbosieve, the pre-adsorption of nonane leads to complete blockage of the pore structure. The effect of progressively removing the pre-adsorbed nonane from a supermicroporous carbon is shown in Figure 9.13. The adsorbent used in this work was a well-characterized carbon cloth with the following properties: a(BET), 1330 $m^2 g^{-1}$; a(ext), 25 $m^2 g^{-1}$; v_p(mic), 0.44 $cm^3 g^{-1}$; w_p, 0.6–2.0 nm (Carrott *et al.*, 1989).

Inspection of the α_S-plots in Figure 9.13 is instructive. It can be seen that there are two linear sections, back-extrapolation of the first giving a zero intercept when part of the pre-adsorbed nonane was removed by prolonged outgassing at 50°C. We may conclude that the initial stage of nitrogen adsorption is by monolayer adsorption on the walls of the supermicropores. This is followed by the formation of a quasi-multilayer until pore filling is complete at $p/p° \approx 0.4$. Increase of outgassing temperature leads to the progressive removal of nonane from the ultramicropores and narrow entrances and the original nitrogen isotherm is restored after prolonged outgassing at 200°C. Thus, we may compare the change in the extent of total micropore capacity, v_p(mic) (obtained as described earlier by back-extrapolation of the linear multilayer branch), with the magnitude of the restoration of the ultramicropore capacity, v_p(u, mic) (as defined above). The fact that at each stage v_p(mic) > v_p(u, mic) is a

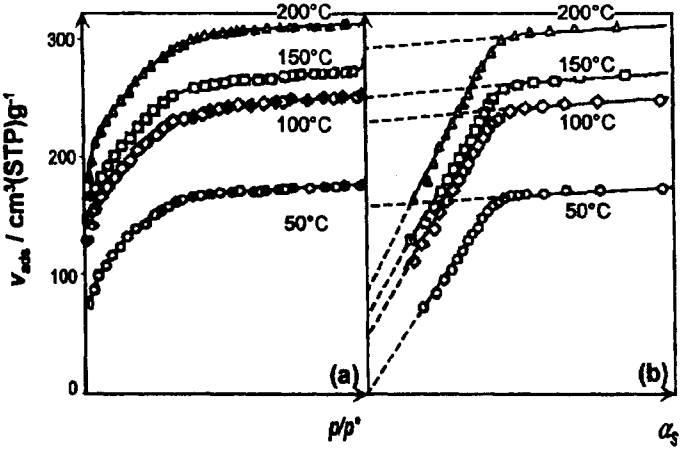

Figure 9.13. Nitrogen adsorption isotherms ar 77 K (a) and corresponding α_S plots (b) for charcoal cloth JF012 after pre-adsorption of nonane followed by outgassing at indicated temperature (after Carrott *et al.*, 1989).

clear indication that the pre-adsorption of nonane has resulted in the blockage of narrow entrances of some supermicropores.

A possible disadvantage of nitrogen is that, because of its diatomic molecular shape and quadrupolar nature, it is an unrepresentative adsorptive for the investigation of micropore filling. It is instructive therefore to compare the results of nitrogen and argon adsorption measurements on a series of activated carbons. For this purpose, adsorption microcalorimetry is an invaluable tool. Differential enthalpies of adsorption for argon and nitrogen are plotted in Figure 9.14 (i.e. $\Delta_{ads}h$ versus θ) for two of the activated charcoals, C1 and C4, featured in Figure 9.12. As expected, over most of the micropore filling range, the nitrogen adsorption energies are appreciably above the corresponding argon energies. As discussed in Chapter 1, this difference is likely to be due to the specific field gradient–quadrupole interaction experienced by nitrogen. However, it is evident that with both C1 and C4 the corresponding adsorption energy curves have the same general appearance.

Inspection of the adsorption enthalpy curves for nitrogen in Figure 9.14 reveals that three characteristic stages of physisorption can be identified: Point A is at the end of the first plateau; Point B is at the beginning of a second, less well-defined, plateau; Point C is the point where the pore-filling curve crosses the corresponding curve for monolayer adsorption on ungraphitized carbon (Spheron 1500). We can attribute the high initial adsorption enthalpies ($\Delta_{ads}h \approx 18$ kJ mol^{-1} for nitrogen and $\approx$16 kJ mol^{-1} for argon) to primary micropore filling within pores of molecular dimensions. This is followed by the transitional region AB and finally the mainly co-operative filling range of BC.

As pointed out in Chapter 1, high physisorption energies are produced by the overlap of the adsorbent–adsorbate interactions in pores of molecular dimensions (Everett and Powl, 1976). In the case of slit-shaped pores in carbons, a significant

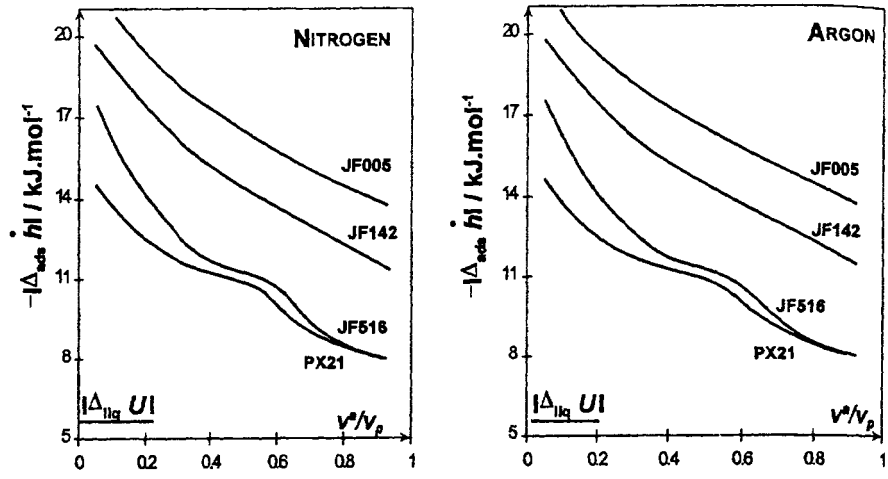

Figure 9.15. Differential enthalpies of adsorption of N_2 and Ar on microporous carbons, plotted versus fractional pore filling (after Atkinson *et al.*, 1987).

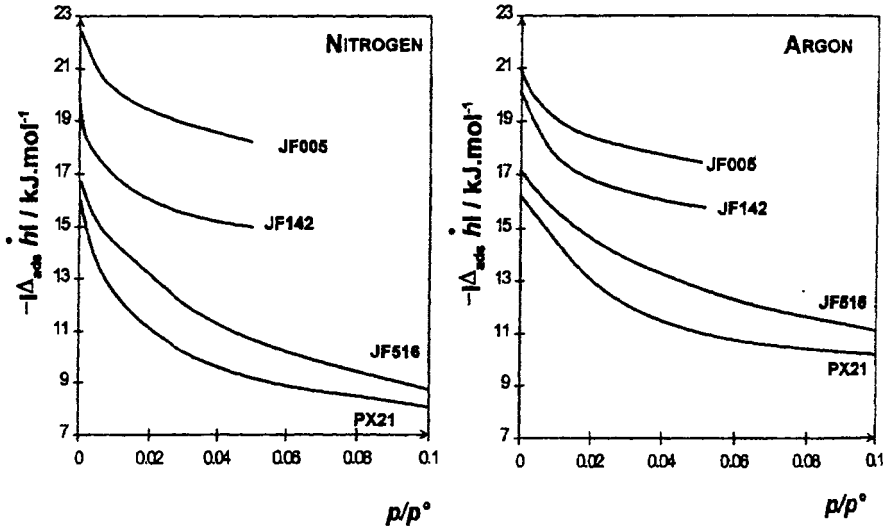

Figure 9.16. Differential enthalpies of adsorption of N_2 and Ar on microporous carbons, plotted versus relative pressure (after Atkinson *et al.*, 1987).

very different in size: the kinetic diameter of N_2 is 0.36 nm and that of CO_2 is 0.33 nm; and the corresponding minimum dimensions are 0.30 and 0.28 nm. However, by far the most important factor in causing the greater uptake of CO_2 is the higher operational temperature (Gregg and Sing, 1982, p. 230).

This effect is exploited to an even greater extent when the carbon dioxide measurements are undertaken at 273 or 298 K. At these temperatures the carbon dioxide saturation pressures are extremely high (e.g. at 298 K $p^\circ = 63.4$ bar) so that the range of p/p° is limited to ≈ 0.02 at sub-atmospheric pressures. This has the advantage that the initial part of the isotherm can be determined with a much greater accuracy than is normally possible with nitrogen at 77 K, and in addition the DR plots are generally more linear (Rodriguez-Reinoso, 1989).

Rodriguez-Reinoso and his co-workers have identified three groups of porous carbons: (a) carbonized materials and activated carbons of low burn-off, giving much larger CO_2 uptake, because of restricted diffusion of nitrogen into very narrow pores; (b) activated carbons of low-to-medium burn-off, having fairly narrow micropores and giving approximately equivalent uptakes of CO_2 and N_2; and (c) activated carbons of medium-to-high burn-off, having a range of wider micropores and giving larger uptakes of N_2 than CO_2.

Recent experiments by Cazorla-Amoros *et al.* (1996) have involved the measurement of CO_2 isotherms up to pressures of 4 MPa at 273 and 298 K. These investigators have confirmed that CO_2 adsorption at subatmospheric pressures is a useful complementary technique for the characterization of very narrow micropores and that at higher pressures the adsorption of CO_2 is similar to nitrogen.

9.5.2. Adsorption of organic vapours

Benzene was the most popular adsorptive in many early studies of the pore structure of activated carbons (Dubinin, 1958, 1966; Cadenhead and Everett, 1958; Smisek and Cerny, 1970). Indeed, in order to construct the characteristic curve for a given microporous carbon, Dubinin and his co-workers (Dubinin, 1966) originally adopted benzene as the standard adsorptive: thus, in the context of the Dubinin theory of the volume filling of micropores (TVFM), the scaling factor β (C_6H_6) = 1 (see Chapter 8).

Polanyi's concept of the temperature invariance of the characteristic curve became an important feature of the TVFM proposed by Dubinin (1966). The approach provided a way of bringing together a family of isotherms determined at different temperatures. The resulting common curve may be regarded as the relation between the fractional filling of the pores of a microporous carbon by a particular adsorptive and the 'adsorption potential', defined as $RT \ln (p^\circ/p)$. An example of a typical characteristic curve is shown in Figure 9.17, where it is evident that for the active carbon CK the common characteristic curve is given by all the benzene isotherms determined over the temperature range of 20–140°C.

Not all characteristic curves are temperature invariant (Aranovich, 1991; Tolmachev, 1993). Invariance over a wide temperature range has thermodynamic implications, which are unlikely to be consistent with the behaviour of many systems – especially when strong adsorbent–adsorbate interactions or a combination of

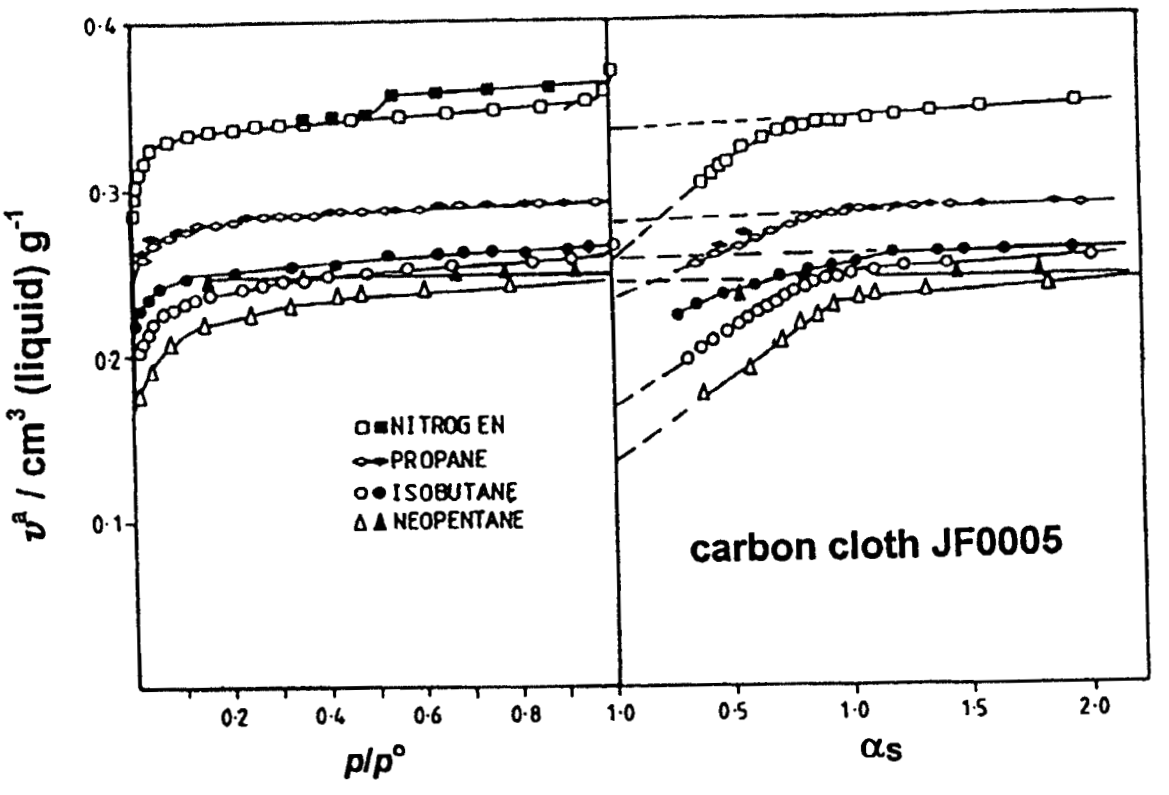

Figure 9.19. Adsorption isotherms and corresponding α_S plots for charcoal cloth JF005 (open symbols, adsorption; solid symbols, desorption) (Carrott *et al.*, 1988b).

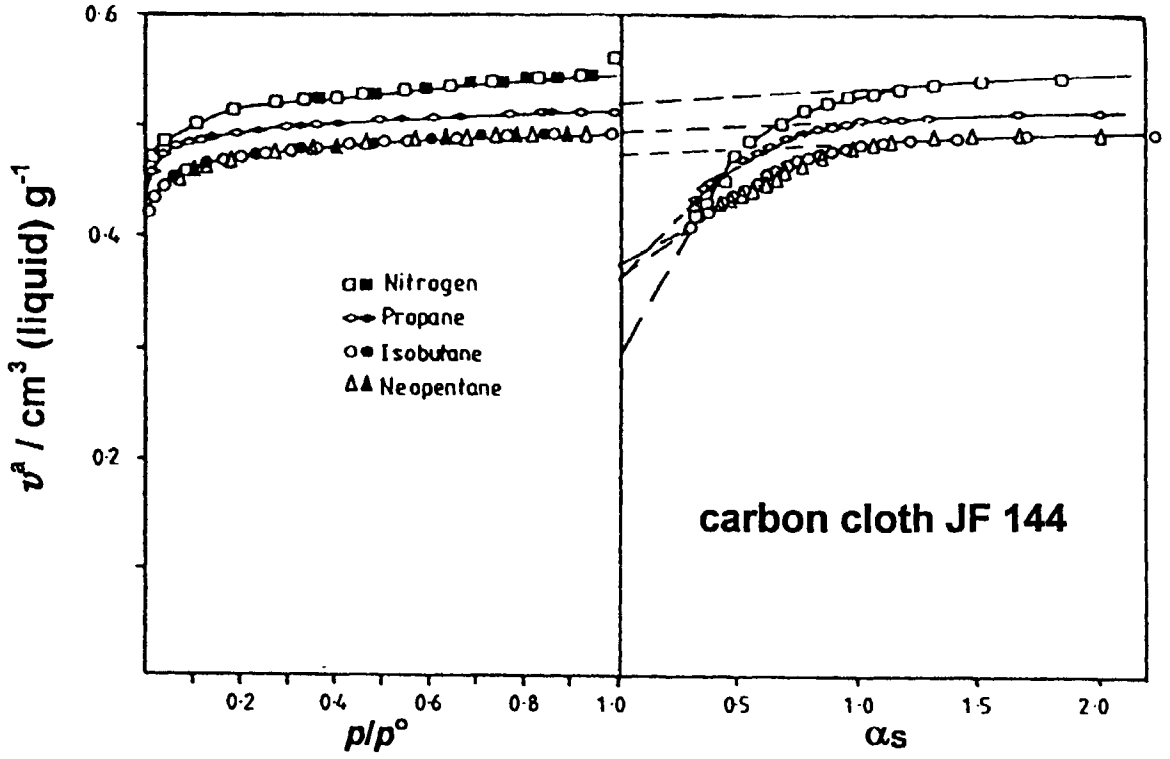

Figure 9.20. Adsorption isotherms and corresponding α_S plots for charcoal cloth JF144 (open symbols, adsorption; solid symbols, desorption) (Carrott *et al.*, 1988b)

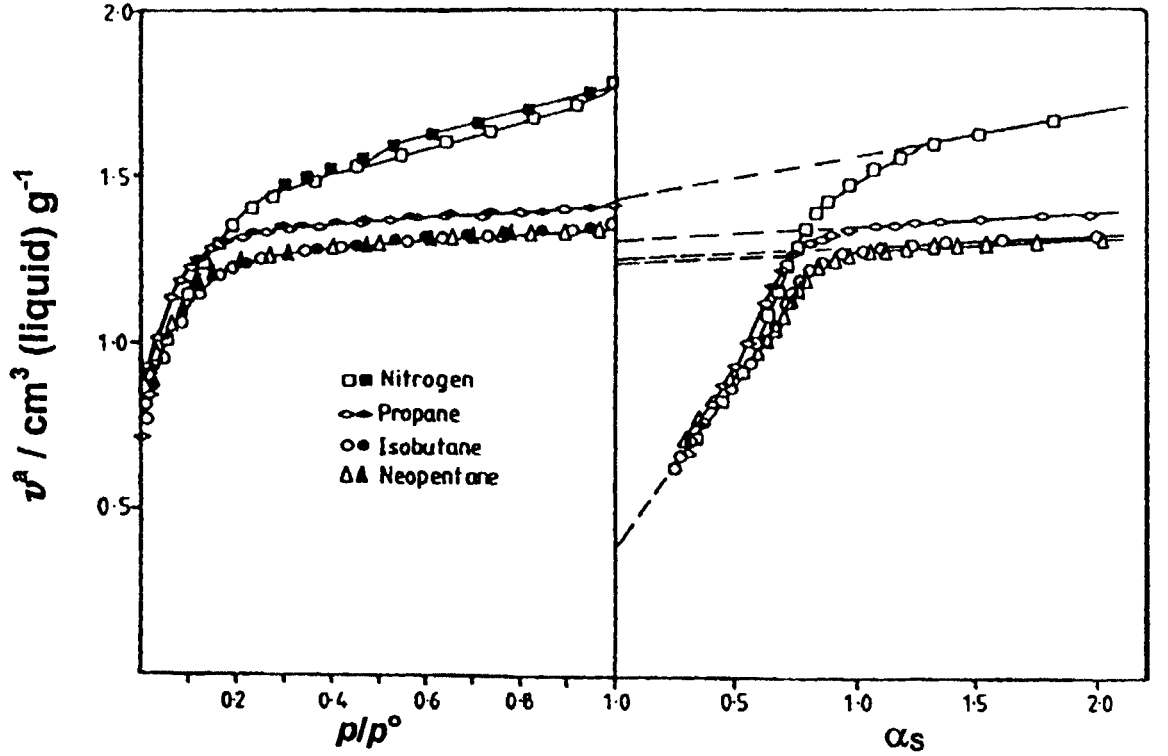

Figure 9.22. Adsorption isotherms and corresponding α_s plots for active carbon AX21 (open symbols, adsorption; solid symbols, desorption) (Carrott *et al.*, 1988b).

Table 9.3. Effective pore sizes of activated carbons

Carbon	Effective pore volume, v_p(mic) ($cm^3\ g^{-1}$)	Pore range, w (nm)
Carbosieve	0.36[a]–0.43[b]	U: 0.4–0.7
JF005	0.28[a]–0.33	U: 0.4–0.8
JF144	0.51[a]–0.55	U + S: 0.4–2
JF518	0.90[a]–0.98	U + S: 0.4–3
AX21	1.29[a]–1.52	U + S: 0.4–3

[a] For propane.
[b] For nitrogen.
U, ultramicroporous; S, supermicroporous.

pore size or volume (Rouquerol *et al.*, 1994) and also specify the adsorptive and operational temperature.

9.5.3. Adsorption of helium

Helium is often used in adsorption manometry for the determination of the 'dead space' volume (see Chapter 3), but this procedure is based on the presupposition that the gas is not adsorbed at ambient temperature and that it does not penetrate into regions of the adsorbent structure which are inaccessible to the adsorptive molecules. In fact, with some microporous adsorbents, significant amounts of helium adsorption can be detected at temperatures well above the normal boiling point (4.2 K). For this reason, the apparent density (or so-called 'true density') determined by helium pycnometry (Rouquerol *et al.*, 1994) is sometimes dependent on the operational temperature and pressure (Fulconis, 1996).

Because of its small size (collision diameter ≈ 0.20 nm), helium would appear to be a useful probe molecule for the study of ultramicroporous carbons. The experimental difficulty of working at liquid helium temperature (4.2 K) is the main reason why helium has not been widely used for the characterization of porous adsorbents. In addition, since helium has some unusual physical properties, it is to be expected that its adsorptive behaviour will be abnormal and dependent on quantum effects.

In their recent investigations of helium adsorption by microporous carbons, Kaneko and his co-workers (Kuwabara *et al.*, 1991; Setoyama *et al.*, 1993; Setoyama and Kaneko, 1995; Setoyama *et al.*, 1996) have obtained strong evidence that the density of physisorbed helium is not the same as that of bulk liquid helium at 4.2 K (i.e. 0.102 g cm^{-3}). By adopting the value 0.202 g cm^{-3}, which had been proposed on theoretical grounds by Steele (1956), Kaneko and his co-workers were able to obtain fairly good agreement between the corresponding uptakes of He and N_2 by certain microporous carbons – as indicated in Figure 9.23. With some other porous carbons, the presence of narrow ultramicropores was demonstrated by the much larger apparent pore volumes available for helium adsorption.

The shapes of a series of helium and nitrogen isotherms are compared in Figures 9.24 and 9.25. To facilitate comparison, the amount adsorbed is expressed in the form

until $p/p^\circ > 0.5$. Another interesting difference between the two water isotherms in Figure 9.26 is the size of their hysteresis loops: the loop given by Carbosieve is steep and narrow, while the loop obtained with AX21 is broader and more rounded.

A qualitative explanation for isotherms of the type shown in Figure 9.26 was first put forward by Pierce and Smith (1950), who postulated that initially a few water molecules are adsorbed on polar sites (e.g. oxygen complexes) and, with increase in p/p°, clusters of molecules are then hydrogen-bonded around these favourable sites. The clusters grow with increased pressure until they merge together and the pores are filled. According to Pierce and Smith, the hysteresis is due to a difference between the steps involved in pore filling and emptying, the latter representing a more stable state. The two-stage process was the basis of the model adopted by Dubinin and Serpinski (1981) and further developed by Barton and Koresh (1983).

The latter authors found that a *reversible* water isotherm was obtained after the low-temperature (i.e. 40°C) evacuation of a carbon cloth, which had been activated by oxidative HNO_3 treatment. The molecular sieve character of this material was reduced by evacuation at 400°C and this also led to the appearance of hysteresis in the water vapour isotherm. Barton and Koresh (1983) conclude that such hysteresis is mainly due to the concentration of surface oxides 'which dictate the adsorption value at which the change from cluster adsorption to a continuous adsorbed phase takes place'. The relationship between the adsorption of water and the surface concentration of chemisorbed oxygen was first established by Walker and Janov (1968). Bansal *et al.* (1978a,b) also investigated the influence of the surface oxygen on the adsorption of water: they concluded that at $p/p^\circ < 0.5$ the level of water uptake is determined by the concentration of surface oxygen-containing structures.

Truly reversible Type V isotherms are quite rare. It is significant that the example reported by Dubinin (1980) was obtained on a low burn-off (5.7%) carbon, which was certainly ultramicroporous. It was pointed out that with an activated carbon obtained by 20% burn-off, the hysteresis extended over virtually the whole range of pore filling – the water isotherm then having a very similar appearance to that of the Carbosieve isotherm in Figure 9.26.

A study of the hydrophilic sites on the surface of activated carbon fibres has been made recently by Kaneko *et al.* (1995) with the aid of X-ray photoelectron spectroscopy (XPS). In this work cellulose (CEL)- and polyacrylonitrile (PAN)-based activated carbon fibres were used and samples were either chemically treated with H_2O_2 or heated in H_2 at 1000°C. As expected, surface oxidation by the H_2O_2 treatment increased the initial uptake of water, while the H_2 reduction caused a marked decrease in the amount of water adsorbed at low p/p°. Measurement of the peak areas of the XPS spectra provided a means of determining the fractional surface coverage by the hydrophilic sites. In this way a linear relationship was found between the low-pressure adsorption of water vapour and the number of hydrophilic sites (mainly —COOH).

The low affinity of the surface of pure carbon for water is associated with the unusually weak non-specific interactions between the non-polar surface and the adsorbate. When certain functional groups are present on the carbon surface, specific interactions come into play and the adsorption affinity is thereby increased (see Chapter 1).

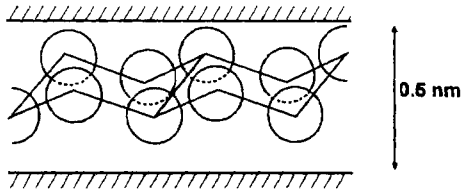

Figure 9.27. Hydrogen-bonded structure of water in a slit-shaped pore (Carrott *et al.*, 1991).

Furthermore, with at least some systems, it has been found that E and N do not vary appreciably with temperature and therefore the temperature-invariance condition is satisfied (Stoeckli *et al.*, 1994b). On the other hand, so far it has not been possible to define the exact meaning of these terms.

Recently, Iiyama *et al.* (1995) have obtained a series of distinctive X-ray diffraction patterns for water adsorbed in the 1.3 nm slit-shaped pores of a supermicroporous carbon. The diffraction patterns and derived electron distribution functions appear to confirm the existence of some long-range order in the structure of the adsorbed water. These interesting results are consistent with the fact that water can be easily accommodated in narrow slit-shaped pores of carbon in contrast to the pore-filling hydrophobicity of the tubular pores of Silicalite (Carrott *et al.*, 1991). As indicated in Figure 9.27, a thin slab of hydrogen-bonded water can be placed in a slit of width greater than ≈0.5 nm with very little distortion of its structure. Moreover, we can begin to see why the size of the hysteresis loop is dependent on pore size as well as surface chemistry. It seems likely that the adsorbate in the central layer will become more liquid-like as the pore width is increased. Therefore, the filling and emptying of a very narrow pore occurs reversibly in one step, whereas a wider pore is filled/emptied in two stages.

A novel method for determining the location of the primary water adsorbing sites has been developed by Bailey *et al.*, (1995). This approach involves the pre-adsorption of naphthalene, which was chosen because of its planar molecular shape and immiscibility with water. With some activated carbons it was found that the growth of the H-bonded water clusters was inhibited by the presence of naphthalene, while in other cases there was very little effect. It was thought that sites in larger micropores were prone to obstruction by the pre-adsorbed naphthalene. It is too early to judge the success of this interesting approach, which may turn out to be a useful alternative to pre-adsorption by *n*-nonane.

9.6. Immersion Microcalorimetry and Adsorption From Solution

9.6.1. Immersion microcalorimetry

Immersion calorimetry can be used to study either the surface chemistry or the texture of active carbons. A sensitive Tian–Calvet microcalorimeter is adaptable for either purpose, the main difference being in the choice of wetting liquids.

References

Amberg C.H., Spencer W.B. and Beebe R.A. (1955) *Canad. J. Chem.* **33**, 305.

Aranovich G.L. (1991) *J. Colloid Interface Sci.* **141**, 30.

Atkinson D., McLeod A.I. and Sing K.S.W. (1984) *J. Chim. Phys.* **81**, 791.

Atkinson D., Carrott P.J.M., Grillet Y., Rouquerol J. and Sing K.S.W. (1987) In: *Proc. 2nd Conf. on Fundamentals of Adsorption* (A.I. Liapis, ed.), Engineering Foundation, New York, p. 89.

Aukett P.N., Quirke N., Riddiford S.M. and Tennison S.R. (1992) *Carbon* **30**, 913.

Avgul N.N. and Kiselev A.V. (1970) *Chem. Phys. Carbon* **1**, 1.

Avgul N.N., Kiselev A.V., Kovalyova N.V. and Khrapova E.V. (1957) In: *Proc. 2nd Int. Congress on Surface Activity*, vol. II (J.H. Schulman, ed.), Butterworths, London, p. 218.

Baker F.S. (1992) In: *Kirk-Othmer Encyclopedia of Chemical Technology*, vol. 4, John Wiley, New York, p. 1015.

Bailey A., Lawrie G.A. and Williams M.R. (1995) *Adsorption Sci. Tech.* **12**, 193.

Balbuena P.B., Lastoskie C., Gubbins K.E. and Quirke N. (1993) In: *Proc. 4th Int. Conf. on Fundamentals of Adsorption* (M. Suzuki, ed.) Kodansha, Tokyo, p. 27.

Balbuena P.B. and Gubbins K.E. (1994) In: *Characterization of Porous Solids III* (J. Rouquerol, F. Rodriguez-Reinoso, K.S.W. Sing and K.K. Unger, eds), Elsevier, Amsterdam, p. 41.

Bansal R.C., Bhatia N. and Dhami T.L. (1978a) *Carbon* **16**, 65.

Bansal R.C., Dhami T.L. and Parkash S. (1978b) *Carbon* **16**, 389.

Bansal R.C., Donnet J.-B. and Stoeckli F. (1988) In: *Active Carbon*, Marcel Dekker, New York.

Barton S.S. and Harrison B.H. (1975) *Carbon* **13**, 47.

Barton S.S. and Koresh J.E. (1983) *J. Chem. Soc., Faraday Trans. I* **79**, 1147–1165.

Barton S.S., Evans M.J.B. and MacDonald J.A.F. (1991) *Carbon* **29**(8), 1099.

Barton S.S., Evans M.J.B. and MacDonald J.A.F. (1992) *Carbon* **30**(1), 123.

Beebe R.A. and Dell R.M. (1955) *J. Phys. Chem.* **59**, 746.

Beebe R.A. and Young D.M. (1954) *J. Phys. Chem.* **58**, 93.

Beebe R.A., Beckwith J.B. and Honig J.M. (1945) *J. Am. Chem. Soc.* **67**, 1554.

Beebe R.A., Biscoe J., Smith W.R. and Wendell C.B. (1947) *J. Am. Chem. Soc.* **69**, 95.

Beebe R.A., Millard B. and Cynarski J. (1953) *J. Am. Chem. Soc.* **75**, 839.

Beebe R.A., Gale R.L. and Kleinsteuber T.C.W. (1966) *J. Phys. Chem.* **70**, 4010.

Bienfait M. (1980) In: *Phase Transitions in Surface Films* NATO ASI B51 (J.G. Dash and J. Ruvalds, eds), Plenum, New York, p. 29.

Bienfait,M. (1985) *Surface Sci.* **162**, 411.

Bienfait M., Zeppenfeld P., Gay J.M. and Palmari J.P. (1990) *Surface Sci.* **226**(3), 327.

Blasinski H., Kamionowska U., Kazmierczak J. and Pustelnik A. (1990) *Adsorption Sci. and Techn.* **7**, 228.

Boehm H.P. (1966) In: *Advances in Catalysis*, vol. 16 (D.D. Eley, H. Pines and P.B. Weisz, eds), Academic Press, New York, p. 179.

Boehm H.P. (1994) *Carbon* **32**, 759.

Bojan M.J. and Steele W.A. (1987) *Langmuir* **3**(6), 1123.

Bonijoly M., Oberlin M. and Oberlin A. (1982) *Int. J. Coal Geol.* **1**, 283.

Bradley R.H. and Rand B. (1995) *J. Colloid Interface Sci.* **169**, 168.

Bradley R.H., Sutherland I. and Sheng E. (1995) *J. Chem. Soc., Faraday Trans.* **91**, 3201.

Breck D.W. (1974) In: *Zeolite Molecular Sieves*, John Wiley, New York, p. 636.

Brauer P., Poosch H.-R., Szombathely M.V., Heuchel M. and Jaroniec M. (1993) In: *Proc. 4th Int. Conf. on Fundamentals of Adsorption* (M. Suzuki, ed.), Kodansha, Tokyo, p. 67.

Brunauer S. (1945) In: *The Adsorption of Gases and Vapours*, Oxford University Press, London, p. 293.

Cadenhead D.A. and Everett D.H. (1958) In: *Industrial Carbon and Graphite*, S.C.I., London, p. 272.

Carrott P.J.M. (1993) *Adsorption Sci Tech* **10**, 63.

Carrott P.J.M. and Sing K.S.W. (1988) In: *Characterization of Porous Solids I* (K.K. Unger, J. Rouquerol, K.S.W. Sing and H. Kral, eds), Elsevier, Amsterdam, p. 77.

Carrott P.J.M. and Sing K.S.W. (1989) *Pure Appl. Chem.* **61**, 1835.

Table 10.2. Standard data for the adsorption of argon at 77 K on non-porous hydroxylated silica

Relative pressure $p/p°$	α_S ($= n/n_{0.4}$)	Relative pressure $p/p°$	α_S ($= n/n_{0.4}$)
0.01	0.243	0.30	0.876
0.02	0.324	0.32	0.900
0.03	0.373	0.34	0.923
0.04	0.413	0.36	0.948
0.05	0.450	0.38	0.973
0.06	0.483	0.40	1.000
0.07	0.514	0.42	1.022
0.08	0.541	0.44	1.048
0.09	0.563	0.46	1.064
0.10	0.583	0.48	1.098
0.11	0.602	0.50	1.123
0.12	0.620	0.52	1.148
0.13	0.638	0.54	1.172
0.14	0.657	0.56	1.198
0.15	0.674	0.58	1.225
0.16	0.689	0.60	1.250
0.17	0.705	0.62	1.275
0.18	0.719	0.64	1.300
0.19	0.733	0.66	1.327
0.20	0.748	0.68	1.354
0.22	0.773	0.70	1.387
0.24	0.801	0.72	1.418
0.25	0.813	0.74	1.451
0.26	0.826	0.76	1.486
0.28	0.851	0.78	1.527

FHH plots have also been constructed from the isotherms of isobutane and neopentane on the pyrogenic silicas (Carrott *et al.*, 1988). Derived values of the FHH exponent, s, for neopentane s (np) and nitrogen s (N_2) are recorded in Table 10.3. Also included in this table are the BET-nitrogen surface areas a(BET-N_2), and the BET C values for nitrogen and neopentane C (N_2) and, C (np). As expected, the high-temperature treatment of TK800 and Aerosil 200 resulted in the removal of a high proportion of the surface OH groups: this in turn led to a significant reduction in the nitrogen–adsorbent interaction energy and consequently a decrease in the values of C (N_2).

The remarkable constancy of the values of s(N_2) and s(np) in Table 10.3 follows from the fact that the linear FHH plots are parallel in the multilayer range. These results confirm that the multilayer character of each adsorptive is rather insensitive to changes in surface chemistry.

The α_S-method has been used for the analysis of the isotherms of the following gases on porous and non-porous silicas: nitrogen (Bhambhani *et al.*, 1972; Carrott and Sing, 1984) argon (Carruthers *et al.*, 1971; Payne *et al.*, 1973) carbon tetrachloride (Cutting and Sing, 1969) and neopentane (Carrott *et al.*, 1988). A consistent pattern of behaviour has emerged from the study of different samples of the pyrogenic silicas. The derived α_S-plots are all linear over the monolayer and lower multilayer range. In

Table 10.4. Comparison of surface areas of pyrogenic silicas evaluated by the BET and α_S-method.

Silica	Outgassing T(K)	a(BET) ($m^2\,g^{-1}$)	a(S) ($m^2\,g^{-1}$)
TK800	298	153	151
	413	158	158
TK900	298	136	136
	413	136	135
Aerosil 200	298	215	213
	413	221	218

area $a(N_2)$ determined by nitrogen adsorption. Thus,

$$\frac{\sigma(\text{np})}{\text{nm}^2} = \frac{1.66a(N_2)/\text{m}^2\,\text{g}^{-1}}{n_m(\text{np})/\mu\text{mol}\,\text{g}^{-1}} \tag{10.2}$$

The five σ(np) values in Table 10.3 are in close agreement (i.e. 0.595 ± 0.015 nm^2), but they are much larger than the value, 0.40 nm^2, calculated for a close-packed monolayer of freely rotating neopentane molecules. However, it must be kept in mind that the C(BET) values are very low (i.e. 6–8) and therefore it is unlikely that n_m(np) represents the true statistical monolayer capacity.

Prolonged storage of a pyrogenic silica can result in slow ageing, as indicated by a loss of BET area. For example, the original specific surface area of a master batch of TK800, as evaluated from the measurements of Payne *et al.* (1973) and Baker and Sing (1976), was 163–166 $m^2\,g^{-1}$. A loss of area of *c.* 6 $m^2\,g^{-1}$, which occurred over a period of eight years, was evidently due to the development of some interparticle mesoporosity since this led to the development of a narrow hysteresis loop in the nitrogen isotherm at high nitrogen $p/p°$ (Carrott and Sing, 1984). A partial restoration in area was achieved by raising the outgassing temperature from 25°C to 140°C (see Table 10.4). This restoration was probably due to the removal of water from the particle interstices: it is likely that the presence of residual water and compaction were together responsible for the loss of area.

A number of detailed studies have been made of the physisorption of gases on compacted silica powders (Avery and Ramsay, 1973; Gregg and Langford, 1977). The changes in the character of nitrogen adsorption as a result of increasing the compacting pressure are shown in Figure 10.4.

It is striking that the isotherms in Figure 10.4 change first from Type II to IV and finally to Type I. Thus, the results of Avery and Ramsay (1973) have clearly demonstrated that mesopores and micropores can be produced by the progressive compaction of a non-porous powder. However, a drastic loss of surface area accompanied this change (from 630 to 219 $m^2\,g^{-1}$) and Avery and Ramsay point out that this was associated with a marked increase in the particle packing density.

The importance of surface silanol (hydroxyl) groups in controlling the specific physisorption interactions was studied by Kiselev (1958, 1971). Kiselev and his co-workers found that fully hydroxylated silica has a surface OH concentration of 7–9 μmol m^{-2}, which corresponds to a surface population, N(OH), of *c.* 5 OH nm^{-2}

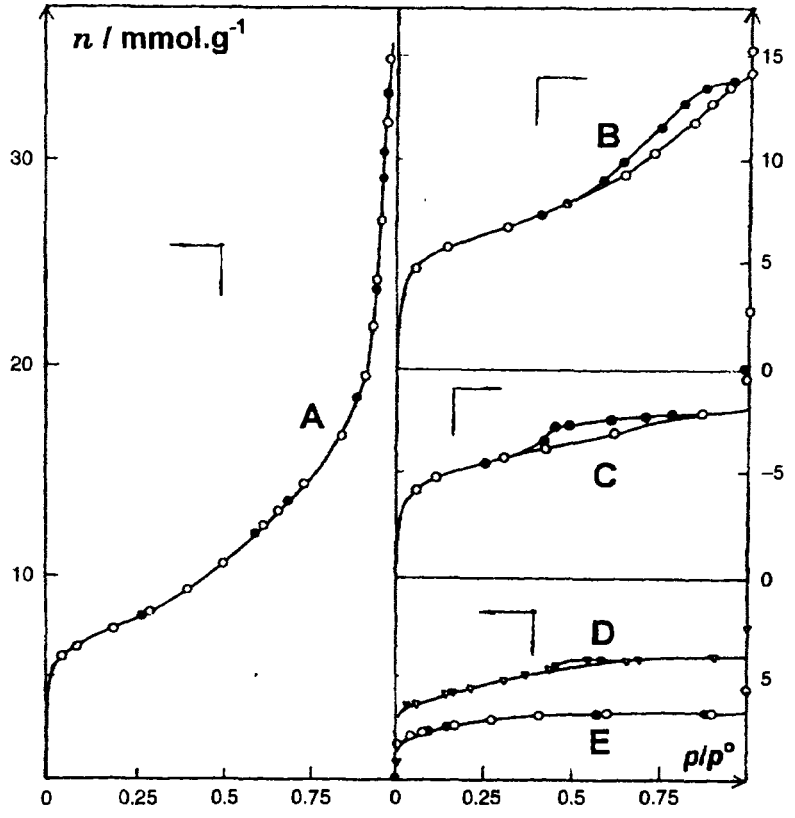

Figure 10.4. Effect of compaction of Aerosil *on* nitrogen adsorption isotherms at 77 K; (A) uncompressed or compressed under (B) 1.5, (C) 6, (D) 7.5 or (E) 15 kbar (reproduced courtesy of Avery and Ramsay, 1973).

(Zhuravlev and Kiselev, 1970). More recently, Zhuravlev (1987) reported a mean N(OH) value of 4.9 OH nm^{-2} (after outgassing at 180–200°C) for 100 fully hydroxylated amorphous silicas. This value is not far removed from N(OH) = 4.6 OH nm^{-2}, originally proposed by Vleeskens (see Okkerse, 1970).

A fully hydroxylated state in which all the OH groups are bound to Si atoms (with N(OH) = 4.6 OH nm^{-2}) would correspond to the octahedral, (111), face of β-cristobalite or the basal face of β-tridymite. However, as indicated in Table 10.5, the surface hydroxyl concentrations found on some arc and fume silicas are significantly lower, typical values being in the range 3.4–4 OH nm^{-2} (Baker and Sing, 1976; Unger, 1979, p. 62; Gallas *et al.*, 1991).

As was noted earlier, the level of surface OH concentration has very little effect on either the isotherms or the energetics of adsorption of non-polar molecules such as argon or the alkanes. Specific interactions become significant when the adsorptive

Adsorption microcalorimetry has shown that the surfaces of both amorphous and crystalline silicas are energetically heterogeneous. Furthermore, the IR spectroscopic evidence reveals that their surface structures are dependent on the conditions of preparation and treatment (Unger, 1994).

10.2.2. Precipitated silicas

Although commercially important, the precipitated silicas have received much less attention in the scientific literature than either the Aerosils or silica gels. In certain respects they are similar to pyrogenic silicas: indeed, at one time they were treated as alternative non-porous silicas. Thus, the reversible Type II isotherms of nitrogen and argon obtained by Basset *et al.* (1968) were assumed to represent uncomplicated monolayer–multilayer adsorption. More recent work (Carrott and Sing, 1984) has shown that the Type II character is here the result of adsorption both on the external surface and within some micropores.

In contrast to the general behaviour of the pyrogenic silicas, the level of physisorption by precipitated silicas has been found to be sensitive to changes in the conditions of outgassing. Physisorption equilibration is more difficult to attain and consequently the isotherms often have a more complicated appearance. For example, the behaviour of a batch of VN3 (a Degussa product) is illustrated by the results in Figure 10.5 (Carrott and Sing, 1984). It can be seen that the increase in outgassing temperature from 25°C to 110°C has produced a significant upward movement in the nitrogen isotherm. In addition it has led to the appearance of a small step in the amount adsorbed at $p/p^\circ \approx 0.6$ and to the development of a small amount of low pressure hysteresis. Similar features are exhibited by the isotherms determined after outgassing at the temperatures of 200°C and 300°C, but in the latter case the step is located at a much lower relative pressure ($p/p^\circ \approx 0.2$) and the open hysteresis extends over the complete isotherm. It is evident that these steps cannot be explained in terms of any well-defined phase transitions. They are more likely to be due to the slow diffusion of the adsorptive molecules into inner regions of the particles, which are not easily accessible.

The α_S-plots for nitrogen on VN3 in Figure 10.5 have been constructed from the *desorption* isotherms. In each case, the back-extrapolated linear portion gives a positive intercept on the n axis and an upward deviation can be seen at $p/p^\circ \approx 0.7$. This behaviour is typical of adsorption at low p/p° occurring both on the external surface and within narrow micropores. At higher p/p°, the upward deviation indicates that the multilayer adsorption on the external surface is accompanied by interparticle capillary condensation, which is partly responsible for the narrow hysteresis loop.

The α_S-plots in Figure 10.5 have been analysed by the method described in Chapter 8. The values of the external surface area, a(ext, S), and micropore volume, v_p(mic, S), in Table 10.6 have been calculated from the slope and intercept, respectively, of each α_S-plot. It can be seen that the external area does not change to any significant extent over the range 110–300°C and that the changes in the BET area, a(BET), are due to the development of a small micropore volume.

Further confirmation of the development of microporosity has been obtained by the application of the nonane pre-adsorption method of Gregg and Langford (1969).

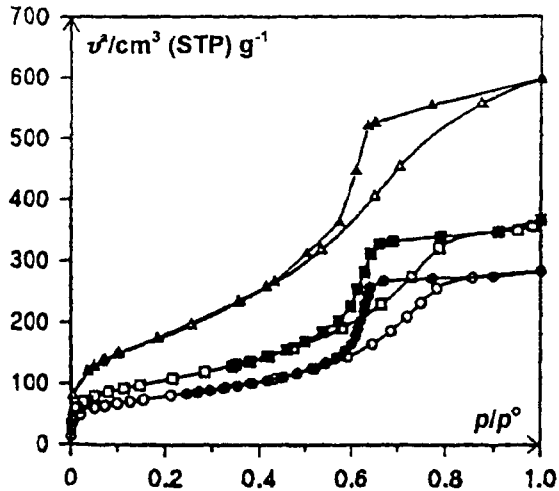

Figure 10.7. Nitrogen isotherms at 77 K for xerogel (circles), acid-washed xerogel (squares; HCl, pH2, 24 h) and alcogel (triangles) (Kenny and Sing, 1994).

The most striking result in Figure 10.7 was obtained when the hydrogel was washed with ethyl alcohol. The vacuum-dried material, which we shall refer to as an 'alcogel', gave a much larger uptake of nitrogen over the complete range of $p/p°$: $a(\text{BET}) = 641\ \text{m}^2\,\text{g}^{-1}$ and $v_p = 0.93\ \text{cm}^3\,\text{g}^{-1}$. It is evident that by replacing water as the continuous liquid phase, it was possible to reduce the large capillary forces which are responsible for the considerable shrinkage normally found when water is removed from the hydrogel.

An even larger pore volume can be obtained if the liquid phase is removed under supercritical conditions to give an 'aerogel'. This type of gel has an extremely high surface area and pore volume (see Table 10.7), but it tends to be mechanically weak and unstable when exposed to water vapour because the particle coordination number is low. The upper limiting area of a silica composed of discrete primary particles would be $\approx 2000\ \text{m}^2\,\text{g}^{-1}$, but specific surface areas of this magnitude are unlikely to be attained.

Barby (1976) has defined two types of conventional silica xerogels (Table 10.7). The S-type gels can be either microporous or mesoporous and are produced in the normal way, which allows considerable loss of suface area and pore volume to occur during the removal of water from the hydrogel. If the hydrogel is subjected to hydrothermal treatment, the primary particles undergo more drastic aggregation-cementation with the result that after drying the porosity is largely confined to the interstitial space between the secondary particles, as in Figure 10.6. The resulting G-type xerogel has a somewhat lower surface area, but a larger and more uniform pore volume (Barby, 1976).

In view of the complexity of the structure of most silica xerogels, it is to be expected that their adsorptive behaviour would be equally complex. The following

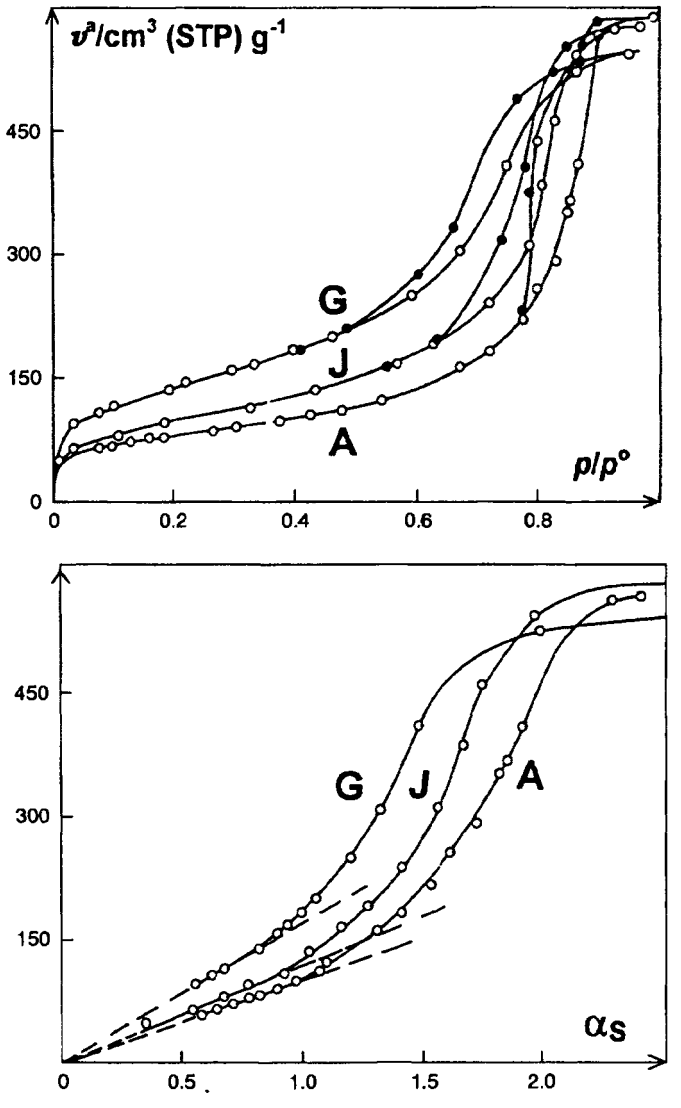

Figure 10.8. Nitrogen isotherms (top) and α_S-plots (bottom) for mesoporous silica gels A, J and G (from Bhambhani *et al.*, 1972).

As explained in Chapter 8, the external surface area, a(ext, S), available for multilayer adsorption can be calculated from the high p/p° section of an α_S-plot, provided that there is an adequate range of linearity to confirm the absence of capillary condensation. This condition is clearly fulfilled with gels D and E, and their external areas are therefore recorded in Table 10.8.

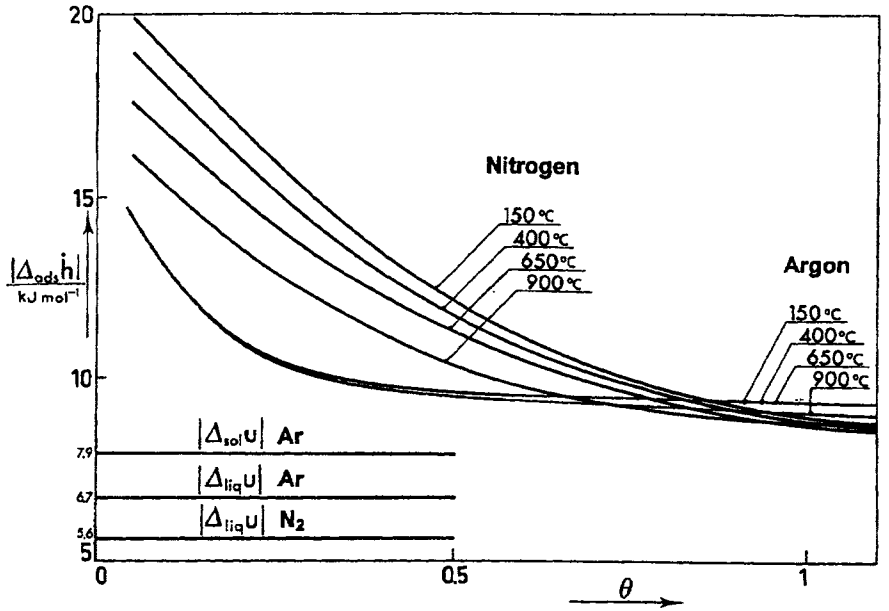

Figure 10.12. Differential enthalpies of adsorption of argon and nitrogen on a mesoporous silical gel: effect of outgassing at different temperatures (Rouquerol *et al.*, 1979b).

energetic heterogeneity is a feature of the adsorption of both gases, with Ar the variation of adsorption enthalpy is virtually unchanged over the outgassing temperature range 150–900°C. The striking difference in the behaviour of N_2 can only be due to the weakening of the specific field gradient–quadrupole interactions which is the result of the reduction in the number of surface hydroxyls. It is evident that the location of the N_2 curve on the 900°C sample is not far removed from the common Ar curve. This is to be expected because of the similarity of the non-specific interactions for both Ar and N_2 with the dehydroxylated surface. The remaining difference is probably due to the specific interaction of N_2 with the remaining isolated hydroxyls on the 900°C surface.

As noted in Chapter 1, the specific interactions between polar molecules and silica are virtually eliminated by the removal of all the surface hydroxyls and therefore the effect of partial dehydroxylation is to drastically reduce the adsorption energies of certain molecules. The polar adsorptives studied by Kiselev and his co-workers included alcohols, ketones, ethers and amines (Kiselev, 1965, 1971): with each adsorptive, the reduction in the adsorbent–adsorbate interaction energy was accompanied by a substantial change in the isotherm character.

It might be expected that a dehydroxylated silica surface would be more energetically homogeneous than the parent hydroxylated surface, and this is found in practice – as exemplified in Figure 10.12. However, the effect of outgassing a silica gel at high temperature may lead to the development of ultramicroporosity. To overcome this problem, much of the later work by Kiselev's group was undertaken on hydrother-

of hydrophobicity shown by all dehydroxylated silicas. The surface rehydroxylation was very slow at $p/p^\circ < 0.3$, but became rapid in the multilayer range; this phenomenon was evidently responsible for the low-pressure hysteresis. Indeed, it was found that the *desorption* branches of the isotherms on gels E and J were remarkably similar to the corresponding parts of the water isotherms on the two hydroxylated gels (Baker and Sing, 1976). We may conclude that the micropores in the rehydroxylated gel E regained their high affinity for water.

10.3. Aluminas: Structure, Texture and Physisorption

10.3.1. Activated alumina

The name 'activated alumina' is generally applied to an adsorbent alumina (usually an industrial product) prepared by the heat treatment of some form of hydrated alumina (i.e. a crystalline hydroxide, oxide-hydroxide or hydrous alumina gel). It has been known for many years that certain forms of activated alumina can be used as powerful desiccants or for the recovery of various vapours. It was apparent at an early stage that the adsorbent activity was dependent on the conditions of heat treatment. For example, in 1934 Bayley reported that the adsorption of H_2S by a commercial sample of activated alumina was affected by prior heating of the adsorbent at different temperatures, the maximum uptake being obtained after heat treatment at 550°C. During an investigation of the catalytic dehydration of alcohols, Alekseevskii (1930) found that a calcination temperature of *c.* 400°C was required to optimize the adsorption of the alcohol reactants, whereas calcination at 600°C was preferable for the adsorption of the olefine products.

Somewhat later it began to appear that there was a lack of agreement between the recorded dependence of surface area on the temperature of calcination (e.g. in the work of Krieger, 1941; Feachem and Swallow, 1948; Taylor, 1949; Gregg and Sing, 1951; de Boer, 1957). In fact, such differences are not really surprising. To obtain reproducible adsorbent properties it is necessary to control: (a) the chemical and physical nature of the starting material (i.e. its structure, crystal/particle size, amount of sample purity); (b) the conditions of heat treatment (type of furnace, atmosphere, time – temperature profile – preferably by a controlled rate thermal analysis (CRTA) heating procedure); and (c) the methods used to interpret the adsorption data (BET, BJH, etc.).

10.3.2. Aluminium trihydroxides

Although various modifications of aluminium trihydroxide, $Al(OH)_3$, have been described in the literature, there are only three common forms: gibbsite (originally also called hydrargillite) bayerite and nordstrandite. Gibbsite is the best known and most abundant. It is the main constituent of North and South American bauxite and is obtained as an intermediate product (i.e. 'Bayer Hydrate') in the Bayer process for the production of aluminium from bauxite.

between two adjacent A (or B) layers is 0.28 nm whereas the A–B distance is 0.20 nm.

Bayerite does not occur in nature, but it can be made in a number of different ways (e.g. by the hydrolysis of an aluminium alkoxide). The OH layers in bayerite appear to be stacked in the order ABABAB.... Within the double layer the A–B distance is 0.21 nm and between the double layers the A–B distance is 0.26 nm. The density of bayerite is correspondingly a little higher than that of gibbsite.

Although deposits of nordstrandite have been found, this modification is not easy to prepare in a relatively pure form. For this reason, the exact structure is still under discussion. However, the layer stacking is likely to be made up of a combination of both bayerite and gibbsite.

In its most common industrial form, gibbsite is a sandy material, of *c.* 50–100 μm grain size. Each grain is itself a dense agglomerate of smaller hexagonal crystals, typically 5–15 μm in size, and the BET-nitrogen surface area is usually not more than 0.2 $m^2 g^{-1}$. Other forms of gibbsite have also been subjected to physisorption studies. These include loose, thin hexagonal crystals with BET-nitrogen areas of 5 and 15 $m^2 g^{-1}$ corresponding to mean crystal sizes of 1 and 0.2 μm, respectively (Rouquerol *et al.*, 1975), and also porous aggregates. For example, Ramsay and Avery (1979) found that a batch of very pure gibbsite powder gave a Type IV nitrogen isotherm with an H1 hysteresis loop at high $p/p°$. It appeared that the gibbsite was mesoporous and possibly also macroporous, the effective pore width being mainly > 20 nm. The BET-nitrogen area was 41 $m^2 g^{-1}$, which was consistent with the mean thickness of *c.* 25 nm of the thin hexagonal platelets, as determined by electron microscopy and X-ray line broadening. This rather ill-defined porosity was ascribed to the space between the gibbsite crystallites and was found to persist after heat treatment at 400°C. A batch of gibbsite of lower BET-nitrogen area (5.6 $m^2 g^{-1}$) was used by Stacey (1987). In this case, the polycrystalline grains of mean diameter 75 μm were composed of 0.3 μm platy crystallites.

A sample of microcrystalline nordstrandite was found to be somewhat mesoporous by Aldcroft and Bye (1967). The nitrogen hysteresis loop was Type H3, which indicated the existence of slit-shaped pores between the crystallites. The BET-nitrogen area of 34 $m^2 g^{-1}$ appeared to represent the external area of the crystallites.

A relatively low-area (8 $m^2 g^{-1}$) aged sample of bayerite (Bye and Robinson, 1964) which gave a reversible Type II nitrogen isotherm, was shown to be essentially non-porous (Payne and Sing, 1969). Electron microscopy revealed that this sample was composed of discrete conical crystals.

10.3.3. Aluminium oxide-hydroxides

There are two well-known oxide-hydroxides (AlOOH) with closely related structures: diaspore and boehmite. Diaspore occurs in some types of clay and bauxite. It has been produced by the hydrothermal treatment of corundum, α-Al_2O_3. Whereas boehmite is characterized by cubic close-packing of the anions, diaspore has a hexagonal close-packed structure. This difference probably accounts for the direct thermal transformation of diaspore to corundum at relatively low temperatures (450–600°C).

of the products are usually complex. As in other thermal decomposition studies, control of the dehydration reactions and sintering/ageing processes is considerably improved by the application of CRTA (controlled rate thermal analysis), together with the use of finely divided and well-characterized gibbsite. In this manner, Rouquerol and co-workers (Rouquerol *et al.*, 1975, 1979a; Rouquerol and Ganteaume, 1975) were able to obtain the results in Figures 10.17 and 10.18 and hence extend the work of Papée.

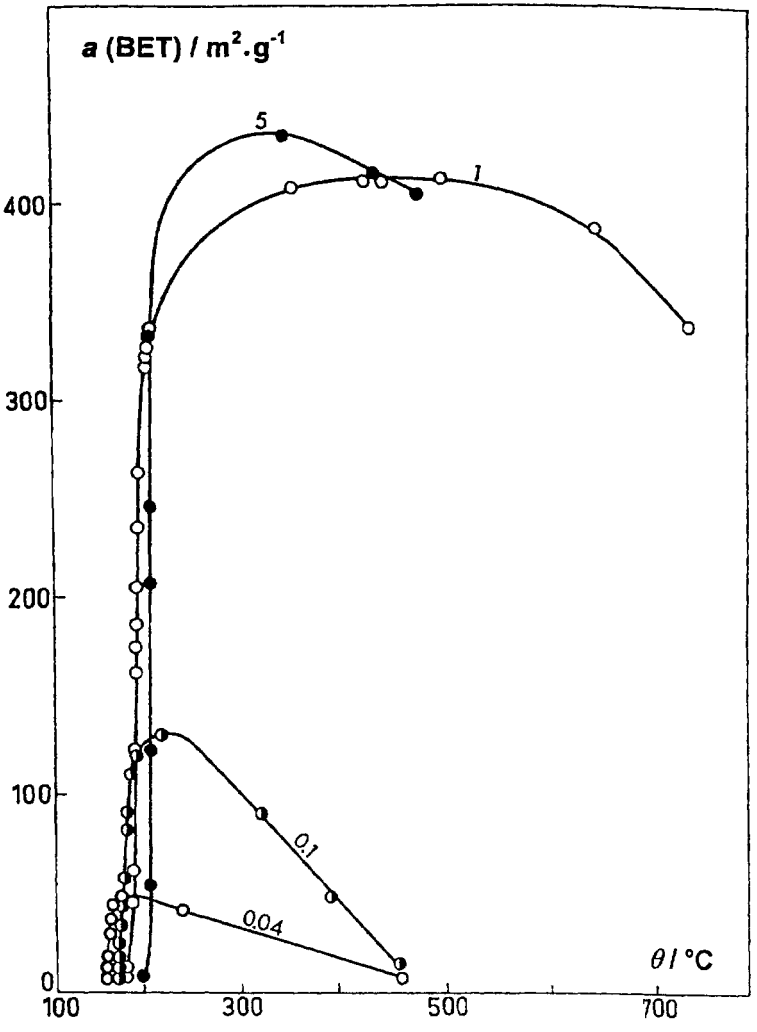

Figure 10.17. Development of the BET-nitrogen surface area during the dehydration, by CRTA, of a sample of fine gibbsite, 1 μm grain size. CRTA conditions: controlled pressure indicated in mbar on the curve; rate of dehydration, 11.4 mg h^{-1} g^{-1} (Rouquerol and Ganteaume, 1977).

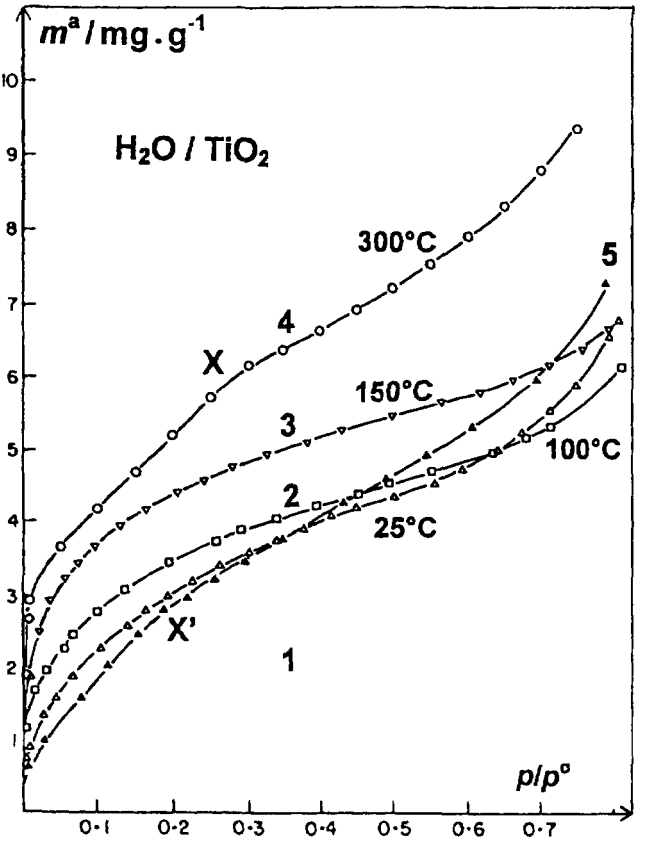

Figure 10.22. Isotherms of water vapour on rutile, outgassed between 25°C and 300°C. Run 5 follows run 4 with simple intermediate outgassing at 25°C (Furlong *et al.*, 1986).

and other bases. On the other hand, there appears to be no indication of Bronsted acidity, although this can be produced by surface treatment (e.g. with HCl). It is not surprising that the dehydrated surface of rutile can interact specifically with a wide range of polar molecules (Parkyns and Sing, 1975).

Parfitt and his co-workers pointed out (Day, Parfitt and Peacock, 1971) that there is an important difference between ethanol and isopropanol in their interactions with rutile. Whereas ethanol can displace water and undergo dissociative chemisorption to form the surface ethoxide, isopropanol is more readily adsorbed in the molecular form. This is consistent with the hydrophobic nature of ethanol-treated TiO_2 and the 'autophobic' nature of the ethanol monolayer. The latter effect is manifested in the form of a Type I isotherm, which is remarkably similar to that given by ethanol on alumina (see Figure 10.15).

A fairly low-area sample of polycrystalline TiO_2 (98.5% rutile) was used by Grillet

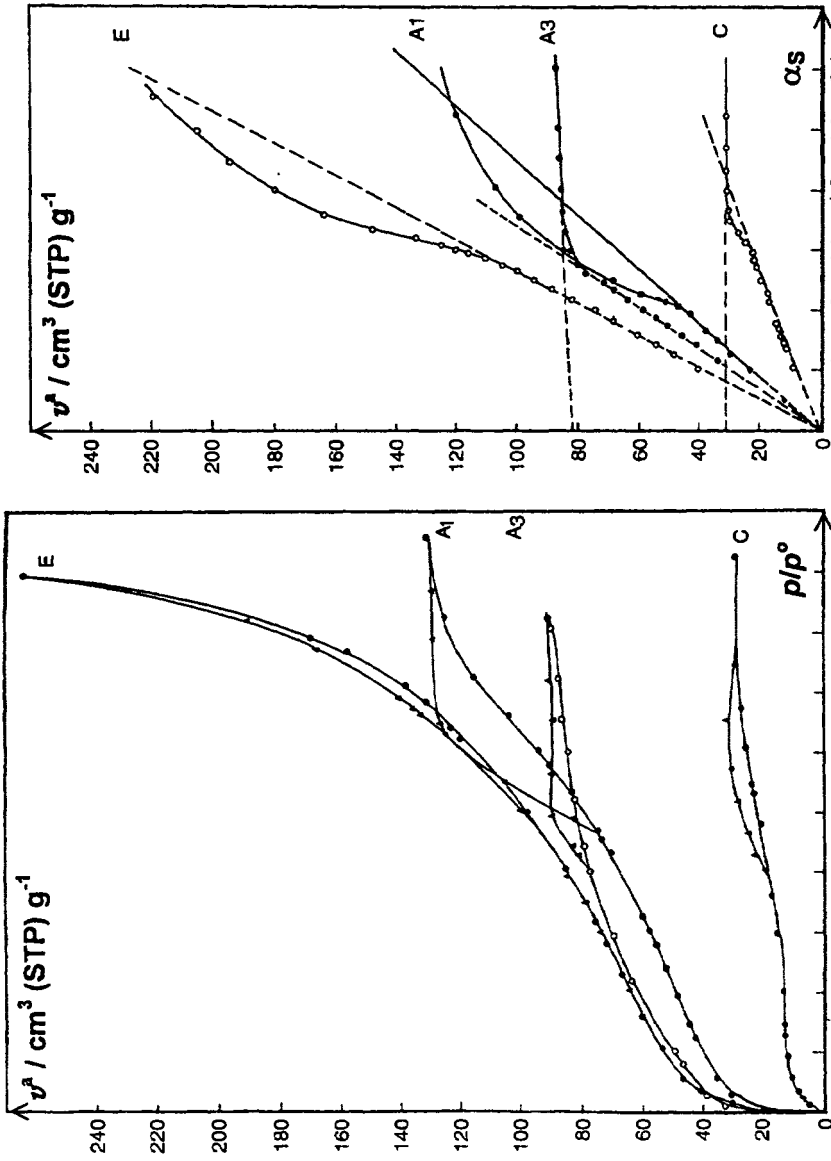

Figure 10.24. Adsorption isotherms of N_2 at 77 K on a selection of hydrous TiO_2 gels (left) and corresponding α_s-plots (right) (Ragai and Sing, 1984).

Vilches, 1984). The deleterious effect of water vapour was attributed to the formation of surface layers of $Mg(OH)_2$. This conclusion was consistent with the inferior quality (i.e. non-stepwise character) of isotherms determined on MgO prepared by the thermal decomposition of $Mg(OH)_2$.

A family of isotherms for the Xe/MgO(1 0 0) system is shown in Figure 10.25. Similar results were obtained for the Kr/MgO(1 0 0) system (Coulomb *et al.*, 1984). The vertical risers corresponding to first and second layer formation are clearly evident, as are the first layer sub-steps. As with other systems, the sub-steps were attributed to 2-D 'fluid–solid' transitions. By following the approach adopted by Larher, Coulomb *et al.* (1984) were able to estimate the 2-D triple and critical points for Xe/MgO and Kr/MgO.

The Ar/MgO(1 0 0) isotherms determined by Coulomb *et al.* (1984) over the temperature range 48–69 K also exhibited well-defined first and second layer risers, but at these temperatures there appeared to be no first-layer sub-steps. This absence of monolayer phase transitions in the p–T range studied seemed to be associated with a large 2-D liquid–vapour coexistence region. However, subsequent work (Coulomb, 1991) revealed the existence of a 2-D solid-type structure at lower temperatures, with all the Ar atoms appearing to lie along the channels formed by the small Mg^{2+} ions. At a temperature of *c.* 38 K, the long-range order along the channels is lost.

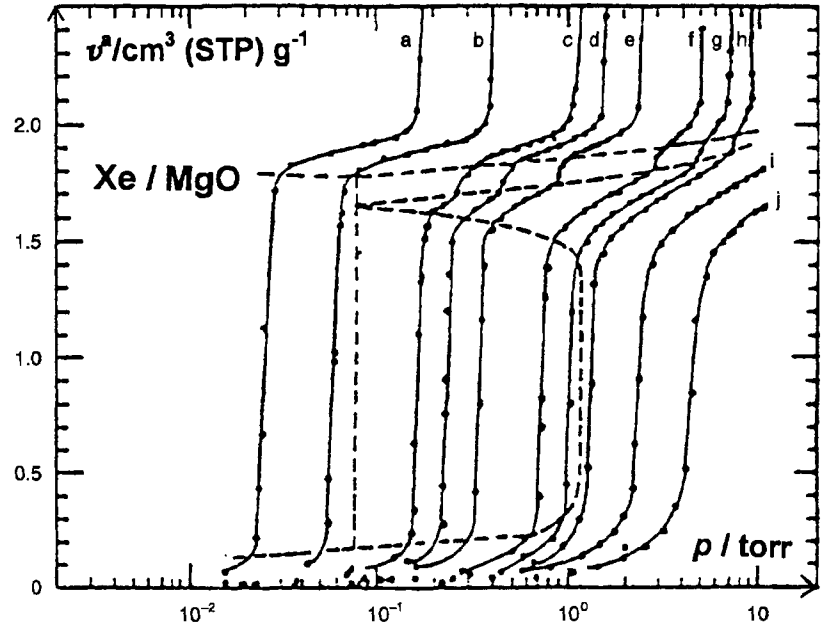

Figure 10.25. Isotherms of Xe on MgO at (a) 96.86, (b) 100.47, (c) 106.20, (d) 108.44, (e) 111.02, (f) 116.14, (g) 118.72, (h) 121.15, (i) 126.17 and (j) 131.19 K. Phase boundaries indicated by dashed lines (Coulomb *et al.*, 1984).

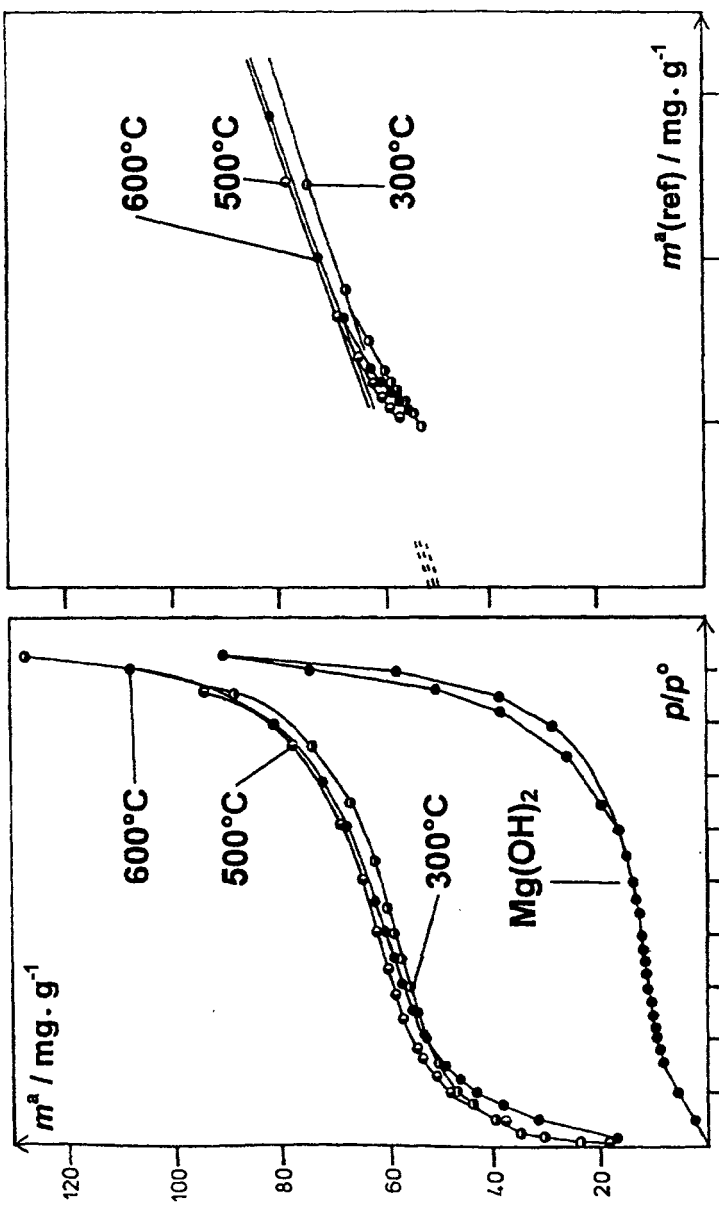

Figure 10.28. Neopentane isotherms at 273 K on partially decomposed and on starting $Mg(OH)_2$ (left) and corresponding comparison plots with undecomposed $Mg(OH)_2$ as reference (right) (Ribeiro Carrott *et al.*, 1991a).

Table 11.3. Henry's law constants and low coverage energies of adsorption for various alkanes on NaY and HY

Adsorptive	NaY		HY	
	$k_H \times 10^5$ (mol g^{-1})	E_0 (kJ mol^{-1})	$k_H \times 10^5$ (mol g^{-1})	E_0 (kJ mol^{-1})
n-Hexane	1.9	45.5	1.7	44.2
2-Methylpentane	2.0	45.3	1.7	44.2
3-Methylpentane	2.0	44.5	1.7	43.5
2,3-Dimethylbutane	2.0	44.1	1.8	43.5
2.2-Dimethylbutane	2.1	43.2	1.8	43.5
n-Heptane	4.4	51.9	3.6	50.1
2,3-Dimethylpentane	5.1	50.6	3.6	50.1
n-Octane	10	57.5	7.9	56.0
2-Methylheptane	10	57.2	7.9	55.7
2,5-Dimethylexane	11	57.1	8.3	56.0
n-Nonane	23	63.4	17	62.0

From Denayer and Baron, (1997).

and branched paraffins by various forms of zeolite Y. By measuring the retention times corresponding to the perturbation of the adsorption system at different loadings, it was possible to derive the adsorption isotherm for each component. The measurements were made over the range 275–400°C. This study of the effect of chain length and branching of alkanes (from C_6 to C_{12}) followed earlier investigations of the adsorption of lower hydrocarbons by the faujasite zeolites (e.g. the work of Atkinson and Curthoys, 1981; Thamm *et al.*, 1983). Our present interest is in the behaviour of NaY and HY. Selected values of Henry's law constant, k_H, and low-coverage energy of adsorption, E_0, are given in Table 11.3.

Inspection of Table 11.3 reveals that there are relatively small differences between the corresponding values of k_H and E_0 for NaY and HY. This is to be expected since the adsorbent–adsorbate interactions are essentially non-specific (see Chapter 1). Decationization of zeolite Y thus has a minimal effect on the energetics of adsorption of the paraffins. The molecular shape of the adsorptive is also unimportant. In accordance with the results in Figures 1.5 and 1.6, the molar mass (number of carbon atoms) is much more important than the molecular shape. As before, there is a linear relation between E_0 and N_c. An exponential increase of k_H with N_c is of course consistent with the form of Equation (4.3).

The interaction of polar molecules with ionic and polar surfaces was briefly discussed in Chapter 1. A simplified form of Equation (1.6) was given as

$$E_0 = E_{ns} + E_{sp} \tag{11.3}$$

where E_{ns} represents the non-specific adsorbent-adsorbate interactions and E_{sp} the various specific contributions. When zeolites are used as adsorbents the E_{sp} term becomes extremely important (Kiselev, 1967; Barrer, 1978). The magnitude of the specific contributions is illustrated by the low-coverage adsorption calorimetric data in Table 11.4.

Comparison of the values of E_0 is made in Table 11.4 for pairs of molecules of very

clear, but it seems likely that the chromatographic results are in part due to a very high degree of interconnectivity within the pore structure of AX21.

In this book we have generally adopted the convention of expressing the adsorption as the amount adsorbed by *unit mass* of the outgassed adsorbent. From a technological standpoint, however, it is sometimes more important to consider the amount adsorbed per *unit volume* of the adsorbent. It is evident that when this change is made for a powder of low bulk density such as AX21 (bulk density ≈ 0.3 g cm^{-3}) the available adsorbing capacity is much less impressive (Sing, 1989). For this reason, for a particular purpose it may be necessary to employ an adsorbent of moderate activity rather than one of very high specific activity.

12.2.2. Activated carbon fibres and carbon cloth

The first high-strength carbon fibres were produced in the 1950s (see Donnet and Bansal, 1984). The early carbonized products were rayon-based, but it was soon found that the mechanical properties and the carbon yield could be improved by the use of polyacrylonitrile (PAN) as the precursor. Also, less expensive fibres of somewhat lower strength and modulus could be made from various other precursors including petroleum pitch and lignin. However, cotton and other forms of natural cellulose fibres possess discontinuous filaments and the resulting mechanical properties were consequently found to be inferior to those of the rayon-based fibres.

It was not long before the first *activated* carbon fibres (ACFs) were developed. In the work of Economy and Lin (1971, 1976) highly porous carbon fibres were prepared from Kynol, a fibrous phenolic precursor. Carbonization was carried out in nitrogen at 800°C and activation occurred in steam at 750–1000°C. The products appeared to be predominantly microporous and were found to be effective for the removal of low levels of certain pollutants (e.g. phenol and pesticides) from air or aqueous solutions.

Another important development was the disclosure by Bailey and Maggs (1972; Bailey *et al.*, (1973) of a novel procedure for the manufacture of 'charcoal cloth'. The continuous process developed in the laboratories of the Chemical Defence Establishment, Porton Down, England, involved three main stages: (1) immersion of the roll of viscose rayon cloth in an aqueous solution of inorganic chlorides (e.g. $ZnCl_2$, $AlCl_3$ and NH_4Cl); (2) oven drying in nitrogen; (3) carbonization and activation in carbon dioxide.

The Type I character of the nitrogen and toluene isotherms displayed in Figure 12.1 indicates that a typical sample of activated charcoal cloth produced by the original Porton process had novel adsorbent properties. The activated material was strong and flexible and had a BET area of over 1200 m^2 g^{-1}, a wide distribution of micropores (no detectable mesoporosity) and a small external surface area (Atkinson *et al.*, 1982; Hall and Williams, 1986). In view of its early promise, it was logical to attempt to control the pore structure of charcoal cloth. A systematic study of the development of porosity was therefore undertaken by Atkinson *et al.* (1982, 1984) and Freeman *et al.* (1987–1991).

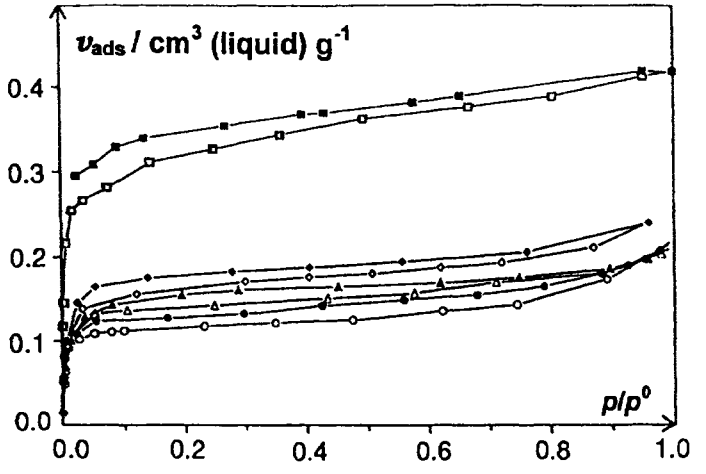

Figure 12.15. Adsorption–desorption isotherms on VPI-5 of methanol (squares), isobutane (diamonds), neopentane (circles) and propane (triangles) determined at 298, 261, 273 and 196 K, respectively (Kenny *et al.*, 1992).

this form of hysteresis cannot be attributed to capillary condensation, and is instead indicative of a more complex change in the adsorption system (e.g. activated entry of adsorptive molecules or swelling of the adsorbent).

Values of apparent specific micropore volume, v_p, of VPI-5 evaluated from the uptakes determined by Kenny *et al.* (1992) of various adsorptives at $p/p^\circ = 0.4$ are recorded in Table 12.7. As before, the adsorbate densities are assumed equal to the respective liquid densities at the operational temperatures. Also included in Table 12.7 are values of v_p derived from the measurements of Davis *et al.* (1989b), Schmidt *et al.* (1992) and Reichert *et al.* (1994). The complexity of the behaviour of VPI-5 is

Table 12.7. Values of apparent micropore volume, v_p, of VPI-5 evaluated from the adsorption capacities of different vapours at $p/p^\circ = 0.4$ (Kenny *et al.*, 1992).

Adsorptive	Kinetic diameter (nm)	Temperature (K)	Apparent v_p (cm^3 g^{-1})
Water	0.27	298	0.31–0.35[a]
Methanol	0.38	298	0.32
Oxygen	0.35	77	0.23[a]
Argon	0.34	77	0.17[b]
Nitrogen	0.36	77	0.187, 0.184[c], 0.146[b]
Methane	0.38	77	0.17[b]
Propane	0.43	196	0.17
Isobutane	0.50	261	0.18
Neopentane	0.62	273	0.12, 0.15[a]

[a] Davis *et al.* (1989b).
[b] Reichert *et al.* (1994).
[c] Schmidt *et al.* (1992).